UvA-DARE (Digital Academic Repository)

The Five Year Fermi/GBM Magnetar Burst Catalog

Collazzi, A.C.; Kouveliotou, C.; van der Horst, A.J.; Younes, G.A.; Kaneko, Y.; Göğüş, E.; Lin, L.; Granot, J.; Finger, M.H.; Chaplin, V.L.; Huppenkothen, D.; Watts, A.L.; von Kienlin, A.; Baring, M.G.; Gruber, D.; Bhat, P.N.; Gibby, M.H.; Gehrels, N.; Mcenery, J.; van der Klis, M.; Wijers, R.A.M.J.

[Link to publication](#)

THE FIVE YEAR *FERMI*/GBM MAGNETAR BURST CATALOG

A. C. Collazzi[1], C. Kouveliotou[2,3], A. J. van der Horst[2], G. A. Younes[2,4], Y. Kaneko[5], E. Göğüş[5], L. Lin[6], J. Granot[7],
M. H. Finger[4], V. L. Chaplin[8], D. Huppenkothen[9,10], A. L. Watts[11], A. von Kienlin[12], M. G. Baring[13], D. Gruber[14],
P. N. Bhat[15], M. H. Gibby[16], N. Gehrels[17], J. McEnery[17], M. van der Klis[11], and R. A. M. J. Wijers[11]

[1] SciTec, Inc., 100 Wall Street, Princeton, NJ 08540, USA; acollazzi@scitec.com
[2] Department of Physics, The George Washington University, 725 21st Street NW, Washington, DC 20052, USA
[3] Space Science Office, ZP12, NASA/Marshall Space Flight Center, Huntsville, AL 35812, USA
[4] Universities Space Research Association, NSSTC, 320 Sparkman Drive, Huntsville, AL 35805, USA
[5] Sabancı University, Orhanlı-Tuzla, Istanbul 34956, Turkey
[6] François Arago Centre, APC, 10 rue Alice Domon et Léonie Duquet, F-75205 Paris, France
[7] Department of Natural Sciences, The Open University of Israel, 1 University Road, P.O. Box 808, Raanana 43537, Israel
[8] School of Medicine, Vanderbilt University, 1161 21st Avenue S, Nashville, TN 37232, USA
[9] Center for Data Science, New York University, 726 Broadway, 7th Floor, New York, NY 10003, USA
[10] Center for Cosmology and Particle Physics, Department of Physics, New York University, 4 Washington Place, New York, NY 10003, USA
[11] Anton Pannekoek Institute, University of Amsterdam, Postbus 94249, 1090 GE Amsterdam, The Netherlands
[12] Max-Planck-Institut für extraterrestrische Physik, Giessenbachstrasse 1, D-85748 Garching, Germany
[13] Department of Physics and Astronomy, Rice University, MS-108, P.O. Box 1892, Houston, TX 77251, USA
[14] Planetarium Südtirol, Gummer 5, I-39053 Karneid, Italy
[15] CSPAR, University of Alabama in Huntsville, 320 Sparkman Drive, Huntsville, AL 35899, USA
[16] Jacobs Technology, Inc., Huntsville, AL, USA
[17] NASA Goddard Space Flight Center, Greenbelt, MD 20771, USA

ABSTRACT

Since launch in 2008, the *Fermi* Gamma-ray Burst Monitor (GBM) has detected many hundreds of bursts from magnetar sources. While the vast majority of these bursts have been attributed to several known magnetars, there is also a small sample of magnetar-like bursts of unknown origin. Here, we present the *Fermi*/GBM magnetar catalog, providing the results of the temporal and spectral analyses of 440 magnetar bursts with high temporal and spectral resolution. This catalog covers the first five years of GBM magnetar observations, from 2008 July to 2013 June. We provide durations, spectral parameters for various models, fluences, and peak fluxes for all the bursts, as well as a detailed temporal analysis for SGR J1550–5418 bursts. Finally, we suggest that some of the bursts of unknown origin are associated with the newly discovered magnetar 3XMM J185246.6+0033.7.

Key words: catalogs – pulsars: individual (SGR J1550–5418, SGR J0501+4516, 1E1841–045, SGR J0418+5729, SGR 1806–20, SGR J1822.3–1606, AXP 4U 0142+61, AXP 1E 2259+586, 3XMM J185246.6+0033.7) – stars: neutron – X-rays: bursts

1. INTRODUCTION

In 1979, Mazets et al. (1979a, 1979b) reported the detection with the *Venera* satellites of a series of short, energetic events apparently originating from the same directions on the sky. Although their durations would place them in the short gamma-ray burst class, Mazets et al. (1979a) argued that the recurrent nature of the emission indicated that we were looking at a new phenomenon. In the following decade, these sources were indeed recognized as a different class of objects, called soft gamma repeaters (SGRs), based on their repeated high-energy burst activity (Golenetskii et al. 1984; Atteia et al. 1987; Laros et al. 1987; Kouveliotou et al. 1987). In the late 1990s, it was discovered that these objects were isolated neutron stars characterized by extremely strong dipole magnetic fields of $\sim 10^{14}–10^{15}$ G (Kouveliotou et al. 1998, 1999), right along the lines of their theoretical prediction by Duncan & Thompson (1992). Currently, the bulk of the magnetar population comprises two main classes of objects: SGRs and Anomalous X-ray Pulsars (AXPs). Their distinguishing traits are slow spin periods ($\sim 2–12$ s), large period derivatives ($\sim 10^{-13} – 10^{-10}$ s s^{-1}), and periods of activity during which they emit multiple bursts in the hard X-ray/soft γ-ray energy range. With respect to the latter burst characteristic, magnetars seem to fall into two groups: sources that emit a few hundreds to a thousand bursts

per active episode and sources emitting only a handful of bursts when active (e.g., Göğüş 2014). For detailed reviews of magnetars, see Woods & Thompson (2006) and Mereghetti (2008).

The magnetar discovery rate increased significantly when wide field-of-view monitors with location capabilities became operational, or when multiple instruments in space allowed for triangulation of their signals to be performed. The first wave of discoveries in the late 1980s was primarily enabled by the *Vela* and *Prognoz* satellites. This was followed by the synergistic era of the Burst And Transient Source Experiment (BATSE) on board the *Compton Gamma Ray Observatory* (*CGRO*), the *Rossi X-ray Timing Explorer* (*RXTE*), and *BeppoSaX* in the 1990s, and, finally, in the mid to late 2000s, the start of the era of NASA's *Swift* and *Fermi* observatories. The latter have on board detectors dedicated to monitoring the high-energy transient sky (the *Swift*/Burst Alert Telescope (BAT) and the *Fermi*/Gamma-ray Burst Monitor (GBM), respectively), and have been extremely efficient in complementing each other in detecting and identifying new magnetar sources.

Since its activation in 2008 July, GBM has recorded several hundreds of bursts from new and known magnetars, and a few magnetar-like bursts from unknown sources within rather large error box regions. A large number of papers has already been published by the GBM magnetar team on some of these sources

with multiple bursts (SGR J1550–5418: Kaneko et al. 2010; Lin et al. 2012; van der Horst et al. 2012; von Kienlin et al. 2012; Huppenkothen et al. 2014; Younes et al. 2014; SGR J0501+4516: Watts et al. 2010; Lin et al. 2011a; Huppenkothen et al. 2013; SGR J0418+5729: van der Horst et al. 2010). Here, we present a comprehensive overview of those magnetars, including bursts that have not been analyzed before, and also for magnetars with only a few events (SGR 1806–20, SGR J1822.3–1606, AXP 4U 0142+61, and AXP 1E 2259+586). We have compiled the entire GBM magnetar burst sample in a catalog for the first five years of the mission. In Section 2, we describe the GBM data types, selection criteria, and analysis methods. We discuss the properties of bursts from confirmed magnetar sources in Section 3. In Section 4, we discuss bursts for which we do not have confirmed source identifications. We conclude in Section 5 with a comparison across the source properties and a discussion of the characteristics of all magnetar bursts detected with GBM.

2. DATA ANALYSIS

GBM is an all-sky monitor with an 8 sr field of view consisting of 12 NaI detectors, covering an energy range from 8 keV to 1 MeV, and 2 BGO detectors, covering 0.2–40 MeV (Meegan et al. 2009). GBM has three data types, of which two (CTIME and CSPEC) are continuously recorded and one (time-tagged event data, or TTE) is recorded only after GBM had triggered on a burst or other selected time intervals during most of the catalog period. This configuration changed after 2012 November, and currently GBM is recording TTE data continuously. While CSPEC data have good spectral resolution (128 energy channels over the full energy range), its temporal resolution of 1.024 s is too long for the ~0.1 s long magnetar bursts. The temporal resolution of CTIME data (64 ms) is better suited in this respect, but the spectral resolution (8 energy channels) is not sufficient to perform detailed spectral analysis. TTE data have the highest temporal (2 μs) and energy (128 energy channels) resolution, and are therefore perfectly suited for magnetar burst analyses. The downside is that this data type is typically only available from ~30 s before a burst trigger to ~300 s afterwards, followed by another ~300 during which no new trigger can take place. For further details on GBM and its data products, see Meegan et al. (2009).

2.1. Data Selection

Given the spectral softness of magnetar bursts, which typically have no emission above 200 keV, we only use NaI data for our analyses. The 12 NaI detectors are oriented in such a way that GBM can monitor the entire sky, which implies that only a subset of the detectors can see one specific location on the sky at any given time. For every burst, we have used only detectors with an angle between the source direction and the detector normal of less than 60°, to ensure a large effective area for these events. We note that in previous studies of GBM bursts the viewing angle varies from 40° to 60°, but this does not have a significant effect on the temporal and spectral results. We have excluded detectors when a source was obstructed by parts of the spacecraft or the Large Area Telescope on board *Fermi*.

We have identified a total of 427 triggered bursts associated with magnetars between 2008 July and 2013 June, the

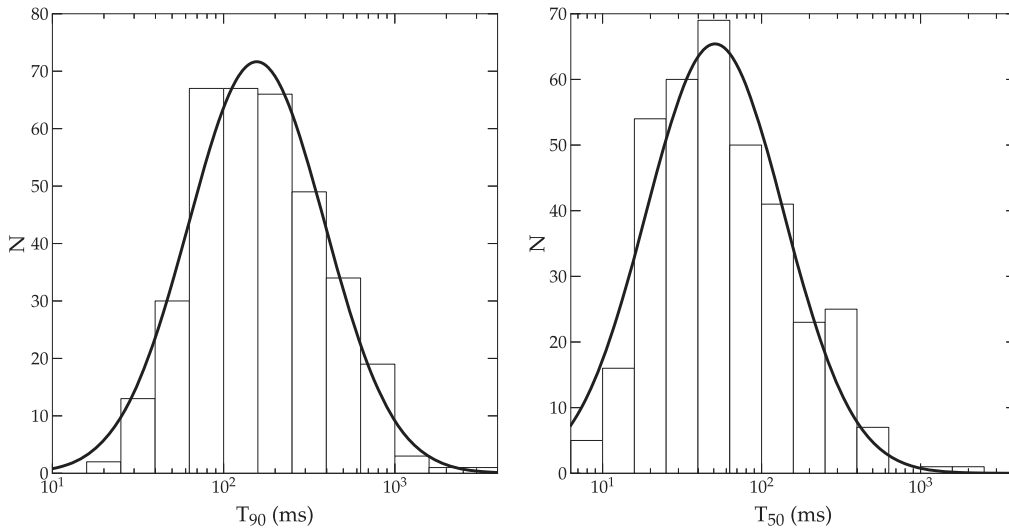**Table 1**
Summary of GBM Magnetar Bursts

Source	Burst Active Periods	Number of Bursts with TTE data
SGR J1550–5418	2008 Oct–2009 Apr	386
SGR J0501+4516	2008 Aug/Sep	29
1E 1841–045	2011 Feb–Jul	6
SGR J0418+5729	2009 Jun	2
SGR 1806–20	2010 Mar	1
SGR J1822.3–1606	2011 Jul	1
AXP 4U 0142+61	2011 Jul	1
AXP 1E 2259+586	2011 Aug	1
Unknown	…	19

associations of which have been established based on localization, detections by other instruments, or source bursting activity. We have also searched for, and included, all untriggered bursts that happened during the 30 s before and 300 s after each trigger, since TTE data were available at these times. Finally, we analyzed 19 magnetar-like bursts during this period, i.e., bursts with durations and spectra similar to those observed in magnetar bursts. Due to the poor positional accuracy of GBM (in particular for spectrally soft events), the crowded areas on the sky where they were found, and the lack of triggers by other gamma-ray instruments, it was not possible to confirm their nature. Several other untriggered bursts were found during the catalog time period, but are not included here since they lack TTE data. In Table 1, we show the magnetars included in this catalog, their burst active periods, and the total number of bursts per magnetar used in our analyses.

2.2. Temporal and Spectral Analysis

The majority of the bursts presented in this catalog have been published (van der Horst et al. 2010, 2012; Lin et al. 2011a, 2011b, 2012; von Kienlin et al. 2012; Younes et al. 2014). For the remaining bursts, we performed temporal and spectral analyses following the techniques and criteria as described in detail in these publications. The T_{90} and T_{50} durations, defined by the time that the cumulative counts rise from 5% to 95% and 25% to 75%, respectively (Kouveliotou et al. 1993), were calculated in photon space, i.e., by using the intrinsic (deconvolved) burst spectra instead of the detector recorded counts to define the durations (for a detailed description, see Lin et al. 2011a). Since many of the bursts consist of multiple peaks, two events qualify as two separate bursts if the time between their peaks is longer than a quarter of the magnetar spin period, and the count rate drops to the background level between the peaks. We excluded the brightest bursts that saturated the High Speed Science Data Bus of GBM from the duration calculations, and for these bursts we only used the non-saturated parts in our spectral analysis. The spectral analyses were performed with the software package *RMFIT*[18] (*v4.3*), using detector response matrices generated with *GBMRSP* (*v2.0*). To generate the response matrices, we used the best available positions from other satellites or telescopes for the magnetar bursts in Section 3, and the GBM positions for the bursts of unconfirmed origin in Section 4. We

---

[18] R.S. Mallozzi, R.D. Preece, & M.S. Briggs, "RMFIT, A Lightcurve and Spectral Analysis Tool" ©2008 Robert D. Preece, University of Alabama in Huntsville, 2008.

Figure 1. Distribution of T_{90} (left panel) and T_{50} (right panel) for all SGR J1550–5418 bursts. A log-normal fit (black line) to the histograms provides $\mu = 2.19 \pm 0.02$ log(ms) and $\sigma = 0.40 \pm 0.02$ log(ms) for T_{90}, and $\mu = 1.71 \pm 0.04$ log(ms) and $\sigma = 0.44 \pm 0.03$ log(ms) for T_{50}.

Table 2
Durations, Phases, Peak Fluxes, and Fluences for SGR J1550–5418 Bursts

Burst (yymmddfff)	T_{90} Start (UT)	T_{90} (ms)	T_{50} Start (UT)	T_{50} (ms)	Phase[c]	4ms Peak Flux[d,e] (erg s^{-1} cm^{-2})	Fluence[d,e] (erg s^{-1} cm^{-2})
081003377a[a]	09:02:46.112	160 ± 29	09:03:46.128	72 ± 11	...	...	4.10E-08 ± 5.00E-09
081003377b	09:03:05.956	276 ± 53	09:03:05.980	120 ± 25	...	...	1.34E-07 ± 9.00E-09
081003377c[a]	09:03:16.144	672 ± 72	09:03:16.176	320 ± 72	...	...	8.10E-08 ± 9.00E-09
081003377d[a]	09:03:33.172	68 ± 25	09:03:33.184	28 ± 11	...	...	6.50E-08 ± 6.00E-09
081003377e[a]	09:04:35.576	128 ± 23	09:04:35.592	56 ± 23	...	...	7.60E-08 ± 7.00E-09
081003377f[a]	09:04:55.520	424 ± 72	09:04:05.544	120 ± 18	...	...	1.31E-07 ± 1.00E-08
081003377 g[a]	09:05:03.504	64 ± 23	09:05:03.520	24 ± 18	...	...	4.50E-08 ± 1.00E-08
081003377 h[a]	09:05:03.904	104 ± 34	09:05:03.912	56 ± 11	...	...	3.60E-08 ± 6.00E-09
081003377i[a]	09:05:35.832	136 ± 18	09:05:35.848	64 ± 11	...	...	1.30E-08 ± 1.00E-09
081003377j[a]	...	...	...	...	...	...	2.30E-08 ± 4.00E-09
081003385a	09:03:05.876	108 ± 18	09:03:05.904	56 ± 34	0.5551	1.61E-06 ± 4.21E-07	5.40E-08 ± 6.00E-09
081003385b[a]	...	...	...	...	0.5163	4.69E-06 ± 7.39E-07	1.27E-07 ± 6.00E-09
081003446a	10:42:52.964	120 ± 14	10:42:52.980	60 ± 11	0.6058	3.63E-06 ± 6.41E-07	1.73E-07 ± 7.00E-09
081003779a	18:41:38.984	104 ± 9	18:41:38.992	60 ± 11	0.6635	5.25E-06 ± 5.27E-07	1.50E-07 ± 5.00E-09
081004050a	01:11:31.980	132 ± 28	01:11:31.988	56 ± 11	0.5523	3.74E-06 ± 5.48E-07	1.30E-07 ± 5.00E-09
081005020a	00:29:08.976	24 ± 16	00:29:08.980	12 ± 6	0.1377	4.21E-06 ± 7.36E-07	3.80E-08 ± 3.00E-09
081010537a	12:53:37.940	60 ± 18	12:53:37.972	24 ± 9	0.6426	2.30E-06 ± 5.30E-07	5.00E-08 ± 3.00E-09
090122037a	00:53:59.329	44^{+31}_{-6}	00:53:59.339	22^{+6}_{-4}	0.4915	2.40E-06 ± 3.98E-07	3.74E-08 ± 3.52E-09
090122037b[a]	00:54:28.769	86^{+37}_{-30}	00:54:28.783	34^{+4}_{-4}	0.7016	4.53E-06 ± 5.86E-07	1.01E-07 ± 6.24E-09
090122037c[a]	00:54:56.702	236^{+29}_{-34}	00:54:56.720	170^{+18}_{-16}	0.1757	8.88E-07 ± 2.89E-07	6.96E-09 ± 1.32E-09
090122037d[a]	00:55:01.268	50^{+17}_{-10}	00:55:01.278	18^{+4}_{-2}	0.3842	9.50E-06 ± 8.26E-07	2.15E-07 ± 7.68E-09
090122037e[a]	00:55:28.102	270^{+8}_{-6}	00:55:28.104	44^{+48}_{-36}	0.3308	2.73E-06 ± 5.18E-07	2.74E-08 ± 3.36E-09
090122037f[a]	00:55:32.314	98^{+24}_{-44}	00:55:32.346	30^{+8}_{-10}	0.3820	1.86E-06 ± 4.16E-07	2.04E-08 ± 2.52E-09
090122037 g[a]	00:55:51.884	118^{+28}_{-20}	00:55:51.924	40^{+4}_{-6}	0.8411	9.97E-06 ± 8.51E-07	3.06E-07 ± 1.06E-08
090122037 h[a]	00:55:54.710	132^{+34}_{-12}	00:55:54.724	52^{+40}_{-8}	0.1789	2.21E-06 ± 5.02E-07	8.96E-09 ± 1.28E-09
090122037i[a]	00:56:02.260	200^{+88}_{-44}	00:56:02.314	76^{+10}_{-14}	0.8595	2.24E-06 ± 4.50E-07	5.82E-08 ± 6.00E-09
090122037j[a]	00:56:08.371	238^{+34}_{-42}	00:56:08.401	146^{+8}_{-18}	0.7779	1.76E-06 ± 4.58E-07	3.01E-08 ± 4.16E-09
090122037k[a]	00:56:14.635	215^{+38}_{-24}	00:56:14.701	132^{+28}_{-12}	0.1057	1.53E-06 ± 4.23E-07	3.44E-08 ± 4.40E-09
090122037 l[a]	00:56:15.263	242^{+31}_{-40}	00:56:15.295	150^{+6}_{-6}	0.1776	2.36E-06 ± 4.93E-07	2.41E-08 ± 3.64E-09
090122037 m[a]	00:56:16.485	764^{+193}_{-36}	00:56:16.523	508^{+34}_{-22}	0.6873	2.50E-06 ± 5.24E-07	3.82E-08 ± 4.68E-09
090122037n[a]	00:56:16.485	764^{+154}_{-36}	00:56:16.523	508^{+30}_{-22}	0.9310	3.96E-06 ± 5.76E-07	2.83E-08 ± 3.48E-09
090122037o[a]	00:56:18.877	90^{+9}_{-20}	00:56:18.933	10^{+2}_{-2}	0.8649	2.32E-05 ± 1.25E-06	2.77E-07 ± 9.88E-09
090122037p[a]	00:56:19.383	206^{+25}_{-12}	00:56:19.417	150^{+14}_{-44}	0.1723	2.32E- 06 ± 5.13E-07	2.82E-08 ± 4.40E-09
090122037q[a]	00:56:24.875	618^{+28}_{-14}	00:56:25.159	250^{+36}_{-48}	0.9445	1.99E-06 ± 4.60E-07	5.37E-08 ± 6.12E-09
090122037r[a]	00:56:27.889	124^{+26}_{-12}	00:56:27.927	60^{+12}_{-8}	0.2052	2.96E-06 ± 5.28E-07	2.95E-08 ± 1.92E-09
090122037 s[a]	00:56:29.235	760^{+18}_{-198}	00:56:29.269	348^{+100}_{-12}	0.0107	4.52E-06 ± 6.11E-07	1.29E-07 ± 1.18E-08
090122037t[a]	00:56:34.528	124^{+21}_{-34}	00:56:34.610	14^{+24}_{-4}	0.4325	4.34E-06 ± 6.01E-07	2.20E-08 ± 2.28E-09
090122037u[a]	00:56:35.317	254^{+59}_{-38}	00:56:35.453	56^{+10}_{-6}	0.8413	9.29E-06 ± 7.91E-07	5.80E-07 ± 1.44E-08

Table 2
(Continued)

Burst (yymmddfff)	T_{90} Start (UT)	T_{90} (ms)	T_{50} Start (UT)	T_{50} (ms)	Phase[c]	4ms Peak Flux[d,e] (erg s^{-1} cm^{-2})	Fluence[d,e] (erg s^{-1} cm^{-2})
090122037v[a,f]	00:56:43.957	164^{+12}_{-24}	00:56:43.963	16^{+6}_{-2}	0.9432	2.40E-05 ± 1.25E-06	1.87E-07 ± 7.00E-09
090122037w[a]	00:56:49.195	160^{+54}_{-32}	00:56:49.221	60^{+6}_{-10}	0.4847	2.34E-06 ± 4.56E-07	3.58E-08 ± 3.08E-09
090122037x[a]	00:56:52.843	104^{+11}_{-14}	00:56:52.859	60^{+8}_{-10}	0.2632	2.90E-06 ± 5.17E-07	7.75E-08 ± 6.76E-09
090122037y[a]	00:56:59.728	432^{+34}_{-56}	00:56:59.802	194^{+50}_{-40}	0.5938	1.45E-06 ± 4.18E-07	2.26E-08 ± 3.36E-09
090122037z[a,f]	00:57:07.432	52^{+13}_{-16}	00:57:07.446	16^{+2}_{-2}	0.2768	1.97E-05 ± 1.21E-06	3.45E-07 ± 1.10E-08
090122037aa[a]	00:57:09.932	766^{+74}_{-14}	00:57:10.082	326^{+50}_{-12}	0.5567	2.89E-06 ± 4.64E-07	1.43E-07 ± 1.02E-08
090122037ab[a]	00:57:13.814	23^{+5}_{-9}	00:57:13.818	8^{+4}_{-2}	0.3540	2.89E-06 ± 5.43E-07	2.58E-08 ± 3.00E-09
090122037ac[a,f]	00:57:20.410	488^{+8}_{-10}	00:57:20.434	412^{+4}_{-6}	0.5404	9.95E-06 ± 8.17E-07	1.14E-06 ± 2.03E-08
090122037ad[a]	00:57:23.967	268^{+72}_{-28}	00:57:23.991	66^{+20}_{-26}	0.2629	1.49E-06 ± 4.05E-07	2.07E-08 ± 3.08E-09
090122037ae[a]	00:57:29.196	112^{+31}_{-20}	00:57:29.210	68^{+8}_{-10}	0.7788	2.09E-06 ± 4.22E-07	9.05E-08 ± 8.12E-09
090122037af[a]	00:57:34.514	628^{+32}_{-8}	00:57:34.544	500^{+30}_{-16}	0.3430	2.42E-06 ± 5.34E-07	1.55E-07 ± 1.29E-08
090122037ag[a]	00:57:43.534	180^{+35}_{-26}	00:57:43.560	86^{+34}_{-42}	0.6954	1.76E-06 ± 5.95E-07	2.34E-08 ± 3.96E-09
090122037ah[a]	00:57:45.890	122^{+26}_{-30}	00:57:45.926	48^{+16}_{-14}	0.8624	3.42E-06 ± 7.04E-07	5.71E-08 ± 5.60E-09
090122037ai[a]	00:57:49.748	362^{+86}_{-100}	00:57:49.802	64^{+30}_{-18}	0.7205	4.18E-06 ± 7.31E-07	6.66E-08 ± 4.32E-09
090122037aj[a]	00:58:00.842	398^{+20}_{-8}	00:58:00.856	296^{+44}_{-156}	0.0531	2.86E-05 ± 1.63E-06	8.82E-07 ± 2.12E-08
090122037ak[a]	00:58:12.995	418^{+116}_{-24}	00:58:13.131	234^{+28}_{-22}	0.0831	2.37E-06 ± 4.49E-07	3.21E-07 ± 1.65E-08
090122037al[a,f]	00:58:19.203	36^{+6}_{-6}	00:58:19.209	12^{+2}_{-2}	0.9137	4.78E-05 ± 1.83E-06	6.78E-07 ± 1.40E-08
090122037am[a]	00:58:45.123	82^{+36}_{-20}	00:58:45.131	24^{+14}_{-2}	0.4254	4.98E-06 ± 6.87E-07	1.31E-07 ± 7.56E-09
090122044a[a]	01:03:26.023	414^{+256}_{-18}	01:03:26.043	182^{+98}_{-20}	0.9897	6.11E-06 ± 7.37E-07	2.85E-07 ± 1.28E-08
090122044b	01:03:53.890	236^{+16}_{-26}	01:03:53.984	20^{+6}_{-2}	0.4849	1.88E-05 ± 1.13E-06	2.90E-07 ± 9.80E-09
090122044c[a]	01:04:02.592	216^{+56}_{-24}	01:04:02.610	106^{+8}_{-8}	0.6466	6.32E-06 ± 6.85E-07	2.43E-07 ± 1.03E-08
090122044d[a]	01:04:25.358	270^{+18}_{-10}	01:04:25.388	154^{+16}_{-14}	0.6365	4.45E-06 ± 6.20E-07	3.61E-07 ± 1.40E-08
090122044e[a]	01:04:46.471	94^{+51}_{-22}	01:04:46.491	32^{+10}_{-8}	0.8368	2.10E-06 ± 4.65E-07	5.54E-08 ± 5.28E-09
090122044f[a]	01:05:04.829	34^{+15}_{-8}	01:05:04.837	16^{+6}_{-6}	0.6853	2.64E-06 ± 5.03E-07	5.54E-08 ± 5.76E-09
090122044 g[a]	01:05:38.031	332^{+38}_{-48}	01:05:38.211	44^{+10}_{-8}	0.7919	1.46E-05 ± 1.03E-06	5.87E-07 ± 1.66E-08
090122044 h[a]	01:06:33.363	94^{+31}_{-8}	01:06:33.391	30^{+6}_{-12}	0.4193	6.08E-06 ± 7.23E-07	6.91E-08 ± 4.32E-09
090122044i[a]	01:07:08.826	138^{+39}_{-18}	01:07:08.862	42^{+6}_{-4}	0.5472	7.47E-06 ± 7.91E-07	3.54E-07 ± 1.15E-08
090122044j[a]	01:07:36.377	42^{+6}_{-8}	01:07:36.383	22^{+6}_{-6}	0.8184	2.34E-06 ± 4.87E-07	2.55E-08 ± 3.64E-09
090122044k[a]	01:08:21.148	122^{+26}_{-12}	01:08:21.156	36^{+4}_{-6}	0.4293	9.69E-06 ± 8.27E-07	2.21E-07 ± 8.32E-09
090122044 l[a]	01:08:39.566	38^{+4}_{-8}	01:08:39.570	12^{+12}_{-2}	0.3154	5.06E-06 ± 5.79E-07	6.16E-08 ± 4.32E-09
090122044 m[a,f]	01:08:41.706	270^{+4}_{-4}	01:08:41.752	186^{+8}_{-4}	0.4539	5.85E-05 ± 2.18E-06	2.13E-06 ± 2.63E-08
090122044n[a]	01:08:42.467	66^{+23}_{-14}	01:08:42.489	20^{+16}_{-10}	0.7295	3.72E-06 ± 5.50E-07	6.84E-08 ± 6.08E-09
090122052a[a]	01:13:50.350	98^{+23}_{-16}	01:13:50.358	46^{+22}_{-14}	0.3067	5.08E-06 ± 6.87E-07	1.48E-07 ± 9.60E-09
090122052b	01:14:14.878	90^{+6}_{-6}	01:14:14.894	32^{+6}_{-2}	0.1546	1.48E-05 ± 1.02E-06	5.59E-07 ± 1.34E-08
090122052c[a]	01:14:29.480	50^{+7}_{-4}	01:14:29.484	42^{+2}_{-4}	0.2105	3.95E-06 ± 6.49E-07	7.54E-08 ± 5.72E-09
090122052d[a]	01:14:37.113	140^{+42}_{-58}	01:14:37.135	40^{+16}_{-18}	0.8915	2.10E-06 ± 4.75E-07	4.93E-08 ± 5.04E-09
090122052e[a,f]	01:14:45.985	118^{+12}_{-12}	01:14:46.029	32^{+2}_{-2}	0.1767	5.85E-05 ± 2.14E-06	2.26E-06 ± 2.55E-08
090122052f[a]	01:14:55.393	360^{+93}_{-76}	01:14:55.471	156^{+34}_{-44}	0.7761	1.46E-06 ± 4.20E-07	5.02E-08 ± 5.32E-09
090122052 g[a]	01:14:58.769	102^{+10}_{-16}	01:14:58.781	58^{+8}_{-14}	0.3436	1.91E-06 ± 4.30E-07	5.38E-08 ± 5.88E-09
090122052 h[a]	01:15:09.296	80^{+20}_{-18}	01:15:09.302	24^{+2}_{-2}	0.4068	1.31E-05 ± 9.77E-07	2.93E-07 ± 9.60E-09
090122052i[a]	01:15:19.897	636^{+34}_{-46}	01:15:20.249	154^{+234}_{-34}	0.7070	3.74E-06 ± 5.75E-07	2.08E-08 ± 2.64E-09
090122052j[a]	01:15:46.002	170^{+50}_{-48}	01:15:46.064	50^{+48}_{-20}	0.1745	9.79E-07 ± 3.77E-07	3.20E-08 ± 4.48E-09
090122052k[a]	01:15:46.616	434^{+40}_{-8}	01:15:46.638	184^{+44}_{-20}	0.4211	7.14E-06 ± 7.57E-07	6.22E-07 ± 1.86E-08
090122052 l[a]	01:16:06.549	268^{+118}_{-26}	01:16:06.583	124^{+22}_{-22}	0.0422	1.37E-06 ± 4.05E-07	9.58E-08 ± 8.40E-09
090122052 m[a]	01:16:08.876	84^{+24}_{-12}	01:16:08.896	40^{+6}_{-8}	0.1802	2.59E-06 ± 5.28E-07	1.22E-07 ± 7.68E-09
090122052n[a]	01:16:19.058	96^{+28}_{-16}	01:16:19.070	42^{+4}_{-4}	0.0798	9.66E-06 ± 8.27E-07	2.32E-07 ± 8.80E-09
090122052o[a]	01:16:25.974	150^{+31}_{-10}	01:16:25.986	36^{+2}_{-4}	0.4190	9.69E-06 ± 8.78E-07	2.31E-07 ± 9.52E-09
090122052p[a]	01:16:26.562	326^{+108}_{-84}	01:16:26.778	36^{+12}_{-6}	0.8129	3.82E-06 ± 5.57E-07	8.88E-08 ± 6.00E-09
090122052q[a,f]	01:16:28.686	84^{+12}_{-8}	01:16:28.704	26^{+2}_{-4}	0.7347	2.67E-05 ± 1.34E-06	8.12E-07 ± 1.51E-08
090122052r[a]	01:16:40.959	1068^{+42}_{-18}	01:16:41.061	374^{+214}_{-134}	0.6429	2.17E-06 ± 4.90E-07	3.72E-08 ± 4.40E-09
090122052 s[a]	01:17:00.894	26^{+8}_{-8}	01:17:00.900	12^{+6}_{-6}	0.2693	1.95E-06 ± 4.55E-07	2.95E-08 ± 4.32E-09
090122052t[a]	01:17:03.119	86^{+18}_{-34}	01:17:03.131	36^{+8}_{-14}	0.3484	9.62E-07 ± 3.29E-07	3.10E-08 ± 3.96E-09
090122052u[a]	01:17:20.673	244^{+60}_{-26}	01:17:20.723	132^{+8}_{-10}	0.8450	5.98E-06 ± 6.28E-07	4.35E-07 ± 1.36E-08
090122052v[a]	01:17:24.737	222^{+68}_{-30}	01:17:24.833	64^{+6}_{-8}	0.8478	4.96E-06 ± 6.10E-07	3.47E-07 ± 1.25E-08
090122052w[a]	01:17:27.976	34^{+13}_{-8}	01:17:27.988	14^{+6}_{-8}	0.3449	3.60E-06 ± 5.08E-07	3.67E-08 ± 4.20E-09
090122052x[a]	01:17:52.194	36^{+22}_{-16}	01:17:52.200	12^{+4}_{-4}	0.0263	3.82E-06 ± 5.68E- 07	5.00E-08 ± 4.80E-09
090122052y[a]	01:17:58.610	128^{+32}_{-34}	01:17:58.628	54^{+16}_{-18}	0.1310	2.51E-06 ± 4.82E-07	4.03E-08 ± 4.32E-09
090122052z[a]	01:18:02.266	78^{+12}_{-26}	01:18:02.276	34^{+18}_{-12}	0.8853	8.84E-07 ± 3.37E-07	3.48E-08 ± 4.80E-09
090122052aa[a,f]	01:18:10.302	84^{+18}_{-18}	01:18:10.330	14^{+2}_{-2}	0.7776	5.72E-05 ± 2.02E-06	9.53E-07 ± 1.68E-08

Table 2
(Continued)

Burst (yymmddfff)	T_{90} Start (UT)	T_{90} (ms)	T_{50} Start (UT)	T_{50} (ms)	Phase[c]	4ms Peak Flux[d,e] (erg s^{-1} cm^{-2})	Fluence[d,e] (erg s^{-1} cm^{-2})
090122052ab[a]	01:18:12.699	48^{+23}_{-10}	01:18:12.709	24^{+14}_{-6}	0.9330	1.35E-06 ± 3.76E-07	3.86E-08 ± 5.04E-09
090122052ac[a,b,f]	01:18:42.351	140^{+10}_{-18}	01:18:42.415	62^{+4}_{-2}			
090122059a	01:25:04.198	586^{+132}_{-74}	01:25:04.320	264^{+44}_{-24}	0.5830	2.23E-06 ± 5.27E-07	3.35E-07 ± 1.42E-08
090122059b[a,f]	01:25:18.640	214^{+12}_{-8}	01:25:18.802	32^{+4}_{-2}	0.5766	4.05E-05 ± 1.77E-06	1.31E-06 ± 2.02E-08
090122059c[a]	01:27:10.561	334^{+56}_{-50}	01:27:10.629	156^{+10}_{-14}	0.5380	1.56E-05 ± 1.13E-06	4.53E-07 ± 1.34E-08
090122059d[a]	01:28:00.599	236^{+70}_{-68}	01:28:00.645	116^{+16}_{-18}	0.7211	2.84E-06 ± 4.69E-07	3.24E-08 ± 3.60E-09
090122059e[a,b,f]	01:28:59.988	146^{+8}_{-8}	01:28:60.002	38^{+2}_{-2}			
090122104a[f]	02:30:09.381	112^{+20}_{-22}	02:30:09.387	42^{+2}_{-4}	0.2844	1.59E-05 ± 1.10E-06	4.00E-07 ± 1.20E-08
090122104b[a,f]	02:32:53.944	132^{+22}_{-40}	02:32:53.956	18^{+2}_{-2}	0.7134	5.97E-05 ± 2.10E-06	9.98E-07 ± 1.52E-08
090122104c[a]	02:34:28.222	356^{+12}_{-6}	02:34:28.236	320^{+4}_{-16}	0.3701	1.74E-05 ± 1.17E-06	6.27E-07 ± 1.90E-08
090122104d[a]	02:34:28.919	184^{+33}_{-18}	02:34:28.955	114^{+16}_{-10}	0.6144	2.10E-06 ± 4.72E-07	1.11E-07 ± 9.40E-09
090122104e[a]	02:34:40.367	94^{+35}_{-20}	02:34:40.377	42^{+10}_{-8}	0.0743	4.00E-06 ± 5.36E-07	2.87E-08 ± 2.80E-09
090122113a	02:42:23.166	86^{+22}_{-32}	02:42:23.168	24^{+4}_{-4}	0.4295	1.66E-05 ± 1.18E-06	1.69E-07 ± 7.48E-09
090122113b[a]	02:44:50.477	62^{+16}_{-10}	02:44:50.481	28^{+2}_{-6}	0.5258	9.53E-06 ± 7.94E-07	1.93E-07 ± 8.32E-09
090122113c[a]	02:45:53.104	138^{+10}_{-2}	02:45:53.106	14^{+2}_{-2}	0.7511	2.88E-05 ± 1.40E-06	3.07E-07 ± 1.01E-08
090122120a	02:53:29.738	152^{+52}_{-20}	02:53:29.784	60^{+14}_{-10}	0.1761	8.89E-06 ± 7.83E-07	2.94E-07 ± 1.01E-08
090122120b[a]	02:53:45.839	958^{+132}_{-54}	02:53:46.079	354^{+164}_{-26}	0.1485	1.37E-06 ± 3.29E-07	8.64E-08 ± 9.60E-09
090122120c[a,b,f]	02:54:00.999	146^{+4}_{-2}	02:54:01.033	80^{+4}_{-2}			
090122120d[a]	02:55:15.998	306^{+104}_{-28}	02:55:16.030	138^{+64}_{-28}	0.4149	1.82E-06 ± 4.42E-07	7.81E- 08 ± 8.68E-09
090122120e[a]	02:56:52.656	268^{+13}_{-20}	02:56:52.662	210^{+8}_{-8}	0.0645	4.28E-06 ± 5.86E-07	1.09E-07 ± 7.80E-09
090122120f[a]	02:56:53.706	258^{+44}_{-40}	02:56:53.758	106^{+32}_{-16}	0.6036	1.62E-06 ± 4.95E-07	5.37E-08 ± 7.04E-09
090122120 g[a]	02:57:04.694	96^{+55}_{-18}	02:57:04.720	40^{+26}_{-6}	0.8874	1.57E-06 ± 4.43E-07	2.74E-08 ± 1.27E-08
090122120 h[a]	02:57:18.399	58^{+27}_{-16}	02:57:18.405	24^{+4}_{-4}	0.4886	3.15E-06 ± 5.96E-07	6.23E-08 ± 6.46E-09
090122173a	04:08:31.632	224^{+54}_{-48}	04:08:31.642	68^{+18}_{-12}	0.8906	7.43E-06 ± 7.88E-07	1.76E-07 ± 8.80E-09
090122173b[a,f]	04:09:08.677	542^{+136}_{-16}	04:09:09.021	74^{+6}_{-8}	0.9511	1.77E-05 ± 1.12E-06	1.07E-06 ± 2.17E-08
090122173c[a]	04:10:50.863	56^{+5}_{-6}	04:10:50.877	32^{+8}_{-2}	0.1015	4.52E-06 ± 6.55E-07	1.30E-07 ± 8.32E-09
090122173d[a]	04:10:59.176	194^{+63}_{-32}	04:10:59.210	102^{+14}_{-8}	0.1083	1.78E-06 ± 4.54E-07	1.31E-07 ± 1.01E-08
090122173e[a,f]	04:12:33.001	694^{+20}_{-56}	04:12:33.107	282^{+8}_{-18}	0.4628	1.64E-05 ± 1.07E-06	1.28E-06 ± 2.17E-08
090122173f[a]	04:13:03.261	100^{+22}_{-24}	04:13:03.305	20^{+6}_{-2}	0.0063	1.44E-05 ± 1.03E-06	3.27E-07 ± 1.01E-08
090122173 g[a]	04:13:22.542	97^{+2}_{-25}	04:13:22.550	22^{+2}_{-4}	0.2964	8.35E-06 ± 7.47E-07	1.42E-07 ± 5.72E-09
090122173 h[a]	04:13:25.401	64^{+25}_{-10}	04:13:25.417	32^{+6}_{-4}	0.6748	2.23E-06 ± 4.55E-07	1.02E-07 ± 8.96E-09
090122180a	04:19:27.598	140^{+24}_{-20}	04:19:27.620	66^{+2}_{-4}	0.4837	9.25E-06 ± 8.30E-07	2.93E-07 ± 1.01E-08
090122180b[a]	04:21:32.321	212^{+6}_{-16}	04:21:32.331	158^{+2}_{-2}	0.7431	2.51E-05 ± 1.31E-06	5.33E-07 ± 1.34E-08
090122180c[a]	04:21:41.874	107^{+5}_{-29}	04:21:41.900	36^{+12}_{-6}	0.2890	4.82E-06 ± 6.02E-07	5.87E-08 ± 6.84E-09
090122180d[a]	04:21:49.444	196^{+21}_{-16}	04:21:49.550	46^{+12}_{-10}	0.9892	3.69E-06 ± 5.77E-07	1.28E-07 ± 7.68E-09
090122180e[a]	04:22:52.287	288^{+22}_{-20}	04:22:52.383	92^{+12}_{-8}	0.3385	6.38E-06 ± 7.09E-07	2.68E-07 ± 1.09E-08
090122180f[a]	04:22:55.927	124^{+19}_{-24}	04:22:55.937	58^{+22}_{-12}	0.0175	1.94E-06 ± 4.54E-07	4.27E-08 ± 4.80E-09
090122180 g[a]	04:23:01.356	110^{+42}_{-30}	04:23:01.368	44^{+4}_{-6}	0.6358	7.29E-06 ± 7.69E-07	2.38E-07 ± 8.64E-09
090122180 h[a]	04:23:35.963	44^{+13}_{-8}	04:23:35.969	20^{+8}_{-4}	0.3412	3.81E-06 ± 5.77E-07	9.63E-08 ± 6.72E-09
090122180i[a]	04:23:56.636	26^{+5}_{-10}	04:23:56.638	10^{+4}_{-2}	0.3151	5.22E-06 ± 6.09E-07	7.78E-08 ± 5.76E-09
090122180j[a]	04:23:59.060	210^{+23}_{-14}	04:23:59.088	98^{+24}_{-18}	0.5048	2.31E-06 ± 5.09E-07	9.04E-08 ± 6.84E-09
090122187a	04:29:27.683	510^{+10}_{-60}	04:29:27.727	194^{+14}_{-12}	0.1847	5.60E-06 ± 6.69E-07	8.13E-08 ± 3.04E-09
090122187b[a]	04:29:51.982	86^{+14}_{-20}	04:29:52.010	36^{+10}_{-16}	0.8410	5.36E-06 ± 7.12E-07	1.15E-07 ± 7.20E-09
090122187c[a]	04:30:14.771	123^{+39}_{-33}	04:30:14.798	28^{+30}_{-6}	0.8307	1.49E-06 ± 4.26E-07	2.18E-08 ± 3.36E-09
090122187d[a,f]	04:30:32.732	216^{+76}_{-14}	04:30:32.750	58^{+2}_{-4}	0.4812	2.56E-05 ± 1.28E-06	1.10E-06 ± 1.87E-08
090122187e[a]	04:31:25.479	330^{+40}_{-90}	04:31:25.563	120^{+28}_{-14}	0.0176	1.42E-06 ± 4.32E-07	3.20E-08 ± 4.76E-09
090122187f[a]	04:32:04.697	524^{+26}_{-12}	04:32:04.711	490^{+4}_{-4}	0.1033	5.73E-06 ± 6.98E-07	1.99E-07 ± 1.57E-08
090122187 g[a]	04:32:10.126	180^{+100}_{-70}	04:32:10.170	30^{+22}_{-10}	0.5087	5.47E-06 ± 6.68E-07	1.07E-07 ± 6.80E-09
090122187 h[a]	04:32:16.354	88^{+60}_{-32}	04:32:16.370	20^{+12}_{-4}	0.4995	4.72E-06 ± 5.58E-07	1.08E-07 ± 6.44E-09
090122187i[a]	04:32:19.025	758^{+16}_{-18}	04:32:19.379	224^{+18}_{-20}	0.9503	9.93E-06 ± 9.18E-07	6.47E-07 ± 1.76E-08
090122187j[a]	04:32:23.897	196^{+39}_{-22}	04:32:23.919	120^{+36}_{-42}	0.1385	3.26E-06 ± 5.59E-07	9.59E-08 ± 9.40E-09
090122187k[a,b,f]	04:32:49.462	526^{+10}_{-12}	04:32:49.516	404^{+4}_{-2}			
090122187l[a]	04:33:02.521	156^{+68}_{-30}	04:33:02.531	44^{+14}_{-8}	0.2898	8.09E-06 ± 8.44E-07	2.71E-07 ± 1.15E-08
090122187m[a]	04:33:18.500	518^{+30}_{-22}	04:33:18.748	240^{+144}_{-142}	0.2318	9.69E-06 ± 8.80E-07	2.50E-07 ± 1.63E-08
090122187n[a,f]	04:33:28.047	74^{+14}_{-12}	04:33:28.053	18^{+2}_{-4}	0.0928	6.36E-05 ± 2.25E-06	7.28E-07 ± 1.40E-08
090122187o[a]	04:33:29.161	86^{+27}_{-16}	04:33:29.211	22^{+6}_{-6}	0.6579	4.70E-06 ± 6.59E-07	1.12E-07 ± 6.80E-09
090122187p[a]	04:33:35.771	360^{+34}_{-20}	04:33:35.801	314^{+4}_{-8}	0.9837	5.98E-06 ± 7.04E-07	2.66E-07 ± 1.52E-08
090122187q[a]	04:33:50.310	648^{+322}_{-174}	04:33:50.332	256^{+20}_{-20}	0.8388	3.10E-06 ± 5.68E-07	1.52E-07 ± 9.40E-09
090122187r[a,b,f]	04:34:09.362	396^{+74}_{-56}	04:34:09.474	84^{+2}_{-2}			

Table 2
(Continued)

Burst (yymmddffff)	T_{90} Start (UT)	T_{90} (ms)	T_{50} Start (UT)	T_{50} (ms)	Phase[c]	4ms Peak Flux[d,e] (erg s^{-1} cm^{-2})	Fluence[d,e] (erg s^{-1} cm^{-2})
090122187s[a]	04:34:12.448	100^{+21}_{-24}	04:34:12.460	28^{+2}_{-6}	0.5245	4.65E-06 ± 6.70E-07	1.30E-07 ± 7.92E-09
090122187t[a,f]	04:34:18.108	338^{+32}_{-78}	04:34:18.116	40^{+4}_{-2}	0.2523	3.21E-05 ± 1.56E-06	8.76E-07 ± 1.66E-08
090122187u[a,f]	04:34:20.687	802^{+88}_{-48}	04:34:20.929	286^{+8}_{-6}	0.7339	1.75E-05 ± 1.10E-06	1.28E-06 ± 2.77E-08
090122194a[a]	04:39:21.048	76^{+12}_{-32}	04:39:21.058	28^{+12}_{-12}	0.4608	1.66E-06 ± 4.61E-07	1.52E-08 ± 2.60E-09
090122194b[a]	04:39:23.670	258^{+39}_{-14}	04:39:23.702	92^{+36}_{-14}	0.7219	2.93E-06 ± 4.56E-07	1.81E-07 ± 1.06E-08
090122194c	04:39:29.942	134^{+13}_{-22}	04:39:29.950	66^{+6}_{-6}	0.7489	7.89E-06 ± 7.72E-07	2.49E-07 ± 9.28E-09
090122194d[a]	04:39:36.640	196^{+36}_{-36}	04:39:36.674	80^{+16}_{-10}	0.0196	3.99E-06 ± 5.68E-07	1.74E-07 ± 8.64E-09
090122194e[a]	04:39:37.361	26^{+7}_{-6}	04:39:37.363	18^{+2}_{-8}	0.3299	9.72E-07 ± 3.62E-07	7.52E-08 ± 1.04E-08
090122194f[a]	04:40:00.058	200^{+8}_{-22}	04:40:00.090	132^{+26}_{-16}	0.3607	8.42E-07 ± 3.87E-07	1.98E-08 ± 3.60E-09
090122194g[a,f]	04:40:04.826	114^{+26}_{-14}	04:40:04.858	38^{+4}_{-8}	0.6039	9.90E-06 ± 7.56E-07	2.57E-07 ± 1.06E-08
090122194h[a]	04:40:05.309	98^{+28}_{-14}	04:40:05.341	48^{+22}_{-20}	0.8529	2.16E-06 ± 4.71E-07	4.97E-08 ± 6.44E-09
090122194i[a]	04:40:06.444	74^{+8}_{-12}	04:40:06.456	26^{+4}_{-2}	0.3747	2.94E-05 ± 1.40E-06	7.74E-07 ± 1.46E-08
090122194j[a]	04:40:09.458	112^{+75}_{-32}	04:40:09.484	32^{+14}_{-8}	0.8356	2.07E-06 ± 5.20E-07	3.28E-08 ± 4.16E-09
090122194k[a]	04:40:10.879	866^{+34}_{-10}	04:40:10.937	394^{+60}_{-46}	0.7028	4.62E-06 ± 6.36E-07	3.76E-07 ± 1.79E-08
090122194l[a]	04:40:22.359	626^{+68}_{-46}	04:40:22.425	338^{+18}_{-12}	0.2148	3.88E-06 ± 5.60E-07	1.40E-07 ± 1.27E-08
090122194m[a]	04:40:26.392	172^{+17}_{-30}	04:40:26.412	72^{+18}_{-20}	0.0005	1.55E-06 ± 4.30E-07	7.30E-08 ± 7.68E-09
090122194n[a]	04:40:27.098	90^{+16}_{-12}	04:40:27.130	16^{+2}_{-2}	0.3480	2.94E-05 ± 1.40E-06	5.13E-07 ± 1.24E-08
090122194o[a]	04:40:28.113	74^{+6}_{-20}	04:40:28.119	28^{+8}_{-6}	0.8345	3.08E-06 ± 5.32E-07	4.32E-08 ± 3.96E-09
090122194p[a]	04:40:28.785	364^{+40}_{-34}	04:40:28.849	192^{+4}_{-6}	0.2679	1.47E-05 ± 1.03E-06	5.71E-07 ± 1.39E-08
090122194q[a]	04:40:33.302	86^{+10}_{-26}	04:40:33.314	32^{+22}_{-10}	0.3321	2.29E-06 ± 4.53E-07	3.12E-08 ± 4.68E-09
090122194r[a]	04:40:54.367	146^{+69}_{-42}	04:40:54.421	26^{+4}_{-4}	0.5250	9.05E-06 ± 7.48E-07	2.59E-07 ± 8.64E-09
090122194s[a]	04:40:55.143	118^{+24}_{-24}	04:40:55.155	28^{+6}_{-6}	0.8735	4.91E-06 ± 5.66E-07	1.00E-07 ± 6.12E-09
090122194t[a]	04:41:01.233	102^{+31}_{-20}	04:41:01.255	50^{+20}_{-10}	0.8054	1.24E-06 ± 4.23E-07	5.92E-08 ± 6.96E-09
090122218a[a]	05:13:37.806	220^{+54}_{-34}	05:13:37.842	94^{+18}_{-36}	0.1102	9.45E-07 ± 3.30E-07	3.12E-08 ± 3.60E-09
090122218b	05:13:40.810	328^{+104}_{-78}	05:13:40.920	120^{+18}_{-22}	0.6541	1.74E-06 ± 3.68E-07	1.38E-07 ± 9.84E-09
090122218c[a]	05:13:46.180	380^{+83}_{-50}	05:13:46.202	134^{+26}_{-32}	0.1547	2.67E-06 ± 4.62E-07	1.35E-07 ± 9.12E-09
090122218d[a]	05:13:49.705	454^{+44}_{-44}	05:13:49.735	310^{+26}_{-36}	0.8627	1.95E-06 ± 4.84E-07	6.84E-08 ± 6.08E-09
090122218e[a,b,f]	05:14:03.372	618^{+2}_{-4}	05:14:03.73	190^{+4}_{-2}			
090122218f[a,f]	05:14:29.229	434^{+43}_{-38}	05:14:29.281	170^{+12}_{-10}	0.9539	1.33E-05 ± 9.32E-07	1.66E-06 ± 2.30E-08
090122218g[a]	05:14:31.579	606^{+70}_{-32}	05:14:31.931	172^{+34}_{-22}	0.2363	2.67E-06 ± 5.39E-07	7.70E-08 ± 8.00E-09
090122218h[a]	05:14:42.033	200^{+56}_{-32}	05:14:42.187	22^{+4}_{-4}	0.1838	6.04E-06 ± 6.78E-07	1.07E-07 ± 6.24E-09
090122218i[a]	05:14:49.635	456^{+48}_{-116}	05:14:49.801	146^{+42}_{-32}	0.8639	9.14E-07 ± 2.98E-07	5.00E-08 ± 7.00E-09
090122218j[a]	05:15:06.270	118^{+52}_{-22}	05:15:06.282	52^{+10}_{-8}	0.8062	3.51E-06 ± 5.44E-07	1.24E-07 ± 7.20E-09
090122218k[a]	05:15:07.403	84^{+11}_{-28}	05:15:07.419	28^{+4}_{-8}	0.3593	3.74E-06 ± 5.65E-07	9.73E-08 ± 6.40E-09
090122218l[a]	05:15:42.906	272^{+27}_{-38}	05:15:42.958	38^{+16}_{-8}	0.5103	5.04E-06 ± 5.90E-07	7.98E-08 ± 5.32E-09
090122218m[a]	05:15:44.014	466^{+70}_{-20}	05:15:44.042	372^{+12}_{-24}	0.0277	2.17E-06 ± 5.21E-07	1.87E-07 ± 9.12E-09
090122218n[a]	05:16:04.675	964^{+54}_{-18}	05:16:05.001	534^{+40}_{-204}	0.2741	1.67E-06 ± 4.73E-07	2.49E-07 ± 1.99E-08
090122218o[a,f]	05:16:06.849	86^{+6}_{-6}	05:16:06.889	26^{+2}_{-2}	0.0623	6.25E-05 ± 2.24E-06	2.30E-06 ± 2.60E-08
090122218p[a]	05:16:18.303	506^{+42}_{-18}	05:16:18.375	192^{+38}_{-14}	0.6083	8.71E-06 ± 8.03E-07	6.46E-07 ± 1.72E-08
090122218q[a]	05:16:31.043	240^{+18}_{-40}	05:16:31.089	100^{+20}_{-18}	0.7431	1.75E-06 ± 4.96E-07	1.31E-07 ± 9.36E-09
090122218r[a,f]	05:16:44.241	102^{+12}_{-18}	05:16:44.269	30^{+2}_{-2}	0.0999	5.55E-05 ± 2.13E-06	9.53E-07 ± 1.72E-08
090122218s[a]	05:16:45.009	350^{+90}_{-44}	05:16:45.025	52^{+6}_{-2}	0.4643	1.49E-05 ± 9.83E-07	3.94E-07 ± 1.12E-08
090122218t[a]	05:17:01.802	210^{+64}_{-26}	05:17:01.826	82^{+40}_{-14}	0.5712	2.05E-06 ± 5.12E-07	6.86E-08 ± 7.28E-09
090122218u[a]	05:17:03.301	214^{+108}_{-26}	05:17:03.309	90^{+8}_{-8}	0.2884	1.20E-05 ± 9.84E-07	2.60E-07 ± 1.04E-08
090122218v[a]	05:17:10.340	144^{+59}_{-54}	05:17:10.370	32^{+10}_{-8}	0.6987	4.62E-06 ± 6.42E-07	2.39E-07 ± 1.18E-08
090122243a	05:49:18.344	370^{+88}_{-118}	05:49:18.540	48^{+8}_{-10}	0.8296	5.73E-06 ± 7.02E-07	1.46E-07 ± 7.04E-09
090122243b[a]	05:49:46.224	58^{+20}_{-12}	05:49:46.232	22^{+4}_{-4}	0.6660	3.77E-06 ± 5.98E-07	7.87E-08 ± 5.76E-09
090122243c[a,b,f]	05:52:15.165	252^{+76}_{-24}	05:52:15.171	66^{+4}_{-6}			
090122252a[f]	06:03:35.989	178^{+10}_{-12}	06:03:36.051	52^{+4}_{-8}	0.1675	9.58E-05 ± 3.63E-06	3.11E-06 ± 3.67E-08
090122252b[a]	06:06:41.652	160^{+54}_{-26}	06:06:41.668	56^{+12}_{-6}	0.7352	8.47E-06 ± 1.11E-06	3.62E-07 ± 1.62E-08
090122283a[a,f]	06:49:08.655	532^{+38}_{-28}	06:49:08.859	236^{+12}_{-10}	0.1535	2.16E-05 ± 1.17E-06	2.38E-06 ± 2.99E-08
090122283b[a,f]	06:49:14.841	1246^{+6}_{-6}	06:49:14.889	118^{+4}_{-2}	0.0238	5.31E-05 ± 1.96E-06	5.29E-06 ± 4.08E-08
090122283c[a]	06:49:21.450	198^{+121}_{-38}	06:49:21.562	30^{+10}_{-6}	0.2154	4.94E-06 ± 6.65E-07	9.66E-08 ± 6.44E-09
090122283d[a]	06:49:27.734	128^{+90}_{-34}	06:49:27.758	38^{+8}_{-4}	0.2034	1.25E-05 ± 9.77E-07	3.15E-07 ± 1.12E-08
090122283e[a]	06:49:29.530	116^{+20}_{-16}	06:49:29.536	46^{+8}_{-6}	0.0606	2.96E-05 ± 1.42E-06	5.36E-07 ± 1.28E-08
090122283f[a]	06:49:31.170	222^{+47}_{-46}	06:49:31.226	70^{+10}_{-10}	0.8830	4.54E-06 ± 6.15E-07	3.22E-07 ± 1.27E-08
090122283g[a,f]	06:49:32.952	424^{+26}_{-16}	06:49:32.994	238^{+8}_{-8}	0.7223	1.38E-05 ± 9.69E-07	1.78E-06 ± 2.22E-08
090122283h[a,f]	06:49:44.192	534^{+16}_{-10}	06:49:44.274	394^{+14}_{-32}	0.3542	2.24E-05 ± 1.22E-06	1.53E-06 ± 2.42E-08
090122283i[a,b,f]	06:49:48.471	616^{+6}_{-8}	06:49:48.609	216^{+4}_{-4}			

Table 2
(Continued)

Burst (yymmddffff)	T_{90} Start (UT)	T_{90} (ms)	T_{50} Start (UT)	T_{50} (ms)	Phase[c]	4ms Peak Flux[d,e] (erg s^{-1} cm^{-2})	Fluence[d,e] (erg s^{-1} cm^{-2})
090122283j[a]	06:50:03.397	474^{+86}_{-36}	06:50:03.447	120^{+6}_{-8}	0.4312	1.75E-05 ± 1.03E-06	1.44E-07 ± 8.28E-09
090122283k[a,b,f]	06:50:08.622	258^{+14}_{-14}	06:50:08.668	152^{+2}_{-2}			
090122283l[a,f]	06:50:12.076	172^{+44}_{-42}	06:50:12.096	42^{+2}_{-4}	0.6012	3.59E-05 ± 1.66E-06	1.54E-06 ± 2.24E-08
090122283m[a,f]	06:50:14.271	164^{+30}_{-16}	06:50:14.339	44^{+8}_{-4}	0.6948	2.57E-05 ± 1.31E-06	1.19E-06 ± 1.98E-08
090122283n[a]	06:50:17.509	46^{+10}_{-6}	06:50:17.517	26^{+2}_{-2}	0.7364	5.65E-06 ± 7.12E-07	1.36E-07 ± 7.68E-09
090122283o[a]	06:50:22.533	1296^{+130}_{-86}	06:50:22.797	266^{+44}_{-32}	0.7789	6.12E-06 ± 7.12E-07	5.88E-07 ± 1.74E-08
090122283p[a]	06:50:30.041	124^{+28}_{-14}	06:50:30.055	52^{+8}_{-6}	0.2708	6.16E-06 ± 6.42E-07	1.91E-07 ± 1.02E-08
090122283q[a]	06:50:34.275	66^{+12}_{-8}	06:50:34.293	26^{+4}_{-4}	0.3230	1.48E-05 ± 9.98E-07	4.23E-07 ± 1.14E-08
090122283r[a]	06:50:37.614	278^{+110}_{-70}	06:50:37.630	106^{+18}_{-12}	0.9239	4.44E-06 ± 6.19E-07	2.24E-07 ± 1.02E-08
090122283s[a,b,f]	06:50:49.339	192^{+202}_{-78}	06:50:49.351	32^{+2}_{-2}			
090122283t[a]	06:50:50.911	1766^{+38}_{-36}	06:50:51.189	1192^{+146}_{-116}	0.6026	4.38E-06 ± 6.53E-07	4.40E-07 ± 1.97E-08
090122283u[a,b,f]	06:50:57.268	156^{+2}_{-4}	06:50:57.300	92^{+2}_{-2}			
090122283v[a]	06:51:08.154	730^{+122}_{-124}	06:51:08.232	262^{+18}_{-20}	0.6950	1.95E-05 ± 1.17E-06	4.61E-07 ± 1.23E-08
090122283w[a]	06:51:12.100	208^{+20}_{-42}	06:51:12.192	76^{+54}_{-22}	0.6347	1.64E-06 ± 4.60E-07	4.97E-08 ± 9.20E-09
090122283x[a,b,f]	06:51:14.791	440^{+70}_{-74}	06:51:14.917	204^{+2}_{-4}			
090122283y[a]	06:51:28.561	110^{+38}_{-38}	06:51:28.571	18^{+2}_{-4}	0.5114	7.41E-06 ± 6.66E-07	1.16E-07 ± 6.48E-09
090122283z[a]	06:51:31.162	218^{+38}_{-64}	06:51:31.248	62^{+18}_{-14}	0.8203	1.45E-06 ± 2.74E-07	6.40E-08 ± 4.00E-09
090122283aa[a]	06:51:37.296	832^{+98}_{-114}	06:51:37.752	156^{+28}_{-22}	0.9603	3.81E-06 ± 4.88E-07	3.63E-07 ± 8.96E-09
090122283ab[a]	06:51:40.773	187^{+8}_{-9}	06:51:40.788	38^{+118}_{-8}	0.4155	9.27E-07 ± 2.70E-07	3.22E-08 ± 4.68E-09
090122283ac[a]	06:51:42.138	36^{+21}_{-8}	06:51:42.144	18^{+4}_{-6}	0.0618	2.78E-06 ± 4.99E-07	3.30E-08 ± 3.92E-09
090122283ad[a]	06:51:43.910	44^{+25}_{-16}	06:51:43.912	12^{+2}_{-4}	0.9160	5.06E-06 ± 6.05E-07	6.24E-08 ± 5.20E-09
090122283ae[a]	06:51:47.436	652^{+50}_{-16}	06:51:47.460	540^{+44}_{-28}	0.6279	2.78E-06 ± 4.92E-07	2.28E-07 ± 1.34E-08
090122283af[a,b,f]	06:52:00.167	100^{+6}_{-8}	06:52:00.177	30^{+2}_{-2}			
090122283ag[a,f]	06:52:03.979	388^{+30}_{-36}	06:52:04.047	88^{+6}_{-4}	0.6354	3.22E-05 ± 1.40E-06	2.44E-06 ± 2.50E-08
090122283ah[a]	06:52:20.032	538^{+62}_{-16}	06:52:20.208	202^{+32}_{-28}	0.5169	1.94E-05 ± 1.07E-06	8.34E-07 ± 1.67E-08
090122283ai[a]	06:52:51.117	80^{+18}_{-8}	06:52:51.123	22^{+4}_{-4}	0.3551	1.48E-05 ± 9.50E-07	2.89E-07 ± 9.72E-09
090122291a	06:58:24.212	98^{+18}_{-22}	06:58:24.238	30^{+6}_{-6}	0.1284	4.90E-06 ± 5.24E-07	1.42E-07 ± 6.96E-09
090122291b[a]	06:58:35.785	62^{+39}_{-14}	06:58:35.793	14^{+8}_{-2}	0.7067	5.46E-06 ± 5.77E-07	8.68E-08 ± 5.20E-09
090122291c[a,b,f]	06:59:35.546	240^{+10}_{-10}	06:59:35.590	118^{+4}_{-2}			
090122291d[a]	07:00:00.458	554^{+40}_{-78}	07:00:00.602	106^{+66}_{-26}	0.6431	2.33E-06 ± 4.02E-07	4.62E-08 ± 4.80E-09
090122291e[a]	07:00:16.919	493^{+11}_{-35}	07:00:16.979	396^{+16}_{-34}	0.7278	2.19E-06 ± 3.65E-07	5.99E-08 ± 5.04E-09
090122291f[a]	07:00:23.307	548^{+36}_{-68}	07:00:23.511	188^{+28}_{-30}	0.7395	1.26E-06 ± 3.68E-07	5.21E-08 ± 4.96E-09
090122291g[a]	07:00:45.277	296^{+47}_{-144}	07:00:45.465	38^{+28}_{-8}	0.3010	1.63E-06 ± 3.93E-07	4.84E-08 ± 4.16E-09
090122291h[a]	07:00:50.275	326^{+33}_{-86}	07:00:50.435	58^{+32}_{-12}	0.7002	2.17E-06 ± 3.86E-07	7.02E-08 ± 5.40E-09
090122291i[a]	07:00:54.775	320^{+47}_{-28}	07:00:54.789	138^{+46}_{-40}	0.7901	6.37E-06 ± 5.87E-07	6.48E-08 ± 4.80E-09
090122291j[a,b,f]	07:00:58.715	308^{+26}_{-20}	07:00:58.765	90^{+4}_{-2}			
090122310a[f]	07:26:29.656	828^{+12}_{-10}	07:26:30.046	396^{+6}_{-4}	0.9337	9.41E-06 ± 8.80E-07	1.30E-06 ± 2.65E-08
090122310b[a]	07:30:15.629	290^{+20}_{-28}	07:30:15.715	132^{+6}_{-8}	0.7294	9.91E-06 ± 8.29E-07	6.07E-07 ± 1.64E-08
090122310c[a,b,f]	07:31:14.748	566^{+28}_{-50}	07:31:14.910	202^{+4}_{-4}			
090122317a[f]	07:36:28.741	330^{+24}_{-40}	07:36:28.749	94^{+2}_{-6}	0.7010	3.64E-05 ± 1.52E-06	7.55E-07 ± 1.18E-08
090122317b[a]	07:37:59.919	676^{+23}_{-114}	07:37:59.983	188^{+26}_{-32}	0.7180	3.47E-06 ± 5.53E-07	2.37E-07 ± 1.06E-08
090122317c[a]	07:39:44.368	185^{+34}_{-25}	07:39:44.389	44^{+22}_{-10}	0.1263	1.91E-06 ± 3.82E-07	2.21E-08 ± 2.56E-09
090122317d[a]	07:40:15.327	103^{+6}_{-4}	07:40:15.343	44^{+6}_{-6}	0.0634	5.81E-06 ± 5.75E-07	1.56E-07 ± 6.72E-09
090122317e[a,b,f]	07:40:15.939	468^{+26}_{-38}	07:40:15.955	146^{+4}_{-4}			
090122352a	08:26:14.513	46^{+50}_{-16}	08:26:14.517	14^{+4}_{-4}	0.7170	1.32E-05 ± 1.79E-06	1.63E-07 ± 1.39E-08
090122352b[a]	08:26:16.073	144^{+72}_{-16}	08:26:16.085	38^{+6}_{-8}	0.4839	1.30E-05 ± 1.62E-06	4.40E-07 ± 2.07E-08
090122359a[b,f]	08:36:30.674	260^{+114}_{-78}	08:36:30.814	42^{+2}_{-2}			
090122359b[a]	08:36:40.490	188^{+56}_{-48}	08:36:40.494	50^{+6}_{-2}	0.8361	1.19E-05 ± 1.05E-06	2.37E-07 ± 1.09E-08
090122359c[a]	08:40:56.330	184^{+37}_{-22}	08:40:56.374	100^{+24}_{-14}	0.3334	1.80E-06 ± 4.19E-07	2.60E-08 ± 3.64E-09
090122380a	09:07:38.613	182^{+62}_{-22}	09:07:38.655	32^{+20}_{-8}	0.6486	6.49E-06 ± 8.13E-07	9.72E-08 ± 7.20E-09
090122380b[a]	09:08:15.574	102^{+84}_{-18}	09:08:15.592	46^{+14}_{-6}	0.4767	1.77E-06 ± 3.95E-07	1.01E-07 ± 7.20E-09
090122390a	09:21:00.370	214^{+72}_{-78}	09:21:00.384	46^{+8}_{-10}	0.5753	9.95E-06 ± 1.18E-06	2.36E-07 ± 1.23E-08
090122419a[b,f]	10:03:04.670	152^{+12}_{-12}	10:03:04.698	46^{+4}_{-2}			
090122419b[a]	10:08:01.834	128^{+20}_{-12}	10:08:01.844	42^{+2}_{-4}	0.2925	3.95E-05 ± 1.56E-06	1.36E-06 ± 1.76E-08
090122428a	10:16:39.335	92^{+28}_{-16}	10:16:39.343	42^{+8}_{-4}	0.0571	3.12E-06 ± 4.28E-07	7.07E-08 ± 5.20E-09
090122428b[a]	10:16:40.374	334^{+70}_{-36}	10:16:40.406	54^{+2}_{-4}	0.5875	1.11E-05 ± 6.59E-07	8.07E-07 ± 1.16E-08
090122451a	10:49:30.135	98^{+34}_{-16}	10:49:30.195	20^{+4}_{-2}	0.2580	8.69E-06 ± 1.02E-06	2.42E-07 ± 1.15E-08
090122451b[a]	10:52:11.895	64^{+8}_{-22}	10:52:11.925	22^{+10}_{-8}	0.3094	3.42E-06 ± 6.99E-07	7.78E-08 ± 1.01E-08
090122491a	11:46:21.307	382^{+62}_{-108}	11:46:21.327	124^{+22}_{-18}	0.5565	3.20E-06 ± 5.91E-07	1.90E-07 ± 9.76E-09

Table 2
(Continued)

Burst (yymmddfff)	T_{90} Start (UT)	T_{90} (ms)	T_{50} Start (UT)	T_{50} (ms)	Phase[c]	4ms Peak Flux[d,e] (erg s^{-1} cm^{-2})	Fluence[d,e] (erg s^{-1} cm^{-2})
090122491b[a]	11:49:44.170	202^{+20}_{-60}	11:49:44.210	64^{+12}_{-8}	0.4804	2.09E-06 ± 4.79E-07	7.84E-08 ± 8.40E-09
090122498a[f]	11:57:34.040	44 ± 9	11:57:34.048	20 ± 9	0.2464	3.13E-06 ± 5.27E-07	7.77E-08 ± 6.66E-09
090122498b[a]	12:00:47.292	244 ± 9	12:00:47.360	120 ± 6	0.5690	3.99E-06 ± 5.35E-07	4.80E-07 ± 1.43E-08
090122498c[a]	12:00:48.740	244 ± 13	12:00:48.784	86 ± 6	0.2554	7.98E-06 ± 7.69E-07	1.07E-06 ± 2.03E-08
090122551a	13:13:14.497	240^{+32}_{-46}	13:13:14.511	126^{+20}_{-32}	0.5884	1.50E-06 ± 3.21E-07	4.33E-08 ± 5.32E-09
090122624a	14:57:52.699	26^{+18}_{-8}	14:57:52.705	10^{+2}_{-2}	0.6398	1.15E-05 ± 1.16E-06	1.87E-07 ± 1.04E-08
090122624b[a]	14:57:57.528	190^{+49}_{-32}	14:57:57.554	72^{+40}_{-18}	0.9868	1.84E-06 ± 5.39E-07	9.21E-08 ± 1.18E-08
090122624c[a,b,f]	15:02:15.402	94^{+14}_{-12}	15:02:15.412	26^{+4}_{-2}			
090122650a[a,b,f]	15:35:53.655	110^{+2}_{-2}	15:35:53.681	60^{+2}_{-2}			
090122684a	16:24:45.286	64^{+27}_{-10}	16:24:45.292	30^{+2}_{-6}	0.3827	4.81E-06 ± 5.96E-07	1.16E-07 ± 6.48E-09
090122969a[a,b,f]	23:14:54.053	200^{+20}_{-12}	23:14:54.095	70^{+2}_{-2}			
090122694a	16:39:26.485	382^{+55}_{-112}	16:39:26.699	98^{+4}_{-6}	0.8263	6.45E-06 ± 5.50E-07	1.85E-07 ± 7.60E-09
090122848a	20:20:55.676	210^{+55}_{-38}	20:20:55.708	66^{+12}_{-8}	0.4473	2.14E-06 ± 4.48E-07	8.80E-08 ± 7.00E-09
090122848b[a]	20:20:56.176	366^{+86}_{-60}	20:20:56.306	126^{+16}_{-18}	0.7576	2.68E-06 ± 4.69E-07	1.54E-07 ± 7.52E-09
090122898a	21:32:53.017	196^{+39}_{-68}	21:32:53.065	48^{+20}_{-12}	0.1461	2.54E-06 ± 5.32E-07	8.70E-08 ± 8.00E-09
090122980a	23:31:19.876	450^{+64}_{-44}	23:31:19.906	134^{+8}_{-6}	0.0929	1.11E-05 ± 8.23E-07	9.33E-07 ± 1.71E-08
090123042a	01:01:14.539	260^{+66}_{-40}	01:01:14.547	74^{+48}_{-20}	0.7531	1.70E-05 ± 1.24E-06	5.28E-07 ± 1.68E-08
090123055a[f]	01:19:42.448	78^{+10}_{-10}	01:19:42.458	24^{+2}_{-2}	0.9466	9.91E-05 ± 4.03E-06	3.15E-06 ± 4.18E-08
090123113a[a,b,f]	02:42:10.695	324^{+16}_{-26}	02:42:10.749	78^{+2}_{-2}			
090123313a	07:31:26.632	253^{+26}_{-43}	07:31:26.679	98^{+26}_{-14}	0.6148	3.35E-06 ± 7.03E-07	2.11E-07 ± 1.32E-08
090123348a	08:21:37.609	98^{+14}_{-12}	08:21:37.623	50^{+2}_{-6}	0.7808	9.58E-06 ± 7.37E-07	3.25E-07 ± 9.60E-09
090123552a	13:14:33.803	78^{+35}_{-20}	13:14:33.813	22^{+4}_{-4}	0.5745	4.37E-06 ± 5.73E-07	1.00E-07 ± 6.40E-09
090123577a	13:50:58.095	36^{+22}_{-14}	13:50:58.105	8^{+6}_{-2}	0.7796	8.86E-06 ± 1.09E-06	1.18E-07 ± 8.36E-09
090123617a	14:48:26.077	182^{+46}_{-26}	14:48:26.097	108^{+2}_{-4}	0.8725	9.95E-06 ± 7.89E-07	3.17E-07 ± 1.06E-08
090123683a	16:22:53.577	298^{+236}_{-112}	16:22:53.597	46^{+14}_{-8}	0.7080	9.64E-06 ± 1.18E-06	2.82E-07 ± 1.56E-08
090123705a[f]	16:54:38.064	78^{+10}_{-6}	16:54:38.072	32^{+2}_{-2}	0.3407	9.78E-05 ± 3.55E-06	2.03E-06 ± 2.88E-08
090124175a	04:11:23.194	462^{+28}_{-28}	04:11:23.218	234^{+36}_{-20}	0.5722	5.05E-06 ± 6.16E-07	1.18E-07 ± 6.80E-09
090124175b[a]	04:11:23.742	56^{+26}_{-14}	04:11:23.764	20^{+6}_{-6}	0.8401	2.77E-06 ± 5.08E-07	5.58E-08 ± 4.80E-09
090125179a	11:17:15.955	80 ± 9	11:17:15.599	36 ± 9	0.4709	7.76E-06 ± 1.08E-06	2.04E-07 ± 1.51E-08
090125277a	06:38:58.324	48 ± 11	06:38:58.328	24 ± 6	0.9677	9.06E-06 ± 1.03E-06	2.94E-07 ± 1.30E-08
090125538a[f]	12:55:21.265	52 ± 6	12:55:21.273	20 ± 6	0.1617	4.42E-05 ± 2.39E-06	8.98E-07 ± 2.23E-08
090125900a	21:36:05.174	368 ± 116	21:36:05.318	80 ± 101	0.4570	1.48E-06 ± 3.31E-07	1.35E-07 ± 1.06E-08
090125911a	21:52:13.115	104 ± 9	21:52:13.159	20 ± 6	0.5565	3.13E-05 ± 1.38E-06	5.66E-07 ± 1.39E-08
090125959a[b]	23:00:36.087	300 ± 9	23:00:36.275	44 ± 6			
090126200a[f]	04:48:05.378	720 ± 6	04:48:05.394	92 ± 9	0.2377	7.21E-05 ± 4.44E-06	3.05E-06 ± 6.12E-08
090126610a	14:37:55.481	104 ± 18	14:37:55.505	40 ± 11	0.5473	3.17E-06 ± 5.09E-07	7.30E-08 ± 8.45E-09
090126748a	17:56:39.210	64 ± 9	17:56:39.222	28 ± 6	0.2769	7.55E-06 ± 7.65E-07	2.65E-07 ± 1.09E-08
090126966a	23:10:20.043	108 ± 13	23:10:20.051	60 ± 6	0.7539	3.17E-06 ± 4.69E-07	1.16E-07 ± 7.30E-09
090127611a	14:39:14.144	48 ± 51	14:39:14.144	32 ± 36	0.6722	2.75E-06 ± 5.03E-07	5.36E-08 ± 6.24E-09
090127632a	15:10:08.920	108 ± 6	15:10:08.928	32 ± 6	0.8272	1.35E-05 ± 7.74E-07	2.77E-07 ± 6.84E-09
090128024a	00:34:45.474	64 ± 23	00:34:45.498	48 ± 23	0.6649	1.74E-06 ± 3.80E-07	4.24E-08 ± 5.12E-09
090129353a	08:27:38.311	70^{+39}_{-16}	08:27:38.325	28^{+4}_{-8}	0.3192	2.44E-06 ± 4.20E-07	5.88E-08 ± 4.68E-09
090129472a	11:19:27.518	68^{+48}_{-20}	11:19:27.540	24^{+4}_{-2}	0.8318	4.57E-06 ± 6.21E-07	1.01E-07 ± 6.40E-09
090129538a	12:54:14.935	176 ± 45	12:54:14.935	84 ± 36	0.7840	4.55E-06 ± 8.32E-07	1.16E-07 ± 1.15E-08
090129588a[f]	14:06:37.759	214^{+36}_{-42}	14:06:37.877	76^{+2}_{-4}	0.8692	4.02E-05 ± 1.68E-06	1.29E-06 ± 2.06E-08
090129936a	22:27:26.775	74^{+26}_{-12}	22:27:26.787	20^{+4}_{-4}	0.2506	2.60E-05 ± 1.73E-06	4.50E-07 ± 1.56E-08
090130290a	06:58:16.537	168 ± 9	06:58:16.549	40 ± 9	0.7340	7.72E-06 ± 7.66E-07	1.94E-07 ± 1.08E-08
090130812a	19:29:41.209	288 ± 9	19:29:41.221	176 ± 6	0.9036	1.32E-05 ± 8.59E-07	5.58E-07 ± 1.39E-08
090130812a[a]	19:29:42.949	64 ± 11	19:29:42.981	24 ± 18	0.7593	3.70E-06 ± 4.80E-07	9.01E-08 ± 6.45E-09
090131080a	01:54:35.570	72 ± 40	01:54:35.578	48 ± 18	0.9083	1.58E-06 ± 3.87E-07	5.20E-08 ± 5.44E-09
090131590a	14:08:54.764	96 ± 36	14:08:54.780	40 ± 11	0.1532	1.81E-06 ± 3.59E-07	9.90E-08 ± 7.36E-09
090201503a	12:04:28.399	368 ± 9	12:04:28.631	88 ± 6	0.8773	4.39E-06 ± 6.16E-07	3.43E-07 ± 1.50E-08
090201684a	16:25:16.332	112 ± 23	16:25:16.348	64 ± 36	0.9127	2.24E-06 ± 5.45E-07	1.04E-07 ± 8.77E-09
090201716a	17:10:45.146	244 ± 11	17:10:45.226	72 ± 9	0.9713	8.53E-06 ± 9.48E-07	6.68E-07 ± 1.84E-08
090201884a	21:12:56.152	228 ± 11	21:12:56.204	76 ± 9	0.0242	7.96E-06 ± 1.23E-06	4.21E-07 ± 2.45E-08
090202321a	07:41:40.006	244 ± 44	07:41:40.014	116 ± 9	0.5926	9.73E-06 ± 7.56E-07	4.68E-07 ± 1.37E-08
090202394a	09:27:26.833	100 ± 29	09:27:26.861	40 ± 11	0.7444	4.88E-06 ± 6.68E-07	1.42E-07 ± 8.85E-09
090202394b[a]	09:30:17.519	60 ± 16	09:30:17.529	32 ± 6	0.1323	1.21E-05 ± 9.80E-07	3.06E-07 ± 1.12E-08
090202440a	10:33:42.000	100 ± 14	10:33:42.016	48 ± 6	0.2807	8.34E-06 ± 8.54E-07	3.81E-07 ± 1.48E-08
090202513a	12:18:58.096	360 ± 23	12:18:58.192	124 ± 6	0.6994	3.11E-06 ± 5.63E-07	4.18E-07 ± 1.71E-08
090202862a	20:40:35.804	396 ± 13	20:40:35.844	180 ± 14	0.6276	3.65E-06 ± 5.30E-07	3.27E-07 ± 1.36E-08
090202862b[a]	20:44:10.904	140 ± 13	20:44:10.924	36 ± 6	0.4440	9.80E-06 ± 6.80E-07	4.51E-07 ± 1.00E-08
090203198a	04:44:51.150	68 ± 38	04:44:51.166	20 ± 6	0.5534	7.00E-06 ± 1.16E-06	1.67E-07 ± 1.50E-08

Table 2
(Continued)

Burst (yymmddfff)	T_{90} Start (UT)	T_{90} (ms)	T_{50} Start (UT)	T_{50} (ms)	Phase[c]	4ms Peak Flux[d,e] (erg s^{-1} cm^{-2})	Fluence[d,e] (erg s^{-1} cm^{-2})
090203206a	04:57:15.387	72 ± 41	04:57:15.411	24 ± 25	0.7532	3.30E-06 $\pm$ 9.24E-07	1.16E-07 $\pm$ 1.53E-08
090203389a	09:19:53.427	44 ± 9	09:19:53.431	16 ± 9	0.0145	2.41E-05 $\pm$ 1.28E-06	4.68E-07 $\pm$ 1.29E-08
090203805a	19:18:47.266	48 ± 29	19:18:47.274	24 ± 11	0.6998	1.78E-06 $\pm$ 3.65E-07	5.36E-08 $\pm$ 6.72E-09
090203834a[f]	20:00:39.494	124 ± 6	20:00:39.518	36 ± 6	0.1867	1.70E-04 $\pm$ 5.62E-06	6.97E-06 $\pm$ 6.35E-08
090204003a	00:04:23.747	96 ± 40	00:04:23.795	24 ± 11	0.2751	3.91E-06 $\pm$ 6.57E-07	5.76E-08 $\pm$ 5.72E-09
090204852a[b]	20:27:20.796	72 ± 6	20:27:20.8	36 ± 6			
090206897a	21:32:18.806	44 ± 9	21:32:18.810	24 ± 6	0.4412	8.74E-06 $\pm$ 1.13E-06	1.52E-07 $\pm$ 1.12E-08
090207834a	20:01:20.021	32 ± 13	20:01:20.025	12 ± 9	0.8989	1.70E-05 $\pm$ 1.55E-06	2.17E-07 $\pm$ 1.30E-08
090208340a	08:09:51.930	40 ± 18	08:09:51.930	24 ± 11	0.4584	5.50E-06 $\pm$ 6.39E-07	8.12E-08 $\pm$ 6.24E-09
090208463a	11:06:07.840	72 ± 13	11:06:07.844	12 ± 6	0.3319	1.34E-05 $\pm$ 1.08E-06	1.84E-07 $\pm$ 1.02E-08
090208682a	16:21:45.781	120 ± 13	16:21:45.785	56 ± 9	0.6437	5.88E-06 $\pm$ 6.29E-07	1.32E-07 $\pm$ 9.22E-09
090209271a	06:29:56.862	96 ± 66	06:29:56.878	64 ± 23	0.0721	1.55E-06 $\pm$ 3.77E-07	6.61E-08 $\pm$ 7.73E-09
090210310a	07:26:04.425	76 ± 6	07:26:04.429	20 ± 6	0.3101	1.76E-05 $\pm$ 9.25E-07	2.42E-07 $\pm$ 7.99E-09
090210415a	09:58:17.431	56 ± 11	09:58:17.447	20 ± 6	0.1511	7.25E-06 $\pm$ 6.32E-07	2.21E-07 $\pm$ 7.78E-09
090210898a	21:33:42.859	76 ± 11	21:33:42.895	20 ± 6	0.9719	2.17E-05 $\pm$ 1.92E-06	4.04E-07 $\pm$ 1.73E-08
090210941a	22:34:25.896	92 ± 11	22:34:25.932	24 ± 6	0.1873	1.18E-05 $\pm$ 8.91E-07	4.14E-07 $\pm$ 1.32E-08
090211264a	06:20:00.863	496 ± 29	06:20:00.927	320 ± 23	0.4932	3.03E-06 $\pm$ 5.69E-07	2.72E-07 $\pm$ 1.65E-08
090211279a[f]	06:41:38.916	36 ± 6	06:41:38.920	16 ± 6	0.8067	6.55E-05 $\pm$ 3.83E-06	1.21E-06 $\pm$ 3.18E-08
090211290a	06:56:58.914	168 ± 29	06:56:58.926	84 ± 11	0.8268	4.18E-06 $\pm$ 7.75E-07	2.55E-07 $\pm$ 1.59E-08
090212968a	23:14:03.128	40 ± 9	23:14:03.140	12 ± 9	0.3348	3.87E-06 $\pm$ 4.84E-07	4.03E-08 $\pm$ 4.90E-09
090214814a[b]	19:31:45.276	64 ± 6	19:31:45.28	20 ± 6			
090217261a	06:16:30.470	40 ± 6	06:16:30.482	12 ± 6	0.9705	2.15E-05 $\pm$ 1.55E-06	3.26E-07 $\pm$ 1.40E-08
090218278a	06:40:11.340	96 ± 13	06:40:11.384	28 ± 6	0.5101	8.45E-06 $\pm$ 7.96E-07	2.60E-07 $\pm$ 1.05E-08
090218491a	11:46:58.874	52 ± 6	11:46:58.882	24 ± 9	0.4040	2.77E-05 $\pm$ 1.85E-06	6.54E-07 $\pm$ 1.93E-08
090221644a[b]	15:27:34.404	116 ± 6	15:27:34.424	68 ± 9			
090221803a	19:16:59.515	80 ± 14	19:16:59.523	28 ± 9	0.6461	8.40E-06 $\pm$ 8.63E-07	2.25E-07 $\pm$ 1.12E-08
090222540a	12:57:06.234	112 ± 68	12:57:06.250	64 ± 36	0.7467	1.65E-06 $\pm$ 4.46E-07	7.43E-08 $\pm$ 8.64E-09
090222906a[b]	21:44:49.908	36 ± 9	21:44:49.912	16 ± 6			
090223128a[b]	03:04:40.789	124 ± 6	03:04:40.809	76 ± 6			
090224694a	16:38:44.089	408 ± 30	16:38:44.121	304 ± 11	0.8687	3.17E-06 $\pm$ 9.83E-07	1.83E-07 $\pm$ 2.34E-08
090224718a	17:13:42.113	284 ± 9	17:13:42.197	128 ± 13	0.3140	9.93E-06 $\pm$ 7.88E-07	5.58E-07 $\pm$ 1.57E-08
090224782a	18:45:57.877	148 ± 29	18:45:57.901	$80 \pm$	0.9721	4.31E-06 $\pm$ 5.10E-07	2.70E-07 $\pm$ 1.05E-08
090322789a	18:56:23.686	592 ± 40	18:56:23.750	360 ± 29	0.4158	2.72E-06 $\pm$ 1.60E-06	3.09E-07 $\pm$ 1.60E-08
090322944a[b]	22:39:15.786	288 ± 6	22:39:15.834	88 ± 6			
090326625a	15:00:35.962	244 ± 30	15:00:36.006	80 ± 6	0.8768	2.44E-06 $\pm$ 4.37E-07	1.32E-07 $\pm$ 9.00E-09
090326625b[a]	15:00:38.216	192 ± 45	15:00:38.282	96 ± 36	09501	1.90E-06 $\pm$ 1.26E-06	9.50E-08 $\pm$ 3.30E-08
090328545a	13:05:12.020	136 ± 37	13:05:12.032	48 ± 9	0.3297	2.73E-06 $\pm$ 5.28E-07	1.26E-07 $\pm$ 6.00E-09
090329754a	18:05:15.732	140 ± 54	18:05:15.748	28 ± 11	0.7721	5.46E-06 $\pm$ 8.12E-07	1.27E-07 $\pm$ 6.00E-09
090330237a	05:41:09.982	124 ± 24	05:41:09.990	32 ± 9	0.4217	2.04E-05 $\pm$ 1.00E-06	5.57E-07 $\pm$ 1.00E-08
090401093a	02:14:28.178	2656 ± 172	02:14:28.402	1632 ± 172	0.6259	9.21E-07 $\pm$ 2.38E-07	2.50E-08 $\pm$ 3.00E-09
090401666a[f]	15:59:36.826	88 ± 6	15:59:36.834	32 ± 6	0.4664	9.66E-05 $\pm$ 3.47E-06	1.87E-06 $\pm$ 2.40E-08
090403592a	14:13:04.284	320 ± 23	14:13:04.460	80 ± 36	0.4952	4.64E-06 $\pm$ 6.78E-07	2.14E-07 $\pm$ 7.00E-09
090403761a	18:15:36.276	136 ± 18	18:15:36.294	48 ± 23	0.1677	2.71E-06 $\pm$ 4.39E-07	8.40E-08 $\pm$ 5.00E-09
090409351a	08:25:23.994	112 ± 18	08:25:24.002	72 ± 18	0.5365	6.40E-06 $\pm$ 6.38E-07	2.33E-07 $\pm$ 7.00E-09
090411917a	22:01:05.250	180 ± 20	22:01:05.282	64 ± 9	0.9203	1.37E-05 $\pm$ 1.07E-06	4.55E-07 $\pm$ 1.00E-08
090413987a	23:41:48.856	72 ± 6	23:41:48.860	28 ± 6	0.8659	2.25E-05 $\pm$ 1.12E-06	3.77E-07 $\pm$ 8.00E-09
090417946a	22:42:11.306	480 ± 69	22:42:11.354	336 ± 23	0.1967	4.78E-06 $\pm$ 6.69E-07	2.27E-07 $\pm$ 1.00E-08

Notes.
[a] Untriggered burst.
[b] Saturated burst.
[c] Phase of the 4 ms peak of the burst.
[d] By COMP model.
[e] 8–200 keV energy range.
[f] Used in Younes et al. (2014).

fitted the time-integrated spectra over an 8−200 keV energy range to different spectral models: a single power law (PL), a blackbody (BB), a Comptonized model (COMP), an optically thin thermal bremsstrahlung model (OTTB), and two BB functions (BB+BB). In each case, we used the Castor C-statistic to determine the model significance. For SGR J1550–5418 we also performed time-resolved spectroscopy of the bursts at 4 ms time resolution to determine their peak fluxes. For this purpose, we only used the COMP model.

Finally, temporal analyses were performed on the whole sample of SGR J1550–5418 bursts, and the methodology and results are discussed in Sections 3.1.4 and 3.1.5.

3. MAGNETAR BURSTS FROM CONFIRMED SOURCES

3.1. SGR J1550–5418

SGR J1550–5418 (R.A. = 15^{h}50^{m}54^s.11, decl. = −54°18′23″.7; Camilo et al. 2007) became active in 2008
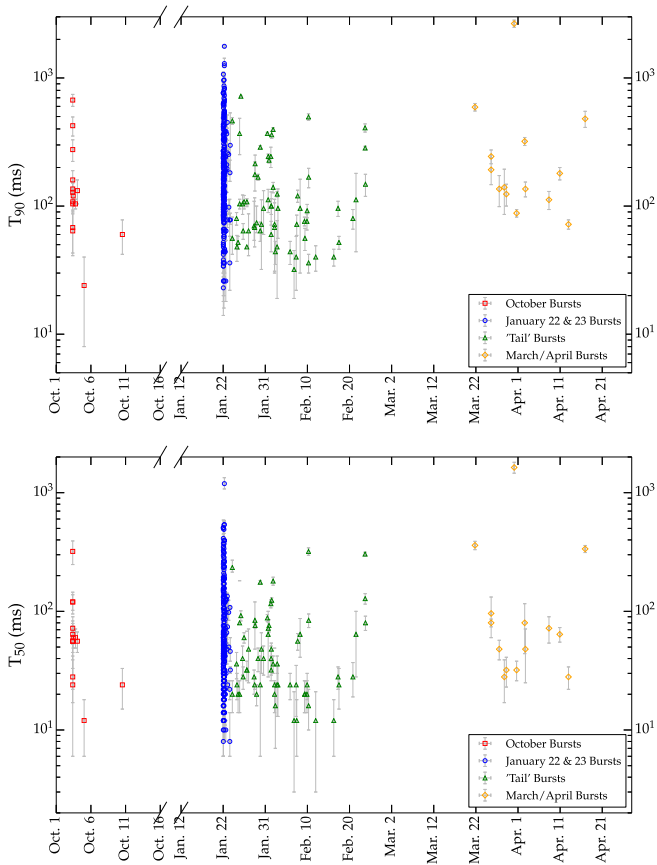
Figure 2. T_{90} and T_{50} for SGR J1550–5418 over the course of all outburst periods. The "tail" bursts in this figure, and the following ones, are bursts detected between January 24 and February 24. We find no trends in these durations over time.

Figure 3. Evolution of the low (top panel) and high (bottom panel) BB temperatures from the BB+BB spectral model over time for SGR J1550–5418 bursts. For the October bursts, we use the values for the single BB fits in both panels (red squares). There is a clear division between these single BB temperatures and the low temperatures of the BB+BB model. However, the former temperatures are similar to the hot BB temperatures of the BB+BB model.

October, when it emitted several hundred magnetar-like bursts (Kouveliotou et al. 2009; Palmer 2009); this activity ceased in April 2009. The source was discovered by the *Einstein* satellite (Lamb & Markert 1981), named 1E 1547.0–5408, and identified as a magnetar candidate following observations with *XMM-Newton* and the *Chandra* X-Ray Observatory (Gelfand & Gaensler 2007). It was later confirmed as a magnetar with a spin period of 2.07 s, a period derivative of 2.32×10^{-11} s/s, and an inferred magnetic field of 2.2×10^{14} G (Camilo et al. 2007; for a detailed description of the history of SGR J1550–5418, see van der Horst et al. 2012 and von Kienlin et al. 2012). Although SGR J1550–5418 was initially classified as an AXP, after this extremely prolific activity, very similar to those from SGRs 1806–20, 1900+14, and 1627–41, it was reclassified as an SGR and renamed SGR J1550–5418 (Kouveliotou et al. 2009; Palmer 2009). The source distance has been estimated to be ~5 kpc (Gelfand & Gaensler 2007; Tiengo et al. 2010).

Throughout this section, we will refer to the activity of SGR J1550–5418 in terms of three active periods: 2008 October (von Kienlin et al. 2012), 2009 January (van der Horst et al. 2012), and 2009 March–April (von Kienlin et al. 2012). von Kienlin et al. (2012) studied the GBM burst data for the first and third periods and found that the spectra of the former were best fit with a single BB, while the latter were best fit with an OTTB. van der Horst et al. (2012) studied the bursts of the first two days of the second period, and found that their

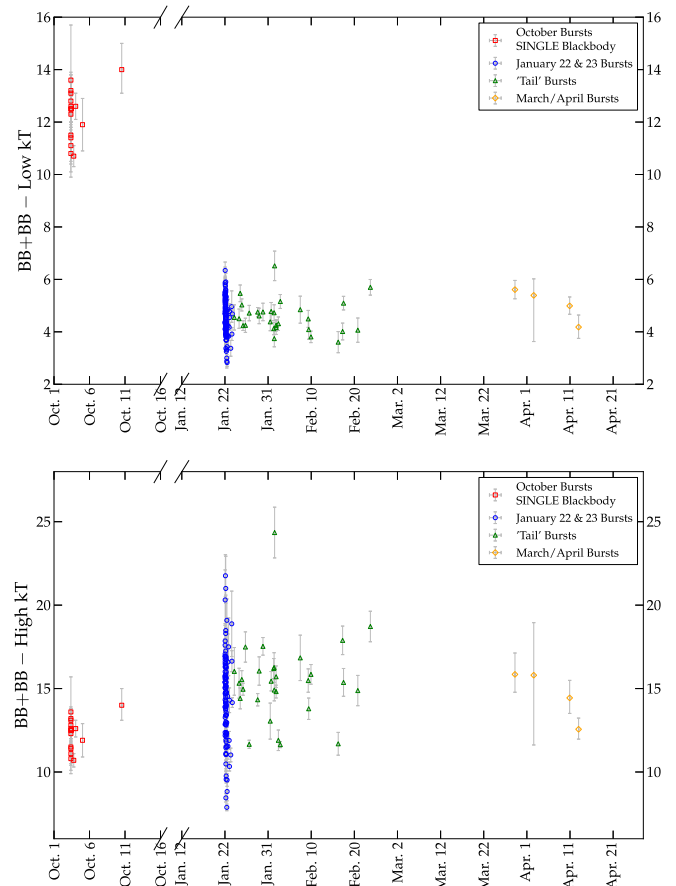spectra were fit equally well with a COMP, an OTTB, and a BB+BB model. Lin et al. (2012) later refined the results of van der Horst et al. (2012), using bursts from the second period which were also seen with the *Swift*/X-ray Telescope (XRT), and established that a BB+BB model best fit these joint spectra. Taken together, these three studies suggest that the first outburst was significantly different than the other two periods, which exhibited similar spectral and temporal properties. Younes et al. (2014) presented time-resolved spectroscopy for the brightest bursts over all three periods, and obtained an estimate of the lower limit on the internal magnetic field. Besides their analysis of these bursts, Kaneko et al. (2010) presented spectral and temporal analyses of enhanced persistent emission during the onset of the second bursting period, resulting in the discovery of the smallest hot spot ever measured for a magnetar. Furthermore, recent detailed variability analysis has revealed candidate quasi-periodic oscillations (QPOs) in bursts during the second emission period (Huppenkothen et al. 2014).

We searched for additional bursts in the GBM data during the gaps between the previously studied bursting periods and found 66 previously unstudied bursts that temporally best belong to the second period (spanning 2009 January 22–February 24). These 66 bursts include 5 untriggered bursts for
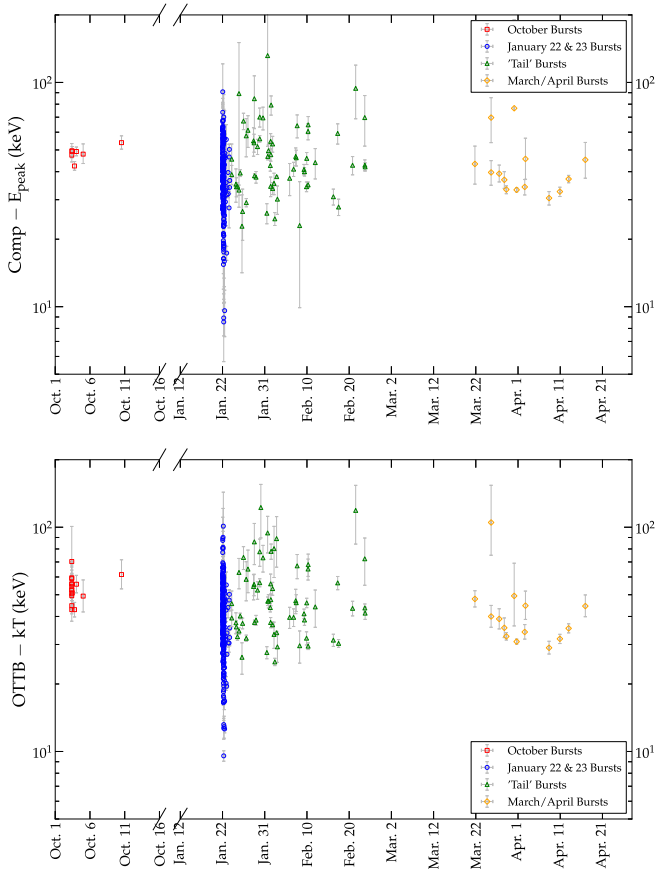
Figure 4. Spectral peak as measured by the Comptonized model (top panel, E_{peak}) and OTTB model (bottom panel, kT) for SGR J1550–5418. Overall, the values are in agreement with each other, and they are both consistent over time.
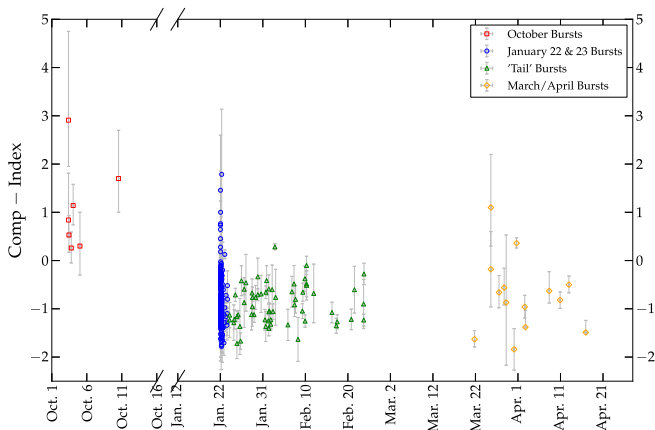
Figure 5. Power-law index of the COMP model for SGR J1550–5418 bursts. The bursts from the October period are clearly different compared to the rest of the sample, confirming the spectral evolution between burst active periods seen with the BB+BB model fits.

which we have TTE data, which were found with the search algorithm described in Kaneko et al. (2010). Between February 24 and March 22, there were no bursts observed from SGR J1550–5418, although the source was still visible in the X-rays (see, e.g., Scholz & Kaspi 2011).

3.1.1. Temporal and Spectral Evolution

Here, we study the statistical properties of all bursts from SGR J1550–5418 detected with GBM and the evolution of the burst activity across the entire 2008–2009 source activation period. Figure 1 displays the T_{90} and T_{50} duration distributions of 354 unsaturated events (see also Table 2). We fit these distributions with a log-normal function (solid line) and find that the T_{90} (T_{50}) duration centers at 155 ± 10 ms (51 ± 5 ms), with a logarithmic width of ~0.4. The duration distribution of the bursts from SGR J1550–5418 is similar to what we have seen in other magnetars (e.g., Woods et al. 1999; Göğüş et al. 2001; Gavriil et al. 2004; Esposito et al. 2008; Lin et al. 2011a). Figure 2 shows the evolution of T_{90} and T_{50} over time. We find no significant trend in the evolution of the burst durations over the entire outburst period of roughly seven months. We note that the longest event in Figure 2 is very faint with a peak flux of 9.2×10^{-7} erg cm^{-2} s^{-1} (see also Lin et al. 2013 for a sample of the very dim but long SGR J1550–5418 bursts detected by *Swift*/XRT).

In Figures 3–5, we present the evolution of time-integrated spectral parameters from the OTTB, COMP, and BB+BB models for the entire sample of SGR J1550–5418 bursts (Table 3; van der Horst et al. 2012; von Kienlin et al. 2012). In Figure 3, we plot the temperatures of our BB+BB fits for the second and third periods along with the temperature of the single BB that best fit the first activity period. The latter is included in both panels (high and low kT) for comparison purposes. As is evident from the lower panel (high kT), the temperature of the single BB is similar to the high kT of the BB+BB model, which means that the lower kT BB is absent in the first activity period. This confirms the suggestion of von Kienlin et al. (2012) that there is a spectral evolution from the first burst active period to the other burst active periods. We note that it would be possible for the lower kT BB to be present below the detection limit of GBM, but this would still indicate a significant change in the spectral shape between the different periods. The burst peak energies, derived with the COMP (E_{peak}) and OTTB (kT) models, are presented in Figure 4 in the upper and lower panels, respectively. We observe no significant evolution across the outburst. However, the evolution of the spectral index of the COMP model (Figure 5) confirms that the bursts of the first burst period are significantly harder.

The distributions of the spectral parameters discussed above are shown in Figures 6–8 . The solid lines represent Gaussian fits, providing results similar to our prior analyses of individual periods (Table 4). We find that the BB+BB low and high temperatures center at ~4.6 and ~15.0 keV, respectively, with the width of the higher kT distribution about three times broader than the lower kT one. The apparent sub-peak around 12 kT for the high kT distribution is caused largely by bursts from the October activity period. The peak energies (Figure 7) from the COMP and OTTB models agree with each other with an average of ~40 keV. Finally, we find the COMP PL index distribution to be narrow with an average of -0.93 ± 0.02 (Figure 8). The significant tail excesses in the OTTB kT and the COMP index distributions, above ~80 keV and 0, respectively, are due to events from all three periods.

3.1.2. Energetics

The fluence range of the SGR J1550–5418 bursts covers over three orders of magnitude, from $\sim7 \times 10^{-9}$ erg cm^{-2} to at

Table 3
Time-integrated Spectral Modeling Results for SGR J1550–5418 Bursts

Burst	OTTB kT (keV)	COMP E_{peak} (keV)	α	BB+BB−Low kT (keV)	R^2 (km)	BB+BB−High kT (keV)	R^2 (km)
081003377a[a]	$44.7^{+9.1}_{-6.6}$	...	...	...	...	...	...
081003377b	$52.5^{+7.2}_{-4.2}$	...	...	...	...	...	...
081003377c[a]	$49.5^{+11.2}_{-8.4}$	...	...	...	...	...	...
081003377d[a]	$59.5^{+10.4}_{-8.8}$	...	...	...	...	...	...
081003377e[a]	$56^{+8.4}_{-6.7}$	...	...	...	...	...	...
081003377f[a]	$52.5^{+7.5}_{-5.4}$	...	...	...	...	...	...
081003377 g[a]	$54.5^{+13.4}_{-10}$	...	...	...	...	...	...
081003377 h[a]	$70.3^{+30.5}_{-0}$	...	...	...	...	...	...
081003377i[a]	$59^{+7.5}_{-5.9}$	...	...	...	...	...	...
081003377j[a]	$42.9^{+17.1}_{-0}$	...	...	...	...	...	...
081003385a	$50.5^{+11.8}_{-6.7}$	$47.4^{+3.2}_{-3.2}$	$2.91^{+1.84}_{-0.96}$	...	...	...	...
081003385b[a]	$55.7^{+6}_{-5.8}$	$49.5^{+3.9}_{-3.4}$	$0.84^{+0.97}_{-0.35}$	...	...	...	...
081003446a	$51^{+4.1}_{-4}$	$49.4^{+2.4}_{-2.2}$	$0.53^{+0.4}_{-0.36}$	...	...	...	...
081003779a	$42.9^{+3.3}_{-3.1}$	$42.4^{+2}_{-1.8}$	$0.26^{+0.33}_{-0.31}$	...	...	...	...
081004050a	$55.7^{+5.3}_{-4.7}$	$49.2^{+2.3}_{-2.1}$	$1.14^{+0.44}_{-0.4}$	...	...	...	...
081005020a	$49.3^{+8.9}_{-7.4}$	$47.9^{+5.3}_{-4.4}$	$0.3^{+0.7}_{-0.6}$	...	...	...	...
081010537a	$61.5^{+10.1}_{-8.4}$	$53.9^{+3.9}_{-3.5}$	$1.7^{+1}_{-0.7}$	...	...	...	...
090122037a	53.67 ± 8.69	51.48 ± 5.16	-0.115 ± 0.529	...	...	...	...
090122037b[a]	56.05 ± 6.11	...	...	...	...	...	...
090122037c[a]	31.98 ± 8.63	33.86 ± 7.64	-0.606 ± 1.01	...	...	...	...
090122037d[a]	36.93 ± 1.88	36.29 ± 2.4	-1.112 ± 0.17	5.469 ± 0.331	$5.65E+01 \pm 1.91E+01$	17.6 ± 1.19	$5.32E-01 \pm 2.15E-01$
090122037e[a]	51.96 ± 11	...	...	...	...	...	...
090122037f[a]	30.09 ± 5.58	31.07 ± 5.77	-0.777 ± 0.751	...	...	...	...
090122037 g[a]	34.51 ± 1.63	33.52 ± 2.21	-1.16 ± 0.158	5.383 ± 0.299	$3.16E+01 \pm 9.82E+00$	16.76 ± 1.13	$3.26E-01 \pm 1.31E-01$
090122037 h[a]	40.45 ± 9.19	...	...	...	...	...	...
090122037i[a]	30.51 ± 4.17	30.42 ± 5.38	-1.024 ± 0.514	...	...	...	...
090122037j[a]	61.17 ± 16.2	58.64 ± 6.36	1.457 ± 1.14	...	...	...	...
090122037k[a]	56.01 ± 12.5	57.1 ± 27.8	-1.621 ± 0.459	...	...	...	...
090122037 l[a]	41.29 ± 9.46	42.84 ± 6.67	-0.226 ± 0.827	...	...	...	...
090122037 m[a]	43.52 ± 8.12	45.81 ± 6.22	-0.446 ± 0.638	...	...	...	...
090122037n[a]	52.88 ± 10.3	52.58 ± 8.44	-0.709 ± 0.565	...	...	...	...
090122037o[a]	44.82 ± 2.5	45.51 ± 1.81	-0.438 ± 0.185	4.381 ± 0.492	$5.60E+01 \pm 3.58E+01$	14.33 ± 0.66	$1.50E+00 \pm 4.13E-01$
090122037p[a]	33.6 ± 7.54	34.22 ± 6.04	-0.412 ± 0.922	...	...	...	...
090122037q[a]	59.86 ± 11.4	63.36 ± 18.2	-1.363 ± 0.416	...	...	...	...
090122037r[a]	50.21 ± 5.36	50.22 ± 5.46	-1.021 ± 0.297	...	...	...	...
090122037 s[a]	54 ± 8.36	54.41 ± 9.54	-1.134 ± 0.4	...	...	...	...
090122037t[a]	50.45 ± 8.43	49.79 ± 6.44	-0.569 ± 0.49	...	...	...	...
090122037u[a]	27.62 ± 0.94	27.18 ± 1.41	-1.062 ± 0.133	4.365 ± 0.233	$8.99E+01 \pm 2.72E+01$	12.37 ± 0.55	$1.72E+00 \pm 4.71E-01$
090122037v[a,b]	35.15 ± 2	37.54 ± 1.54	-0.37 ± 0.22	4.707 ± 0.587	$9.94E+01 \pm 6.92E+01$	12.85 ± 0.78	$3.87E+00 \pm 1.46E+00$
090122037w[a]	33.68 ± 4.03	33.45 ± 4.89	-1.041 ± 0.414	...	...	...	...
090122037x[a]	62.4 ± 9.26	61.97 ± 9.33	-0.949 ± 0.353	...	...	...	...
090122037y[a]	47.68 ± 11	46.24 ± 7.66	-0.435 ± 0.836	...	...	...	...
090122037z[a,b]	32.1 ± 1.38	31.75 ± 1.95	-1.047 ± 0.165	5.266 ± 0.282	$1.24E+02 \pm 3.72E+01$	16.3 ± 1.06	$1.19E+00 \pm 4.65E-01$
090122037aa[a]	38.53 ± 4.17	38.56 ± 4.36	-0.991 ± 0.353	...	...	...	...
090122037ab[a]	62.04 ± 12	62.6 ± 16.9	-1.284 ± 0.478	...	...	...	...
090122037ac[a,b]	39.62 ± 1.16	40.19 ± 1.09	-0.847 ± 0.098	4.115 ± 0.21	$5.42E+01 \pm 1.60E+01$	13.91 ± 0.36	$9.58E-01 \pm 1.48E-01$
090122037ad[a]	49.19 ± 11.3	48.36 ± 7.95	-0.403 ± 0.749	...	...	...	...
090122037ae[a]	52.83 ± 7.56	48.91 ± 3.46	0.644 ± 0.591	...	...	...	...
090122037af[a]	58.83 ± 10.7	62.21 ± 14.7	-1.234 ± 0.412	...	...	...	...
090122037ag[a]	77.14 ± 25.2	67.64 ± 11.8	0.454 ± 1.01	...	...	...	...
090122037ah[a]	40.33 ± 6.76	41.41 ± 3.39	0.733 ± 0.745	...	...	...	...
090122037ai[a]	47.61 ± 4.82	47.77 ± 4.48	-0.898 ± 0.298	...	...	...	...
090122037aj[a]	31.67 ± 1.07	31.75 ± 1.3	-0.984 ± 0.124	5.192 ± 0.227	$3.30E+01 \pm 8.04E+00$	15.03 ± 0.76	$4.55E-01 \pm 1.40E-01$
090122037ak[a]	46.28 ± 3.59	46.46 ± 3.88	-1.092 ± 0.217	...	...	...	...
090122037al[a,b]	33.18 ± 1.12	37.23 ± 0.69	0.278 ± 0.144	5.872 ± 0.598	$1.14E+02 \pm 6.26E+01$	12.19 ± 0.63	$1.16E+01 \pm 4.09E+00$
090122037am[a]	34.59 ± 2.85	34.53 ± 3.35	-1.01 ± 0.284	4.881 ± 0.572	$6.24E+01 \pm 4.11E+01$	14.71 ± 1.46	$1.01E+00 \pm 6.05E-01$
090122044a[a]	57.07 ± 4.32	55.99 ± 3.66	-0.715 ± 0.2	4.338 ± 0.488	$1.38E+01 \pm 8.91E+00$	17.07 ± 0.93	$1.84E-01 \pm 5.80E-02$
090122044b	42.44 ± 2.2	43.05 ± 1.86	-0.727 ± 0.168	5.117 ± 0.396	$2.53E+01 \pm 1.09E+01$	16.01 ± 0.9	$4.62E-01 \pm 1.55E-01$
090122044c[a]	35.75 ± 2.14	36.46 ± 1.9	-0.719 ± 0.211	5.428 ± 0.465	$1.71E+01 \pm 8.08E+00$	15.07 ± 1.3	$3.38E-01 \pm 1.78E-01$
090122044d[a]	59.65 ± 3.85	56.48 ± 2.56	-0.329 ± 0.183	4.318 ± 0.502	$1.65E+01 \pm 1.10E+01$	16.49 ± 0.71	$3.25E-01 \pm 8.12E-02$
090122044e[a]	66.34 ± 11.3	60.9 ± 7.55	-0.418 ± 0.472	...	...	...	...
090122044f[a]	56.81 ± 10.2	51.31 ± 4.39	0.764 ± 0.662	...	...	...	...
090122044 g[a]	55.21 ± 2.63	53.53 ± 1.89	-0.481 ± 0.138	5.049 ± 0.397	$1.29E+01 \pm 5.68E+00$	16.93 ± 0.68	$2.93E-01 \pm 6.92E-02$

Table 3
(Continued)

Burst	OTTB kT (keV)	COMP E_{peak} (keV)	α	BB+BB−Low kT (keV)	BB+BB−Low R^2 (km)	BB+BB−High kT (keV)	BB+BB−High R^2 (km)
090122044 h[a]	42.38 ± 4.1	42.27 ± 4.28	−1.048 ± 0.284	⋯	⋯	⋯	⋯
090122044i[a]	36.48 ± 1.67	36.59 ± 1.81	−0.979 ± 0.155	4.949 ± 0.308	4.08E+01 ± 1.42E+01	15.7 ± 0.87	5.26E-01 ± 1.75E-01
090122044j[a]	41.5 ± 9.01	41.71 ± 8.59	−0.909 ± 0.656	⋯	⋯	⋯	⋯
090122044k[a]	40 ± 2.4	41.1 ± 1.85	−0.523 ± 0.208	5.528 ± 0.54	3.35E+01 ± 1.80E+01	15.36 ± 1.15	8.65E-01 ± 3.95E-01
090122044 l[a]	25.18 ± 2.78	28.16 ± 2.32	−0.126 ± 0.545	⋯	⋯	⋯	⋯
090122044 m[a,b]	34.28 ± 0.6	36.25 ± 0.5	−0.516 ± 0.066	5.211 ± 0.157	9.42E+01 ± 1.57E+01	13.88 ± 0.31	2.65E+00 ± 3.70E-01
090122044n[a]	45.38 ± 6.3	44.76 ± 4.05	−0.179 ± 0.475	⋯	⋯	⋯	⋯
090122052a[a]	60.51 ± 6.61	61.09 ± 8.08	−1.126 ± 0.256	⋯	⋯	⋯	⋯
090122052b	42.45 ± 1.57	43.32 ± 1.32	−0.716 ± 0.121	4.776 ± 0.268	7.55E+01 ± 2.39E+01	15.76 ± 0.57	1.24E+00 ± 2.66E-01
090122052c[a]	87.31 ± 13.3	73.6 ± 7.14	−0.117 ± 0.346	⋯	⋯	⋯	⋯
090122052d[a]	63.93 ± 11.6	60.77 ± 9.98	−0.813 ± 0.44	⋯	⋯	⋯	⋯
090122052e[a,b]	40.76 ± 0.72	42.44 ± 0.53	−0.444 ± 0.061	5.8 ± 0.171	9.33E+01 ± 1.51E+01	15.77 ± 0.34	2.59E+00 ± 3.44E-01
090122052f[a]	42.87 ± 7.15	42.58 ± 6.24	−0.805 ± 0.516	⋯	⋯	⋯	⋯
090122052 g[a]	45.36 ± 7.22	45.51 ± 7.68	−1.074 ± 0.442	⋯	⋯	⋯	⋯
090122052 h[a]	29.72 ± 1.34	28.27 ± 2.26	−1.209 ± 0.158	5.142 ± 0.269	8.25E+01 ± 2.42E+01	15.66 ± 1.05	7.59E-01 ± 3.09E-01
090122052i[a]	61.45 ± 12.5	⋯	⋯	⋯	⋯	⋯	⋯
090122052j[a]	52.53 ± 12.5	51.66 ± 11.2	−0.837 ± 0.668	⋯	⋯	⋯	⋯
090122052k[a]	39.78 ± 1.58	39.82 ± 1.6	−0.981 ± 0.123	5.37 ± 0.271	1.61E+01 ± 4.53E+00	16.61 ± 0.85	2.24E-01 ± 6.84E-02
090122052 l[a]	29.65 ± 3.54	27.33 ± 5.83	−1.331 ± 0.387	⋯	⋯	⋯	⋯
090122052 m[a]	58.36 ± 6.09	58.64 ± 6.9	−1.049 ± 0.255	⋯	⋯	⋯	⋯
090122052n[a]	43.84 ± 2.74	44.23 ± 1.88	−0.374 ± 0.212	5.51 ± 0.612	5.65E+01 ± 1.91E+01	15.4 ± 1.08	5.65E+01 ± 1.91E+01
090122052o[a]	44.39 ± 2.66	43.62 ± 3.18	−1.193 ± 0.172	4.688 ± 0.342	6.24E+01 ± 2.60E+01	17.85 ± 1.04	4.75E-01 ± 1.61E-01
090122052p[a]	37.83 ± 3.95	38.44 ± 3.09	−0.551 ± 0.347	⋯	⋯	⋯	⋯
090122052q[a,b]	27.33 ± 0.7	27.14 ± 1.09	−1.027 ± 0.1	5.303 ± 0.156	1.33E+02 ± 2.18E+01	15.59 ± 0.69	1.12E+00 ± 3.04E-01
090122052r[a]	88.89 ± 21.9	90.83 ± 30.2	−1.043 ± 0.439	⋯	⋯	⋯	⋯
090122052 s[a]	65.86 ± 17.2	55.45 ± 8.15	0.182 ± 0.825	⋯	⋯	⋯	⋯
090122052t[a]	40.89 ± 8.34	42.59 ± 16.5	−1.526 ± 0.474	⋯	⋯	⋯	⋯
090122052u[a]	48.52 ± 2.46	48.09 ± 1.8	−0.501 ± 0.154	4.688 ± 0.405	2.01E+01 ± 9.79E+00	15.38 ± 0.67	4.86E-01 ± 1.25E-01
090122052v[a]	37.65 ± 1.9	37.88 ± 1.88	−0.895 ± 0.165	6.342 ± 0.319	1.38E+01 ± 3.81E+00	20.31 ± 1.8	9.47E-02 ± 4.95E-02
090122052w[a]	48.58 ± 8.64	⋯	⋯	⋯	⋯	⋯	⋯
090122052x[a]	69.42 ± 12.8	61.34 ± 6.77	−0.024 ± 0.519	⋯	⋯	⋯	⋯
090122052y[a]	37.8 ± 5.84	⋯	⋯	⋯	⋯	⋯	⋯
090122052z[a]	66.02 ± 16.9	⋯	⋯	⋯	⋯	⋯	⋯
090122052aa[a,b]	34.1 ± 0.91	36.49 ± 0.67	−0.274 ± 0.103	5.425 ± 0.283	8.43E+01 ± 2.41E+01	13.27 ± 0.47	3.53E+00 ± 7.99E-01
090122052ab[a]	80.67 ± 20.4	66.86 ± 11	−0.134 ± 0.611	⋯	⋯	⋯	⋯
090122059a	30.06 ± 1.83	27.45 ± 3.31	−1.416 ± 0.185	4.788 ± 0.259	1.61E+01 ± 4.94E+00	16.95 ± 1.52	9.25E-02 ± 4.80E-02
090122059b[a,b]	38.62 ± 0.95	39.82 ± 0.76	−0.589 ± 0.08	5.407 ± 0.194	5.75E+01 ± 1.14E+01	15.39 ± 0.46	1.26E+00 ± 2.29E-01
090122059c[a]	51.64 ± 2.41	51.73 ± 2.56	−1.029 ± 0.114	4.088 ± 0.228	3.92E+01 ± 1.27E+01	16.91 ± 0.58	3.42E-01 ± 6.74E-02
090122059d[a]	44.22 ± 9.29	41.54 ± 3.73	1 ± 0.849	⋯	⋯	⋯	⋯
090122104a[f]	33.1 ± 1.39	34.2 ± 1.38	−0.743 ± 0.159	5.501 ± 0.309	6.49E+01 ± 2.02E+01	15.54 ± 1.03	9.50E-01 ± 3.84E-01
090122104b[a,f]	30.99 ± 0.73	34.02 ± 0.55	−0.158 ± 0.096	5.742 ± 0.262	1.24E+02 ± 3.08E+01	12.87 ± 0.51	5.52E+00 ± 1.44E+00
090122104c[a]	41.44 ± 1.69	41.1 ± 1.86	−1.111 ± 0.121	4.612 ± 0.236	3.15E+01 ± 9.17E+00	16.36 ± 0.68	3.28E-01 ± 7.98E-02
090122104d[a]	49.79 ± 6.66	50.36 ± 7.94	−1.161 ± 0.338	⋯	⋯	⋯	⋯
090122104e[a]	27.38 ± 3.68	27.77 ± 5	−0.934 ± 0.57	⋯	⋯	⋯	⋯
090122113a	60.96 ± 4.39	63.01 ± 6.95	−1.357 ± 0.161	4.67 ± 0.354	6.21E+01 ± 2.71E+01	21.76 ± 1.26	2.71E-01 ± 8.92E-02
090122113b[a]	44.94 ± 3.05	45.59 ± 2.48	−0.674 ± 0.21	4.483 ± 0.501	4.92E+01 ± 3.12E+01	15.31 ± 0.89	9.03E-01 ± 3.11E-01
090122113c[a]	38.65 ± 2.12	40.13 ± 1.49	−0.326 ± 0.204	5.221 ± 0.534	2.32E+01 ± 1.31E+01	14.14 ± 0.94	8.00E-01 ± 3.28E-01
090122120a	39.06 ± 2.09	40.02 ± 1.6	−0.533 ± 0.189	5.1 ± 0.45	2.65E+01 ± 1.30E+01	14.66 ± 0.04	6.68E-01 ± 2.08E-01
090122120b[a]	45.62 ± 7.63	42.09 ± 5.19	−0.441 ± 0.537	⋯	⋯	⋯	⋯
090122120d[a]	81.37 ± 14.5	63.75 ± 7.2	−0.123 ± 0.454	⋯	⋯	⋯	⋯
090122120e[a]	37.7 ± 4.72	37.77 ± 3.22	−0.279 ± 0.444	⋯	⋯	⋯	⋯
090122120f[a]	80.21 ± 18.7	⋯	⋯	⋯	⋯	⋯	⋯
090122120 g[a]	90.17 ± 31.1	⋯	⋯	⋯	⋯	⋯	⋯
090122120 h[a]	42.59 ± 5.32	42.27 ± 7.03	−1.285 ± 0.334	⋯	⋯	⋯	⋯
090122173a	40.97 ± 3.15	41.82 ± 2.69	−0.725 ± 0.248	⋯	⋯	⋯	⋯
090122173b[a,f]	25.91 ± 0.69	26.09 ± 0.94	−0.967 ± 0.108	4.88 ± 0.161	3.66E+01 ± 6.75E+00	13.72 ± 0.65	4.49E-01 ± 1.30E-01
090122173c[a,b]	47.73 ± 4.47	47.8 ± 4.13	−0.872 ± 0.269	⋯	⋯	⋯	⋯
090122173d[a]	57.55 ± 7.19	54.85 ± 5.47	−0.568 ± 0.338	⋯	⋯	⋯	⋯
090122173e[a]	31.96 ± 0.81	32.07 ± 0.92	−0.976 ± 0.09	4.983 ± 0.166	3.32E+01 ± 6.16E+00	14.5 ± 0.52	5.03E-01 ± 1.09E-01
090122173f[a]	29.26 ± 1.25	29.55 ± 1.61	−0.945 ± 0.165	5.607 ± 0.251	5.49E+01 ± 1.37E+01	17.25 ± 1.4	3.71E-01 ± 1.81E-01
090122173 g[a]	30.13 ± 1.69	29.19 ± 2.56	−1.154 ± 0.198	5.591 ± 0.307	4.97E+01 ± 1.53E+01	18.3 ± 1.82	2.72E-01 ± 1.60E-01
090122173 h[a]	59.33 ± 7.99	56.74 ± 6.51	−0.676 ± 0.352	⋯	⋯	⋯	⋯
090122180a	33.03 ± 1.6	32.66 ± 1.95	−1.058 ± 0.169	4.527 ± 0.304	6.40E+01 ± 2.44E+01	14.25 ± 0.82	8.94E-01 ± 3.08E-01
090122180b[a]	39.63 ± 1.61	40.82 ± 1.09	−0.248 ± 0.147	⋯	⋯	⋯	⋯
090122180c[a]	56.62 ± 7.6	58.02 ± 11.3	−1.3 ± 0.309	⋯	⋯	⋯	⋯

13

Table 3
(Continued)

Burst	OTTB kT (keV)	COMP E_{peak} (keV)	α	BB+BB−Low kT (keV)	R^2 (km)	BB+BB−High kT (keV)	R^2 (km)
090122180d[a]	35.62 ± 3.24	36.56 ± 2.21	−0.206 ± 0.349	⋯	⋯	⋯	⋯
090122180e[a]	42.19 ± 2.49	41.89 ± 2.67	−1.089 ± 0.175	4.172 ± 0.324	4.52E+01 ± 2.03E+01	15.59 ± 0.83	4.62E-01 ± 1.44E-01
090122180f[a]	68.66 ± 14.4	⋯	⋯	⋯	⋯	⋯	⋯
090122180 g[a]	35.07 ± 1.83	35.91 ± 1.79	−0.819 ± 0.192	5.196 ± 0.364	5.08E+01 ± 1.98E+01	15.6 ± 1.17	7.24E-01 ± 3.27E-01
090122180 h[a]	45.28 ± 4.57	45.3 ± 4.14	−0.869 ± 0.309	⋯	⋯	⋯	⋯
090122180i[a]	41.41 ± 4.59	42.31 ± 3.65	−0.611 ± 0.383	⋯	⋯	⋯	⋯
090122180j[a]	40.73 ± 4.41	41.32 ± 3.74	−0.723 ± 0.349	⋯	⋯	⋯	⋯
090122187a	40.44 ± 2.5	40.73 ± 2.3	−0.872 ± 0.194	4.336 ± 0.377	2.28E+01 ± 1.13E+01	14.78 ± 0.87	3.46E-01 ± 1.20E-01
090122187b[a]	63.8 ± 7.07	58.93 ± 4.72	−0.402 ± 0.285	⋯	⋯	⋯	⋯
090122187c[a]	44.84 ± 11.5	43.96 ± 7.45	−0.255 ± 0.835	⋯	⋯	⋯	⋯
090122187d[a,b]	33.58 ± 0.81	34.98 ± 0.77	−0.708 ± 0.09	5.298 ± 0.189	9.61E+01 ± 1.90E+01	14.78 ± 0.5	1.81E+00 ± 3.77E-01
090122187e[a]	40.47 ± 9.07	40.45 ± 9.2	−1.019 ± 0.622	⋯	⋯	⋯	⋯
090122187f[a]	46.46 ± 4.84	46.4 ± 4.87	−0.979 ± 0.282	4.763 ± 0.584	5.70E+00 ± 3.94E+00	16.82 ± 1.71	7.08E-02 ± 4.17E-02
090122187 g[a]	46.6 ± 4.65	46.44 ± 4.95	−1.075 ± 0.279	⋯	⋯	⋯	⋯
090122187 h[a]	25.59 ± 2.28	26.45 ± 2.59	−0.765 ± 0.374	⋯	⋯	⋯	⋯
090122187i[a]	44.45 ± 1.83	44.28 ± 2.05	−1.141 ± 0.113	4.396 ± 0.224	3.04E+01 ± 8.87E+00	16.32 ± 0.62	3.12E-01 ± 6.87E-02
090122187j[a]	33.91 ± 4.24	31.72 ± 6.38	−1.384 ± 0.354	⋯	⋯	⋯	⋯
090122187 l[a]	36.78 ± 2.22	36.82 ± 2.28	−0.985 ± 0.188	4.923 ± 0.38	2.65E+01 ± 1.15E+01	15.02 ± 1.07	4.28E-01 ± 1.82E-01
090122187 m[a]	57.12 ± 5.77	59.39 ± 8.21	−1.195 ± 0.219	5.128 ± 0.477	5.37E+01 ± 2.82E+01	21 ± 1.93	3.60E-02 ± 1.87E-02
090122187n[a,b]	30.1 ± 0.94	32.88 ± 0.67	−0.065 ± 0.129	5.904 ± 0.332	6.65E+01 ± 2.03E+01	12.87 ± 0.77	2.71E+00 ± 1.07E+00
090122187o[a]	42.76 ± 4.48	43.79 ± 3.11	−0.32 ± 0.328	⋯	⋯	⋯	⋯
090122187p[a]	46.18 ± 3.68	45.82 ± 3.15	−0.759 ± 0.22	4.892 ± 0.501	8.98E+00 ± 5.15E+00	15.87 ± 1.19	1.73E-01 ± 7.58E-02
090122187q[a]	41.66 ± 4.09	41.71 ± 4.9	−1.205 ± 0.263	5.204 ± 0.499	1.11E+01 ± 5.95E+00	18.48 ± 2.12	8.88E-02 ± 5.87E-02
090122187 s[a]	45.16 ± 4.32	44.92 ± 3.04	−0.423 ± 0.288	⋯	⋯	⋯	⋯
090122187t[a,b]	34.53 ± 0.97	35.65 ± 0.91	−0.727 ± 0.099	5.362 ± 0.212	1.09E+02 ± 2.38E+01	15 ± 0.56	2.03E+00 ± 4.65E-01
090122187u[a,b]	45.1 ± 1.34	44.86 ± 1.06	−0.654 ± 0.088	4.867 ± 0.222	2.35E+01 ± 6.00E+00	15.19 ± 0.42	5.45E-01 ± 8.98E-02
090122194a[a]	21.14 ± 4.89	19.69 ± 10	−1.201 ± 1.06	⋯	⋯	⋯	⋯
090122194b[a]	55.97 ± 5.7	52.66 ± 4.08	−0.514 ± 0.266	⋯	⋯	⋯	⋯
090122194c	39.67 ± 2.26	39.8 ± 1.99	−0.809 ± 0.175	3.936 ± 0.36	5.99E+01 ± 3.17E+01	13.39 ± 0.68	1.07E+00 ± 3.21E-01
090122194d[a]	36.37 ± 2.65	34.65 ± 3.61	−1.311 ± 0.215	4.01 ± 0.327	4.11E+01 ± 1.95E+01	15.15 ± 1.09	3.26E-01 ± 1.36E-01
090122194e[a]	64.64 ± 15	67.8 ± 23.7	−1.236 ± 0.466	⋯	⋯	⋯	⋯
090122194f[a]	101.1 ± 42.2	⋯	⋯	⋯	⋯	⋯	⋯
090122194 g[a,b]	40.73 ± 2.35	40.81 ± 2.21	−0.916 ± 0.171	4.822 ± 0.364	2.66E+01 ± 1.13E+01	15.41 ± 0.95	4.29E-01 ± 1.56E-01
090122194 h[a]	51.01 ± 9.85	53.35 ± 14.7	−1.3 ± 0.423	⋯	⋯	⋯	⋯
090122194i[a]	29.74 ± 0.79	30.66 ± 0.9	−0.817 ± 0.1	5.525 ± 0.172	9.92E+01 ± 1.71E+01	15.65 ± 0.7	1.09E+00 ± 2.99E-01
090122194j[a]	39.73 ± 7.2	38.89 ± 5.78	−0.693 ± 0.561	⋯	⋯	⋯	⋯
090122194k[a]	60.78 ± 4.88	56.51 ± 3.8	−0.594 ± 0.193	4.562 ± 0.511	4.97E+01 ± 3.16E+01	16.49 ± 0.95	1.01E-01 ± 3.33E-02
090122194 l[a]	36.84 ± 4.24	37 ± 3.89	−0.866 ± 0.344	⋯	⋯	⋯	⋯
090122194 m[a]	57.92 ± 9.34	57.67 ± 10.2	−0.971 ± 0.358	⋯	⋯	⋯	⋯
090122194n[a]	32.95 ± 1.15	33.71 ± 1.11	−0.818 ± 0.122	4.328 ± 0.234	1.01E+02 ± 3.09E+01	13 ± 0.48	2.09E+00 ± 4.69E-01
090122194o[a]	67.56 ± 10.9	60.25 ± 7.15	−0.44 ± 0.372	⋯	⋯	⋯	⋯
090122194p[a]	43.63 ± 1.55	43.61 ± 1.64	−1.069 ± 0.097	4.713 ± 0.202	2.72E+01 ± 6.58E+00	16.35 ± 0.56	3.33E-01 ± 6.68E-02
090122194q[a]	40.02 ± 8.55	40.14 ± 11.3	−1.303 ± 0.531	⋯	⋯	⋯	⋯
090122194r[a]	29.28 ± 1.46	29.96 ± 1.57	−0.843 ± 0.184	5.023 ± 0.325	4.98E+01 ± 1.79E+01	13.8 ± 1.05	8.29E-01 ± 3.87E-01
090122194 s[a]	45.47 ± 4.7	44.85 ± 3.09	−0.335 ± 0.32	⋯	⋯	⋯	⋯
090122194t[a]	66.23 ± 13.5	59.38 ± 7.78	−0.113 ± 0.516	⋯	⋯	⋯	⋯
090122218a[a]	16.5 ± 3.21	19.04 ± 3.44	−0.265 ± 1.17	⋯	⋯	⋯	⋯
090122218b	53.96 ± 6.73	57.66 ± 10.1	−1.235 ± 0.249	⋯	⋯	⋯	⋯
090122218c[a]	35.88 ± 3.13	33.06 ± 4.71	−1.398 ± 0.249	3.892 ± 0.364	3.42E+01 ± 1.87E+01	15.34 ± 1.3	2.30E-01 ± 1.13E-01
090122218d[a]	64.34 ± 9.73	60.23 ± 7.33	−0.557 ± 0.36	⋯	⋯	⋯	⋯
090122218f[a,b]	16.67 ± 0.3	16.36 ± 0.73	−1.047 ± 0.097	3.367 ± 0.117	2.54E+02 ± 5.15E+01	8.45 ± 0.25	6.64E+00 ± 1.26E+00
090122218 g[a]	58.19 ± 9.47	59.79 ± 13.3	−1.182 ± 0.35	⋯	⋯	⋯	⋯
090122218 h[a]	24.23 ± 1.88	19.2 ± 5.16	−1.498 ± 0.272	3.928 ± 0.388	1.02E+02 ± 5.80E+01	11.92 ± 1.21	1.29E+00 ± 7.92E-01
090122218i[a]	40.84 ± 7.89	40.65 ± 9.37	−1.2 ± 0.5	⋯	⋯	⋯	⋯
090122218j[a]	30.47 ± 2.66	29.83 ± 3.5	−1.138 ± 0.299	⋯	⋯	⋯	⋯
090122218k[a]	17.7 ± 1.66	18.58 ± 2.64	−0.786 ± 0.496	⋯	⋯	⋯	⋯
090122218 l[a]	24.94 ± 2.25	23.34 ± 3.72	−1.224 ± 0.333	⋯	⋯	⋯	⋯
090122218 m[a]	20.16 ± 1.62	⋯	⋯	⋯	⋯	⋯	⋯
090122218n[a]	40.03 ± 4.24	39.69 ± 5.37	−1.273 ± 0.268	4.215 ± 0.423	6.69E+00 ± 3.87E+00	16.25 ± 1.67	5.31E-02 ± 3.12E-02
090122218o[a,b]	32.59 ± 0.59	35.63 ± 0.4	−0.066 ± 0.069	4.52 ± 0.211	2.74E+02 ± 7.14E+01	11.45 ± 0.2	1.82E+01 ± 2.02E+00
090122218p[a]	23.38 ± 0.87	15.43 ± 3.46	−1.675 ± 0.125	4.179 ± 0.149	4.67E+01 ± 9.59E+00	14.25 ± 0.79	2.77E-01 ± 9.06E-02
090122218q[a]	45.76 ± 5.03	44.78 ± 3.3	−0.262 ± 0.339	⋯	⋯	⋯	⋯
090122218r[a,b]	21.17 ± 0.53	22.76 ± 0.76	−0.716 ± 0.12	4.273 ± 0.179	2.21E+02 ± 5.20E+01	10.48 ± 0.44	5.52E+00 ± 1.49E+00
090122218 s[a]	18.48 ± 0.73	18.03 ± 1.65	−1.069 ± 0.197	4.119 ± 0.208	1.57E+02 ± 4.51E+01	11.05 ± 0.86	1.87E+00 ± 9.04E-01
090122218t[a]	63.29 ± 12	56.1 ± 7.55	−0.317 ± 0.483	⋯	⋯	⋯	⋯

14

Table 3
(Continued)

| Burst	OTTB kT (keV)	COMP E_{peak} (keV)	α	BB+BB−Low kT (keV)	BB+BB−Low R^2 (km)	BB+BB−High kT (keV)	BB+BB−High R^2 (km)
090122218u[a]	34.47 ± 2.02	32.15 ± 2.91	−1.305 ± 0.183	4.226 ± 0.276	5.31E+01 ± 2.00E+01	15.39 ± 0.97	4.24E−01 ± 1.56E−01
090122218v[a]	22.42 ± 1.62	21.21 ± 2.98	−1.171 ± 0.3	3.908 ± 0.401	6.81E+01 ± 4.00E+01	11.11 ± 1.19	1.10E+00 ± 7.23E−01
090122243a	36.17 ± 2.62	37.83 ± 1.95	−0.407 ± 0.272	...	...	...	...
090122243b[a]	24.47 ± 2.51	25.83 ± 2.82	−0.746 ± 0.439	...	...	...	...
090122252a[b]	25.3 ± 0.4	26.89 ± 0.51	−0.724 ± 0.067	5.217 ± 0.111	2.68E+02 ± 3.16E+01	13.41 ± 0.39	4.04E+00 ± 7.48E−01
090122252b[a]	22.14 ± 1.34	21.05 ± 2.67	−1.16 ± 0.261	...	...	...	...
090122283a[a,b]	24.28 ± 0.41	24.63 ± 0.6	−0.941 ± 0.071	4.681 ± 0.1	8.61E+01 ± 1.03E+01	12.93 ± 0.37	1.12E+00 ± 1.98E−01
090122283b[a,b]	17.41 ± 0.18	19.15 ± 0.3	−0.655 ± 0.057	4.139 ± 0.07	1.84E+02 ± 1.75E+01	9.56 ± 0.22	4.21E+00 ± 6.34E−01
090122283c[a]	25.17 ± 2.45	...	...	...	...	...	...
090122283d[a]	31.4 ± 1.47	17.55 ± 6.76	−1.78 ± 0.138	3.802 ± 0.186	1.43E+02 ± 4.14E+01	15.66 ± 0.79	5.84E−01 ± 1.71E−01
090122283e[a]	27.45 ± 0.97	29.06 ± 1.02	−0.677 ± 0.146	4.231 ± 0.263	1.22E+02 ± 4.28E+01	11.52 ± 0.51	3.27E+00 ± 8.93E−01
090122283f[a]	28.54 ± 1.49	26.8 ± 2.45	−1.248 ± 0.183	4.406 ± 0.273	4.48E+01 ± 1.58E+01	13.98 ± 0.95	4.67E−01 ± 1.89E−01
090122283 g[a,b]	19.58 ± 0.36	20.72 ± 0.58	−0.795 ± 0.092	3.991 ± 0.128	1.50E+02 ± 2.73E+01	9.76 ± 0.32	3.89E+00 ± 8.15E−01
090122283 h[a,b]	21.82 ± 0.46	18.38 ± 1.25	−1.395 ± 0.083	4.259 ± 0.1	1.03E+02 ± 1.38E+01	12.81 ± 0.43	8.89E−01 ± 1.82E−01
090122283j[a]	32.45 ± 2.5	30.38 ± 3.74	−1.28 ± 0.25	4.362 ± 0.406	4.37E+01 ± 2.32E+01	14.77 ± 1.33	4.25E−01 ± 2.27E−01
090122283 l[a,b]	28.6 ± 0.54	27.28 ± 0.9	−1.164 ± 0.07	4.809 ± 0.109	2.21E+02 ± 2.83E+01	14.8 ± 0.39	2.13E+00 ± 3.43E−01
090122283 m[a,b]	21.66 ± 0.46	20.78 ± 0.94	−1.118 ± 0.093	4.411 ± 0.118	1.93E+02 ± 2.93E+01	12.22 ± 0.45	2.26E+00 ± 5.16E−01
090122283n[a]	28.54 ± 2.12	26.49 ± 3.48	−1.251 ± 0.261	3.683 ± 0.397	1.03E+02 ± 6.52E+01	12.12 ± 0.91	1.39E+00 ± 6.28E−01
090122283o[a]	41.66 ± 1.77	41.59 ± 1.81	−1.029 ± 0.124	4.185 ± 0.238	4.12E+01 ± 1.35E+01	15.12 ± 0.56	4.98E−01 ± 1.08E−01
090122283p[a]	29.63 ± 1.99	22.89 ± 5.57	−1.596 ± 0.21	3.814 ± 0.296	7.06E+01 ± 3.21E+01	13.91 ± 1.04	5.07E−01 ± 2.22E−01
090122283q[a]	28.99 ± 1.07	26.9 ± 1.92	−1.262 ± 0.129	5.334 ± 0.203	8.10E+01 ± 1.72E+01	16.89 ± 1.05	5.34E−01 ± 1.99E−01
090122283r[a]	9.56 ± 0.51	8.55 ± 2.86	−1.19 ± 0.463	...	...	...	...
090122283t[a]	26 ± 1.39	16.4 ± 6.04	−1.746 ± 0.158	3.882 ± 0.221	3.13E+01 ± 1.04E+01	13.41 ± 0.89	2.38E−01 ± 9.27E−02
090122283v[a]	27.94 ± 1.1	28.26 ± 1.33	−0.939 ± 0.146	3.807 ± 0.266	1.02E+02 ± 4.13E+01	11.06 ± 0.46	2.55E+00 ± 6.49E−01
090122283w[a]	59.57 ± 16.4	58.81 ± 17.1	−0.941 ± 0.642	...	...	...	...
090122283y[a]	26.62 ± 2.05	26.18 ± 2.9	−1.065 ± 0.299	3.904 ± 0.435	6.71E+01 ± 4.32E+01	11.81 ± 1.09	1.10E+00 ± 6.14E−01
090122283z[a]	12.7 ± 1.36	...	...	...	...	...	...
090122283aa[a]	13.18 ± 0.58	...	...	3.681 ± 0.127	7.78E+01 ± 1.59E+01	13.42 ± 1.27	1.74E−01 ± 9.68E−02
090122283ab[a]	52.36 ± 11.5	53.31 ± 17.8	−1.374 ± 0.52	...	...	...	...
090122283ac[a]	44.56 ± 7.99	44.57 ± 7.98	−0.994 ± 0.506	...	...	...	...
090122283ad[a]	46.98 ± 5.76	46.36 ± 8.14	−1.363 ± 0.305	...	...	...	...
090122283ae[a]	45.18 ± 4.34	45.2 ± 4.49	−1.031 ± 0.259	4.354 ± 0.501	7.07E+00 ± 4.67E+00	15.99 ± 1.34	8.08E−02 ± 3.91E−02
090122283ag[a,b]	18.85 ± 0.25	8.91 ± 1.5	−1.758 ± 0.056	3.887 ± 0.058	2.42E+02 ± 2.11E+01	12.26 ± 0.27	1.53E+00 ± 2.03E−01
090122283ah[a]	33.75 ± 1.03	27.8 ± 2.4	−1.569 ± 0.088	3.85 ± 0.133	6.35E+01 ± 1.29E+01	14.77 ± 0.45	4.22E−01 ± 7.49E−02
090122283ai[a]	29.63 ± 1.32	27.84 ± 2.11	−1.222 ± 0.161	4.075 ± 0.235	9.88E+01 ± 3.30E+01	13.57 ± 0.69	1.02E+00 ± 3.09E−01
090122291a	43.36 ± 3.14	42.84 ± 3.67	−1.191 ± 0.204	4.069 ± 0.348	3.52E+01 ± 1.76E+01	16.26 ± 1.04	2.66E−01 ± 9.79E−02
090122291b[a]	28.99 ± 2.34	24.47 ± 5.33	−1.473 ± 0.26	3.699 ± 0.417	1.05E+02 ± 6.97E+01	12.37 ± 1.06	1.24E+00 ± 6.32E−01
090122291d[a]	40.61 ± 6.03	41.44 ± 4.64	−0.539 ± 0.518	...	...	...	...
090122291e[a]	39.04 ± 4.82	37.36 ± 6.83	−1.361 ± 0.33	...	...	...	...
090122291f[a]	33.41 ± 5.07	...	...	...	...	...	...
090122291 g[a]	66.04 ± 10.8	70.06 ± 18.2	−1.33 ± 0.322	...	...	...	...
090122291 h[a]	47.64 ± 5.55	46.59 ± 7.68	−1.361 ± 0.294	...	...	...	...
090122291i[a]	37.18 ± 3.99	37.31 ± 4.11	−0.968 ± 0.339	...	...	...	...
090122310a[b]	43.51 ± 1.24	43.36 ± 1.42	−1.166 ± 0.079	4.557 ± 0.151	2.83E+01 ± 5.36E+00	16.73 ± 0.47	2.71E−01 ± 4.41E−02
090122310b[a]	37.59 ± 1.42	35.75 ± 2.03	−1.35 ± 0.108	3.868 ± 0.18	6.77E+01 ± 1.84E+01	14.75 ± 0.52	5.68E−01 ± 1.16E−01
090122317a[b]	30.43 ± 0.71	30.89 ± 0.83	−0.92 ± 0.088	4.803 ± 0.154	1.05E+02 ± 1.89E+01	14.05 ± 0.46	1.56E+00 ± 3.11E−01
090122317b[a]	55 ± 4.26	54.17 ± 3.86	−0.801 ± 0.196	...	...	...	...
090122317c[a]	23.59 ± 4.67	27.73 ± 2.41	1.786 ± 1.35	...	...	...	...
090122317d[a]	33.33 ± 2.14	33.98 ± 2.19	−0.896 ± 0.235	3.253 ± 0.355	1.03E+02 ± 6.79E+01	12.31 ± 0.64	1.17E+00 ± 3.59E−01
090122352a	39.21 ± 4.97	39.91 ± 4.43	−0.803 ± 0.417	...	...	...	...
090122352b[a]	21.84 ± 1.52	23.89 ± 1.63	−0.397 ± 0.355	...	...	...	...
090122359b[a]	26.96 ± 1.61	18.73 ± 5.32	−1.618 ± 0.204	3.314 ± 0.256	2.28E+02 ± 1.06E+02	12.33 ± 0.72	1.66E+00 ± 5.71E−01
090122359c[a]	24.9 ± 5	25.44 ± 6.34	−0.869 ± 0.825	...	...	...	...
090122380a	37.95 ± 4.06	38.03 ± 4.05	−0.973 ± 0.336	...	...	...	...
090122380b[a]	12.91 ± 1.45	...	...	...	...	...	...
090122390a	22.37 ± 1.71	23.04 ± 2.53	−0.86 ± 0.346	...	...	...	...
090122419b[a,b]	29.68 ± 0.53	30.78 ± 0.59	−0.807 ± 0.069	4.645 ± 0.13	1.84E+02 ± 2.90E+01	12.96 ± 0.29	3.86E+00 ± 5.34E−01
090122428a	16.8 ± 1.43	15.93 ± 3.65	−1.065 ± 0.498	2.876 ± 0.255	1.59E+02 ± 8.91E+01	11.52 ± 1.19	4.98E−01 ± 3.00E−01
090122428b[a]	20.75 ± 0.48	23.74 ± 0.53	−0.314 ± 0.123	2.998 ± 0.246	1.51E+02 ± 7.42E+01	7.88 ± 0.2	9.33E+00 ± 1.49E+00
090122451a	45.99 ± 3.35	42.9 ± 5.87	−1.526 ± 0.187	4.277 ± 0.317	5.01E+01 ± 2.17E+01	19.09 ± 1.28	2.05E−01 ± 7.84E−02
090122451b[a]	30.54 ± 5.42	25.57 ± 15.1	−1.582 ± 0.525	...	...	...	...
090122491a	23.66 ± 2.1	...	...	...	...	...	...
090122491b[a]	52.15 ± 8.98	56.26 ± 18.5	−1.539 ± 0.382	...	...	...	...
090122498a[b]	48.01 ± 6.38	46.63 ± 8.71	−1.354 ± 0.351	...	...	...	...
090122498b[a]	12.6 ± 0.49	...	...	2.831 ± 0.147	3.06E+02 ± 9.91E+01	8.831 ± 0.557	2.09E+00 ± 8.05E−01
090122498c[a]	16.75 ± 0.415	9.595 ± 2.25	−1.656 ± 0.117	3.434 ± 0.129	2.08E+02 ± 4.60E+01	9.521 ± 0.379	2.84E+00 ± 7.03E−01

Table 3
(Continued)

Burst	OTTB kT (keV)	COMP E_{peak} (keV)	α	BB+BB−Low kT (keV)	R^2 (km)	BB+BB−High kT (keV)	R^2 (km)
090122551a	50.72 ± 9.77	48.31 ± 6	−0.198 ± 0.582	...	...	...	...
090122624a	35.78 ± 2.75	32.47 ± 4.51	−1.388 ± 0.228	3.833 ± 0.372	1.44E+02 ± 8.21E+01	14.53 ± 1.04	1.16E+00 ± 4.86E−01
090122624b[a]	46.4 ± 8.69	46.03 ± 6.45	−0.503 ± 0.592	...	...	...	...
090122684a	32.48 ± 2.56	29.34 ± 4.66	−1.394 ± 0.244	4.845 ± 0.396	3.33E+01 ± 1.54E+01	16.59 ± 1.68	2.39E−01 ± 1.43E−01
090122694a	31.65 ± 1.84	33.1 ± 1.63	−0.604 ± 0.225	4.225 ± 0.519	2.81E+01 ± 1.95E+01	11.54 ± 0.77	1.06E+00 ± 4.35E−01
090122848a	42.72 ± 4.79	35.76 ± 12.8	−1.707 ± 0.257	3.827 ± 0.425	3.56E+01 ± 2.35E+01	17.5 ± 1.73	1.33E−01 ± 7.52E−02
090122848b[a]	20.14 ± 1.42	...	...	...	...	...	...
090122898a	55.28 ± 7.85	55.67 ± 9.16	−1.132 ± 0.343	...	...	...	...
090122980a	19.55 ± 0.47	17.34 ± 1.25	−1.286 ± 0.108	4.174 ± 0.122	1.01E+02 ± 1.68E+01	11.89 ± 0.54	9.60E−01 ± 2.41E−01
090123042a	33.76 ± 1.53	33.87 ± 1.68	−0.978 ± 0.154	4.543 ± 0.277	4.92E+01 ± 1.70E+01	14.3 ± 0.74	7.07E−01 ± 2.19E−01
090123055a[b]	27.13 ± 0.56	31.54 ± 0.41	0.127 ± 0.091	4.778 ± 0.296	3.81E+02 ± 1.30E+02	10.33 ± 0.27	3.74E+01 ± 6.57E+00
090123313a	43.88 ± 4.42	39.66 ± 8.9	−1.163 ± 0.231	...	...	...	...
090123348a	30.52 ± 1.33	31.88 ± 1.27	−0.72 ± 0.162	3.372 ± 0.302	1.36E+02 ± 7.24E+01	11.02 ± 0.41	3.08E+00 ± 6.85E−01
090123552a	30.44 ± 2.72	27.58 ± 5.12	−1.342 ± 0.301	...	...	...	...
090123577a	47.34 ± 5.02	46.5 ± 6.4	−1.273 ± 0.28	4.963 ± 0.599	3.88E+01 ± 2.65E+01	18.88 ± 1.96	3.01E−01 ± 1.82E−01
090123617a	50.17 ± 2.57	50.26 ± 2.86	−1.097 ± 0.129	3.914 ± 0.244	5.05E+01 ± 1.85E+01	16.64 ± 0.63	3.87E−01 ± 8.43E−02
090123683a	32.23 ± 2.65	34.04 ± 2.13	−0.519 ± 0.304	...	...	...	...
090123705a[b]	35.55 ± 0.73	36.53 ± 0.71	−0.803 ± 0.069	4.686 ± 0.148	3.06E+02 ± 5.44E+01	14.16 ± 0.29	6.02E+00 ± 7.58E−01
090124175a	39.37 ± 3.34	38.82 ± 3.83	−1.131 ± 0.262	4.549 ± 0.48	3.67E+01 ± 2.21E+01	16.03 ± 1.43	3.67E−01 ± 1.92E−01
090124175b[a]	45.64 ± 6.3	45.47 ± 7.67	−1.232 ± 0.365	...	...	...	...
090125179a	37.5 ± 4.03	35.19 ± 5.96	−1.287 ± 0.368	...	...	...	...
090125277a	35.92 ± 2.27	34.25 ± 3.34	−1.221 ± 0.2	4.501 ± 0.367	6.27E+01 ± 2.93E+01	15.32 ± 0.896	6.51E−01 ± 2.29E−01
090125538a[b]	32.52 ± 1.16	34.44 ± 1.25	−0.7117 ± 0.136	5.468 ± 0.318	1.47E+02 ± 4.73E+01	14.41 ± 0.625	3.51E+00 ± 9.72E−01
090125900a	62.85 ± 9.71	89.17 ± 61.4	−1.72 ± 0.311	...	...	...	...
090125911a	34.44 ± 1.17	33.11 ± 1.75	−1.158 ± 0.112	5.026 ± 0.229	4.05E+01 ± 1.05E+01	15.54 ± 0.533	5.24E−01 ± 1.10E−01
090126200a[b]	40.2 ± 1.17	39.45 ± 1.4	−1.124 ± 0.0915	4.237 ± 0.186	8.01E+01 ± 2.03E+01	14.96 ± 0.359	1.01E+00 ± 1.46E−01
090126610a	26.31 ± 4.21	22.85 ± 8.68	−1.366 ± 0.58	...	...	...	...
090126748a	37.28 ± 2.05	26.6 ± 6.84	−1.669 ± 0.169	4.249 ± 0.271	4.29E+01 ± 1.61E+01	17.49 ± 0.908	1.82E−01 ± 5.55E−02
090126966a	73.35 ± 8.58	67.25 ± 5.63	−0.4187 ± 0.31	...	...	...	...
090127611a	58.57 ± 11.6	57.8 ± 11.2	−0.8715 ± 0.515	...	...	...	...
090127632a	31.98 ± 1.04	29.12 ± 1.23	−0.5934 ± 0.115	4.715 ± 0.293	4.82E+01 ± 1.70E+01	11.66 ± 0.244	1.46E+00 ± 2.46E−01
090128024a	65.06 ± 14	61.19 ± 9.88	−0.4603 ± 0.588	...	...	...	...
090129353a	54.45 ± 7.01	54.89 ± 8.01	−1.117 ± 0.323	...	...	...	...
090129538a	86.03 ± 17.9	84.62 ± 22.4	−0.9571 ± 0.407	...	...	...	...
090129472a	55.6 ± 6.1	53.8 ± 4.94	−0.672 ± 0.291	...	...	...	...
090129588a[b]	37.64 ± 0.91	38.36 ± 0.8	−0.764 ± 0.079	4.754 ± 0.174	6.13E+01 ± 1.26E+01	14.33 ± 0.37	1.28E+00 ± 1.99E−01
090129936a	38.52 ± 1.92	37.81 ± 2.25	−1.122 ± 0.158	4.606 ± 0.295	8.90E+01 ± 3.24E+01	16.05 ± 0.85	9.03E−01 ± 2.83E−01
090130290a	52.43 ± 4.72	51.73 ± 4.02	−0.7632 ± 0.247	...	...	...	...
090130812a	56.58 ± 2.33	56.05 ± 1.89	−0.7084 ± 0.123	4.758 ± 0.333	1.86E+01 ± 7.45E+00	17.53 ± 0.528	2.88E−01 ± 5.07E−02
090130812b[a]	77.73 ± 10.8	70.06 ± 6.81	−0.3366 ± 0.387	...	...	...	...
090131080a	122.4 ± 32.8	...	...	...	...	...	...
090131590a	73.04 ± 9.94	69.49 ± 8.07	−0.6918 ± 0.384	...	...	...	...
090201503a	27.62 ± 1.71	26.11 ± 2.68	−1.228 ± 0.216	4.381 ± 0.339	2.02E+01 ± 8.86E+00	13.05 ± 1.08	2.90E−01 ± 1.44E−01
090201684a	94.3 ± 17.5	131.7 ± 79.8	−1.366 ± 0.312	...	...	...	...
090201716a	46.8 ± 2.05	46.78 ± 1.62	−0.657 ± 0.131	4.775 ± 0.344	2.91E+01 ± 1.18E+01	15.44 ± 0.582	6.49E−01 ± 1.45E−01
090201884a	46.83 ± 3.21	49.62 ± 3.23	−0.4156 ± 0.309	...	...	...	...
090202321a	43.83 ± 1.92	42.61 ± 2.39	−1.251 ± 0.127	4.121 ± 0.231	3.56E+01 ± 1.17E+01	16.2 ± 0.599	2.88E−01 ± 6.19E−02
090202394a	55.9 ± 5.9	54.61 ± 4.52	−0.589 ± 0.292	...	...	...	...
090202394b[a]	37.6 ± 1.96	34.41 ± 3.45	−1.405 ± 0.154	4.728 ± 0.304	4.06E+01 ± 1.49E+01	16.26 ± 0.889	3.80E−01 ± 1.23E−01
090202440a	47.53 ± 2.88	47.62 ± 3.08	−1.061 ± 0.156	3.742 ± 0.313	3.49E+01 ± 1.72E+01	14.91 ± 0.647	3.84E−01 ± 9.65E−02
090202513a	78.03 ± 6.1	79.27 ± 7.78	−1.046 ± 0.165	6.516 ± 0.563	2.42E+00 ± 1.16E+00	24.35 ± 1.52	2.54E−02 ± 9.04E−03
090202862a	53.25 ± 3.52	53.17 ± 4.32	−1.226 ± 0.179	4.249 ± 0.219	4.64E+01 ± 1.39E+01	14.82 ± 0.383	4.69E−01 ± 7.78E−02
090202862b[a]	36.74 ± 1.06	33.69 ± 2.07	−1.32 ± 0.122	4.164 ± 0.263	4.42E+01 ± 1.64E+01	15.71 ± 0.645	3.82E−01 ± 9.20E−02
090203198a	33.27 ± 4.45	35.48 ± 3.89	−0.603 ± 0.509	...	...	...	...
090203206a	80.27 ± 20.6	...	...	...	...	...	...
090203389a	25.09 ± 0.941	24.65 ± 1.63	−1.058 ± 0.16	4.309 ± 0.258	9.91E+01 ± 3.37E+01	11.9 ± 0.614	1.84E+00 ± 5.92E−01
090203805a	88.94 ± 22.6	...	...	...	...	...	...
090203834a[b]	33.85 ± 0.488	38.02 ± 0.306	0.2845 ± 0.0615	5.157 ± 0.266	1.99E+02 ± 5.62E+01	11.64 ± 0.18	2.41E+01 ± 2.47E+00
090204003a	29.28 ± 4.31	30.17 ± 4.37	−0.7624 ± 0.58	...	...	...	...
090206897a	39.65 ± 4.28	37.39 ± 6.11	−1.333 ± 0.324	...	...	...	...
090207834a	39.66 ± 3.58	41.05 ± 2.98	−0.6465 ± 0.32	...	...	...	...
090208340a	47.02 ± 5.85	46.77 ± 4.27	−0.484 ± 0.382	...	...	...	...
090208463a	46.06 ± 3.96	46.13 ± 3.74	−0.9176 ± 0.243	4.845 ± 0.515	1.97E+01 ± 1.18E+01	16.84 ± 1.36	2.62E−01 ± 1.24E−01
090208682a	67.26 ± 8.31	64.12 ± 7.52	−0.8036 ± 0.284	...	...	...	...
090209271a	29.62 ± 4.85	23 ± 13.1	−1.634 ± 0.456	...	...	...	...
090210310a	41.12 ± 2.02	40.9 ± 2.19	−1.047 ± 0.154	4.493 ± 0.323	4.35E+01 ± 1.79E+01	15.48 ± 0.7	5.72E−01 ± 1.53E−01

Table 3
(Continued)

| Burst | OTTB | COMP | | BB+BB−Low | | BB+BB−High | |
| | kT | E_{peak} | α | kT | R^2 | kT | R^2 |
	(keV)	(keV)		(keV)	(km)	(keV)	(km)
090210415a	38.57 ± 2.06	39.98 ± 1.73	-0.6559 ± 0.188	4.085 ± 0.368	$5.70E+01 \pm 2.98E+01$	13.79 ± 0.641	$1.03E+00 \pm 2.85E-01$
090210898a	32.01 ± 2.16	34.28 ± 1.7	-0.3765 ± 0.262	...	...	...	...
090210941a	46 ± 2.22	45.87 ± 2.83	-1.254 ± 0.127	3.808 ± 0.219	$6.09E+01 \pm 2.07E+01$	15.85 ± 0.59	$4.54E-01 \pm 9.72E-02$
090211264a	65.12 ± 6.97	60.51 ± 5.04	-0.4823 ± 0.27	...	...	...	...
090211279a[b]	29.5 ± 1.02	34.94 ± 1.04	-0.1003 ± 0.189	...	...	...	...
090211290a	68.11 ± 7.76	64.72 ± 5.73	-0.5136 ± 0.302	...	...	...	...
090212968a	44.13 ± 8.34	43.91 ± 6.79	-0.6809 ± 0.607	...	...	...	...
090217261a	31.37 ± 1.96	30.92 ± 2.52	-1.077 ± 0.214	3.607 ± 0.403	$1.01E+02 \pm 6.64E+01$	11.69 ± 0.683	$1.89E+00 \pm 6.60E-01$
090218278a	56.47 ± 3.83	59.24 ± 6.14	-1.352 ± 0.155	4.013 ± 0.32	$3.51E+01 \pm 1.65E+01$	17.89 ± 0.854	$2.20E-01 \pm 6.01E-02$
090218491a	30.35 ± 1.22	27.83 ± 2.33	-1.269 ± 0.146	5.094 ± 0.259	$1.35E+02 \pm 3.87E+01$	15.37 ± 0.833	$1.45E+00 \pm 4.80E-01$
090221803a	43.49 ± 3.26	42.73 ± 4	-1.219 ± 0.213	4.064 ± 0.463	$4.67E+01 \pm 3.09E+01$	14.88 ± 0.907	$5.82E-01 \pm 2.09E-01$
090222540a	118.9 ± 34.8	94.15 ± 25.3	-0.6042 ± 0.484	...	...	...	...
090224694a	72.31 ± 17.2	69.7 ± 17.7	-0.9007 ± 0.509	...	...	...	...
090224718a	43.65 ± 1.83	42.77 ± 2.37	-1.233 ± 0.123	5.698 ± 0.298	$1.36E+01 \pm 3.99E+00$	18.72 ± 0.914	$1.44E-01 \pm 4.15E-02$
090224782a	41.4 ± 2.58	42.03 ± 1.76	-0.2778 ± 0.221	...	...	...	...
090322789a	$47.9^{+4.2}_{-3.8}$	$43.3^{+8.7}_{-8.1}$	$-1.63^{+0.18}_{-0.16}$	...	...	...	...
090326625a	$40^{+4.8}_{-4.2}$	$39.7^{+5.1}_{-4.9}$	$1.1^{+1.1}_{-0.8}$	...	...	...	...
090326625b[a]	$105^{+48.8}_{-30}$	$69.7^{+15.8}_{-15.8}$	$-0.18^{+0.78}_{-0.78}$	...	...	...	...
090328545a	$39^{+4.3}_{-3.8}$	$39.2^{+3.6}_{-3.2}$	$-0.66^{+0.35}_{-0.32}$	...	...	...	...
090329754a	$35.6^{+3.8}_{-3.4}$	$36.8^{+3.2}_{-3.1}$	$-0.56^{+0.4}_{-0.36}$	...	...	...	...
090330237a	$32.6^{+1.3}_{-1.4}$	$33.3^{+1.3}_{-1.4}$	$-0.87^{+1.4}_{-1.3}$	$5.61^{+0.35}_{-0.35}$	$8.45E+01 \pm 2.90E+01$	$15.85^{+1.28}_{-1.07}$	$1.14E+00 \pm 5.05E-01$
090401093a	$49.4^{+19.7}_{-13.1}$	76.7^{+114}_{-114}	$-1.84^{+0.43}_{-0.43}$	...	...	...	...
090401666a[b]	$30.9^{+0.8}_{-0.8}$	$33.2^{+0.7}_{-0.1}$	$0.36^{+0.11}_{-0.1}$	...	...	...	...
090403592a	$34.1^{+2.7}_{-2.4}$	$34.2^{+2.7}_{-2.7}$	$-0.96^{+0.24}_{-0.23}$	$5.39^{+0.63}_{-1.76}$	$1.90E+01 \pm 3.25E+01$	$15.8^{+3.15}_{-4.18}$	$2.36E-01 \pm 5.76E-01$
090403761a	$44.7^{+7.2}_{-5.9}$	$45.6^{+10.8}_{-8.6}$	$-1.38^{+0.35}_{-0}$	...	...	...	...
090409351a	$29^{+2}_{-1.8}$	$30.5^{+2.1}_{-2.1}$	$-0.63^{+0.4}_{-0.25}$	...	...	...	...
090411917a	$31.8^{+1.5}_{-1.5}$	$32.6^{+1.5}_{-1.6}$	$-0.82^{+0.17}_{-0.17}$	$4.99^{+0.34}_{-0.32}$	$4.48E+01 \pm 1.68E+01$	$14.44^{+1.05}_{-0.93}$	$6.96E-01 \pm 2.83E-01$
090413987a	$35.4^{+1.7}_{-1.6}$	$37.1^{+1.4}_{-1.4}$	$-0.5^{+0.18}_{-0.17}$	$4.18^{+0.46}_{-0.43}$	$1.25E+02 \pm 7.76E+01$	$12.56^{+0.67}_{-0.59}$	$3.76E+00 \pm 1.12E+00$
090417946a	$44.5^{+5.4}_{-4.6}$	$45.2^{+8.8}_{-7.8}$	$-1.49^{+0.25}_{-0}$	...	...	...	...

Notes.
[a] Untriggered burst.
[b] Used in Younes et al. (2014).
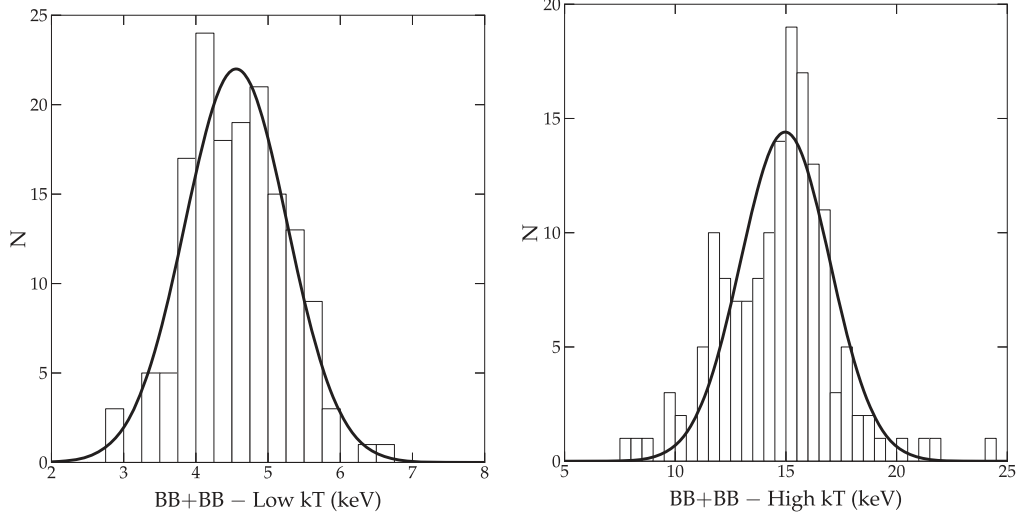
Figure 6. Low (left panel) and high (right panel) BB temperatures for all bursts of SGR J1550–5418. We fit these histograms to a Gaussian (black line) with $\mu = 4.55 \pm 0.05$ keV and $\sigma = 0.71 \pm 0.05$ keV for the low kT BB, and $\mu = 14.96 \pm 0.16$ keV and $\sigma = 2.03 \pm 0.16$ keV for the high kT BB.

least $\sim 1 \times 10^{-5}$ erg cm^{-2} (8–200 keV). The corresponding total energy range is $\sim 2 \times 10^{37}\ d_5^2$ erg to $\sim 3 \times 10^{40}\ d_5^2$ erg (with d_5 the distance to the source divided by its estimated distance of 5 kpc). Compared to the other prolific magnetars, these bursts are brighter than those reported for SGR 1806–20 (1.2×10^{-10}–1.9×10^{-7} erg cm^{-2}; 3.0×10^{36}–4.9×10^{39} erg; for $E > 25$ keV; Göğüş et al. 2001) and SGR 1900+14 (1.2×10^{-10}–3.3×10^{-7} erg cm^{-2}; 7×10^{35}–2×10^{39} erg; for
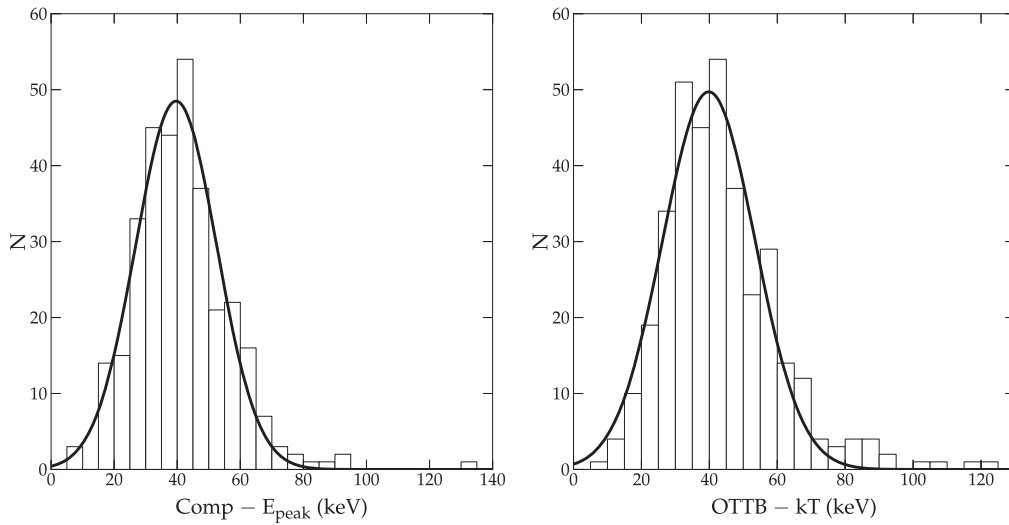
Figure 7. E_{peak} as measured by the COMP and OTTB models for SGR J1550–5418 bursts. We fit these histograms to Gaussians (black line). For the COMP model, we find E_{peak} to have $\mu = 39.6 \pm 0.6$ keV and $\sigma = 12.9 \pm 0.6$ keV. For the OTTB model, we find kT to have $\mu = 39.8 \pm 0.7$ keV and $\sigma = 13.7 \pm 0.7$ keV.
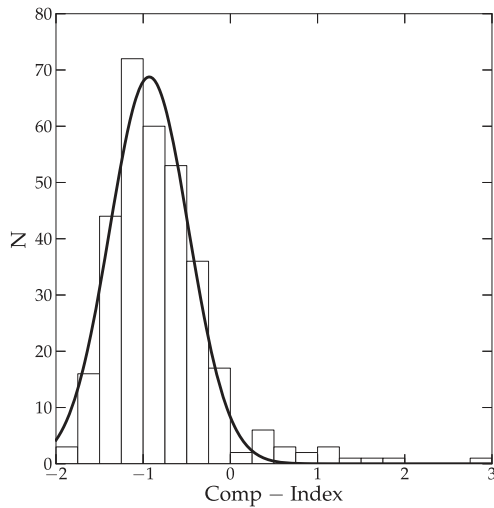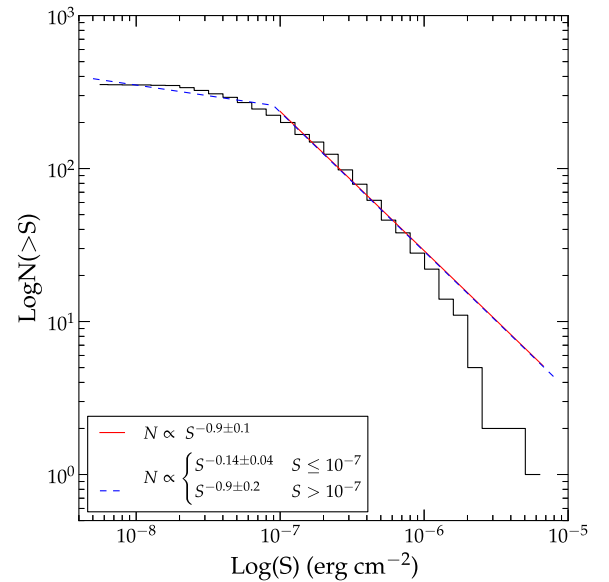

Figure 8. Power-law spectral index as measured by the COMP model for all bursts of SGR J1550–5418. The distribution was fit to a Gaussian (black line) with $\mu = -0.93 \pm 0.02$ and $\sigma = 0.45 \pm 0.02$.

Figure 9. Log $N(>S)$ − Log (S) diagram of SGR J1550–5418 bursts. The data are fit to a single PL (red solid line) and a broken PL (blue dashed line). For the single PL, we only fit the data with $S > 1 \times 10^{-7}$ erg cm^{-2}.

Table 4
Distribution Average and Spread for Parameters of SGR J1550–5418 Bursts

| Value	Fit μ	Fit σ
T_{90} (log (ms))	2.19 ± 0.02	0.40 ± 0.02
T_{50} (log (ms))	1.71 ± 0.04	0.44 ± 0.03
OTTB–kT (keV)	39.8 ± 0.7	13.7 ± 0.7
Comp–E_{peak} (keV)	39.6 ± 0.6	12.9 ± 0.6
Comp–α	-0.93 ± 0.02	0.45 ± 0.02
BB+BB low kT (keV)	4.55 ± 0.05	0.71 ± 0.05
BB+BB high kT (keV)	14.96 ± 0.16	2.03 ± 0.16

$E > 25$ keV; Göğüş et al. 2001). Woods et al. (1999) provide the peak luminosity range of SGR 1627–41 bursts to be $10^{39}-10^{42}$ erg s^{-1} ($E > 25$ keV), which corresponds (assuming a burst average duration of 0.1 s) to an energy range of $10^{38}-10^{41}$ erg, indicating that these bursts were at the higher end of the energy distribution. However, since these data were obtained with a higher threshold instrument with limited trigger

algorithm options for very short events (*CGRO*/BATSE), the non-detection of a fainter subset may well have been an instrumental effect. SGR J1550–5418 bursts are an order of magnitude fainter than those of SGR J0501+4516 (4×10^{-8}–2×10^{-5} erg cm^{-2}; $2.0 \times 10^{37} - 1.0 \times 10^{40}$ erg; for 8–200 keV; Lin et al. 2011a). Finally, all SGR bursts are significantly more energetic when compared to bursts from AXP 1E2259+586, which range between 5×10^{34} and 7×10^{36} erg (2–60 keV; Gavriil et al. 2004).

Next, we derive a lower limit on the total energy fluence emitted by bursts from the source. The limit takes into account that we could not include bursts that occurred when *Fermi* was in the South Atlantic Anomaly, when the Earth occulted the source, or when no TTE data existed. For this limit, we include the unsaturated parts of the saturated bursts across all outburst periods. We obtain a value of 2.2×10^{-4} erg cm^{-2}, which corresponds to an (lower limit) energy release of 6.6×10^{41}
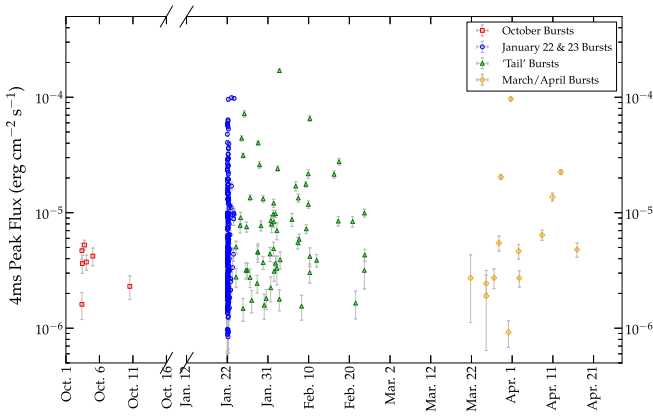
Figure 10. Evolution of the 4 ms peak flux of all SGR J1550–5418 bursts as measured by the COMP model. The October bursts were faint compared to the other periods, but there is no other distinct evolution in the peak flux of the bursts over time.

Table 5
Correlation Coefficient and Probability between Parameters of
SGR J1550–5418 Bursts

Parameters	Coefficient	Probability
E_{peak} –Fluence	−0.400	9.7×10^{-14}
T_{90} –Fluence	0.194	2.5×10^{-4}
T_{50} –Fluence	0.086	1.1×10^{-1}
Comp Index–Fluence	−0.082	1.4×10^{-1}
E_{peak} –Peak Flux	−0.463	1.8×10^{-18}
T_{90} –Peak Flux	−0.084	1.2×10^{-1}
T_{50} –Peak Flux	−0.240	7.1×10^{-6}
Comp Index–Peak Flux	−0.010	8.6×10^{-1}
Peak Flux–Phase	−0.013	8.1×10^{-1}
Fluence–Phase	0.039	4.8×10^{-1}
E_{peak} –Phase	0.127	2.3×10^{-2}
T_{90} –Phase	0.085	1.2×10^{-1}
T_{90} –E_{peak}	0.001	9.9×10^{-1}
T_{50} –E_{peak}	0.112	4.6×10^{-2}
Fluence–Peak Flux	0.831	3.0×10^{-89}

d_5^2 erg (8–200 keV). This is four orders of magnitude above the upper limit derived for bursts from AXP 1E2259+586 (2–60 keV; Gavriil et al. 2004).

In Figure 9, we present a Log $N(>S)$–Log (S) diagram for all 354 unsaturated events, where S is the energy fluence (8–200 keV). We fit this histogram with both a PL and a broken PL. For the single PL, we only fit the bins $\geqslant 1 \times 10^{-7}$ erg cm^{-2}, obtaining an index of -0.9 ± 0.1. We find that the broken PL fits the data best with a break at 1×10^{-7} erg cm^{-2} and indices of -0.14 ± 0.04 and -0.9 ± 0.1 below and above the break, respectively. The PL slope above the break is steeper than what has been found for other magnetars with a large sample of bursts, ranging from −0.5 to −0.7 (Göğüş et al. 1999, 2001; Woods et al. 1999; Aptekar et al. 2001; Gavriil et al. 2004), although a similar slope has been found for a large sample of SGR 1806–20 bursts (Götz et al. 2006). The PL slope below the break is clearly much shallower, which is due to the lower sensitivity of the instrument to faint bursts. Regarding the PL slope at high fluences, the energy and fluence ranges probed in our SGR J1550–5418 sample differ from
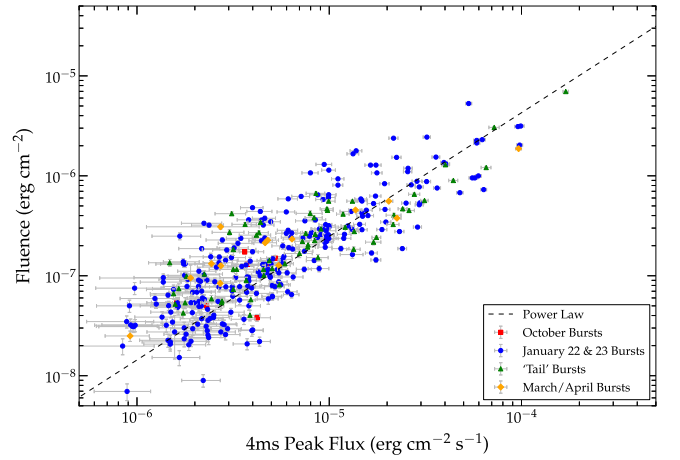

Figure 11. Integrated fluence of SGR J1550–5418 bursts vs. their peak flux. There is a strong correlation between these two parameters, and a PL fit results in a slope of 1.2 ± 0.4.
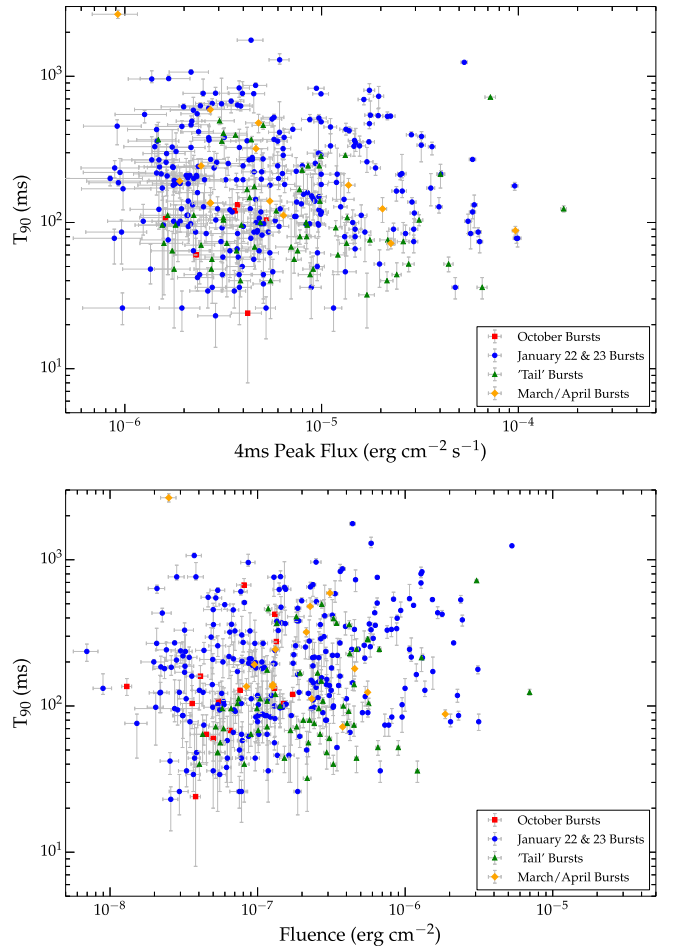

Figure 12. T_{90} duration vs. peak flux (top panel) and fluence (bottom panel) for all SGR J1550–5418 bursts. There is a marginally significant correlation between T_{90} and the fluence, but not between T_{90} and the peak flux.

those in other magnetar samples, making a clear direct comparison unfeasible.

Finally, we find that the 4 ms peak fluxes of SGR J1550–5418 bursts range from $\sim 8 \times 10^{-7}$ to $\sim 2 \times 10^{-4}$ erg s^{-1} cm^{-2}, corresponding to a peak luminosity range of $\sim 5 \times 10^{38}$ to $\sim 1 \times 10^{41}$ erg s^{-1}. The 4 ms fluxes extend the peak
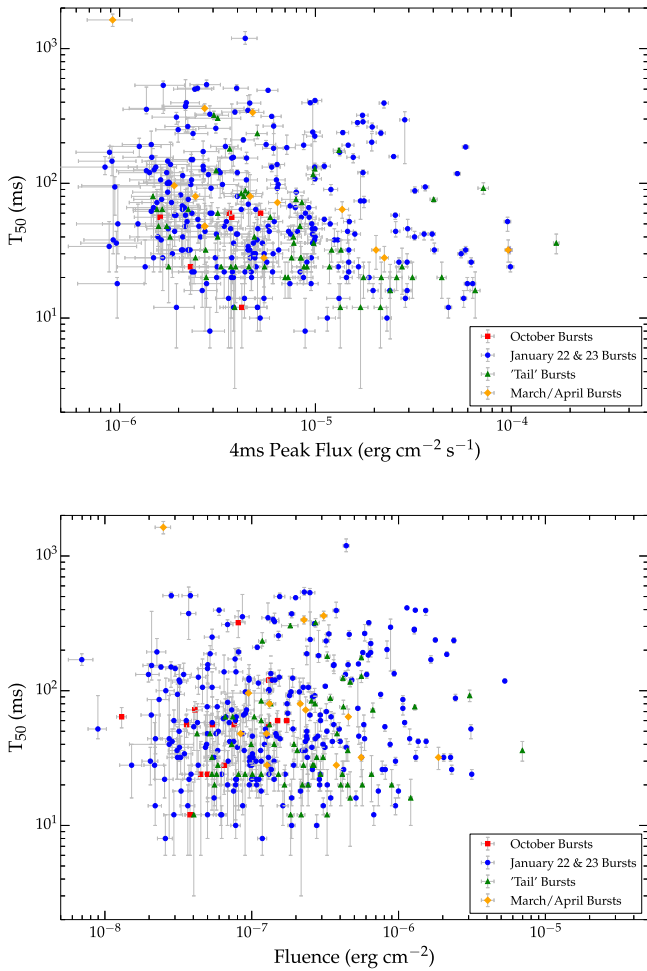
Figure 13. T_{50} duration vs. peak flux (top panel) and fluence (bottom panel) for all SGR J1550–5418 bursts. There is a marginally significant correlation between T_{50} and the peak flux, but not between T_{50} and the fluence.
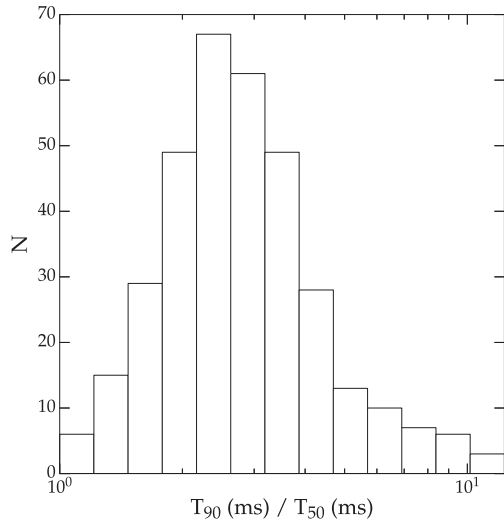

Figure 14. Histogram of the T_{90} / T_{50} ratio for SGR J1550–5418 bursts, showing that the distribution is broad, extending a factor of ~10.

flux range to about a full order of magnitude higher than was covered with the average fluxes from this source (Lin et al. 2012; van der Horst et al. 2012; von Kienlin et al. 2012). Figure 10 shows the evolution of peak fluxes across the
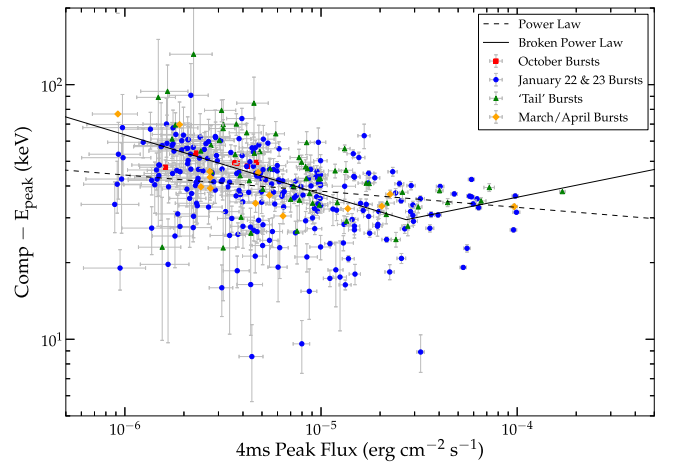
Figure 15. $E_{\rm peak}$ from the COMP model vs. the 4ms peak flux of SGR J1550–5418 bursts. We fit this correlation with a PL (dashed line) and a broken PL (solid line).
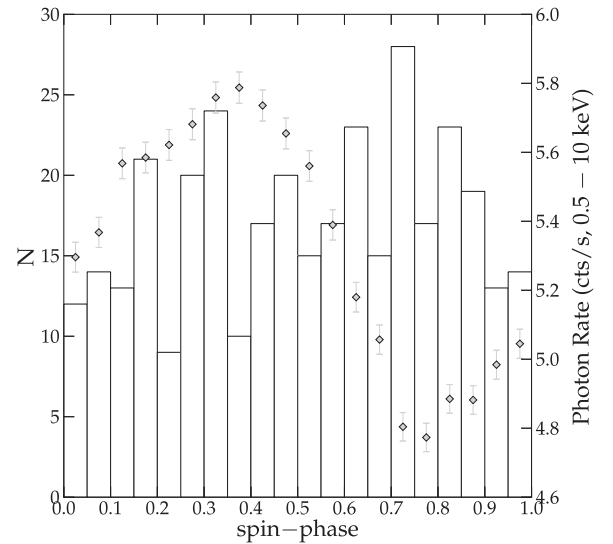

Figure 16. Distribution of the phase of the peak of all the SGR J1550–5418 bursts. We do not find a preferred spin phase for burst peaks, which is consistent with what has been found for other magnetars.

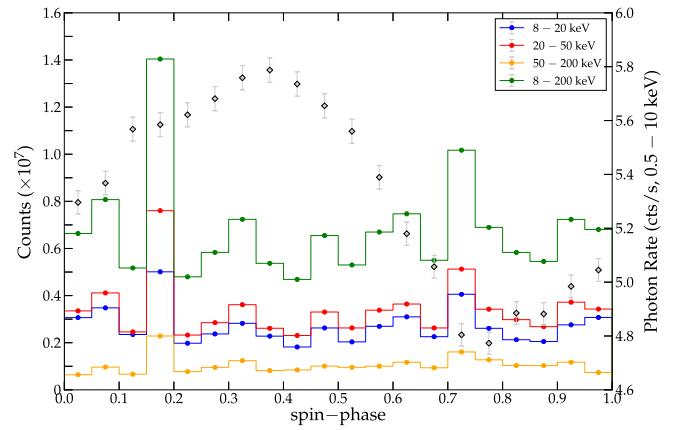outburst and demonstrates the uniformly low peak fluxes of the events of the first period.

3.1.3. Correlations

We searched for correlations among the burst properties across the entire burst activity from the source, using the Spearman rank order correlation test. We considered multiple combinations of parameters and estimated the Spearman coefficient and probability for each; the results are listed in Table 5. In most cases, the significance of the correlation was very low, but we identified the following significant correlations: fluence–peak flux, $E_{\rm peak}$–fluence, and $E_{\rm peak}$–peak flux (all determined using the COMP model). Figure 11 exhibits the strong correlation between the fluence and peak flux; the data are fit with a PL with an index 1.2 ± 0.4. The $E_{\rm peak}$–fluence correlation is moderately weaker than that previously reported for bursts of only the second period (van der Horst et al. 2012), but there still is a very small chance probability of 9.7×10^{-14}. We previously found a marginal correlation between T_{90} and
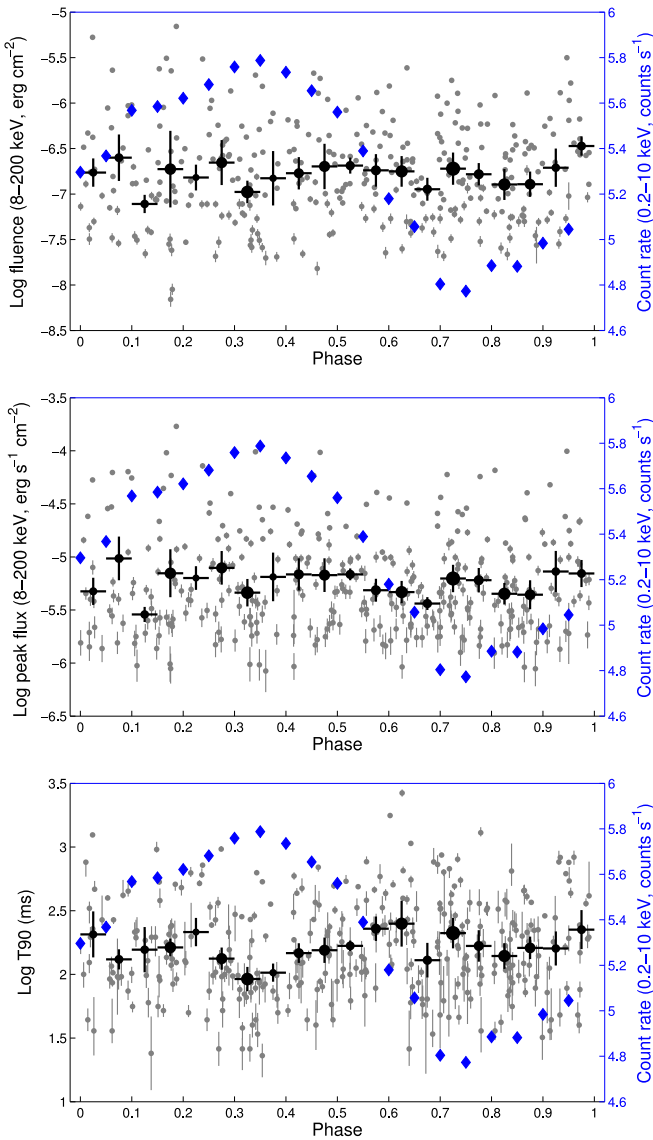
Figure 17. Fluence (top panel), peak flux (middle panel), and T_{90} (bottom panel) of SGR J1550–5418 bursts compared to the spin phase. The gray dots represent each individual burst, and the black dots represent the weighted average of these gray dots grouped by phase. The sizes of the black dots represent how many bursts are in each group. The blue diamonds indicate the 0.2–10 keV pulse profile (Lin et al. 2012). There are no correlations between the fluence, peak flux, or T_{90} and the spin phase.

Figure 18. Folded light curve of all bursts from SGR J1550–5418 in 3 channels: 8–20 keV (blue), 20–50 keV (red), and 50–200 keV (yellow). The sum of all three channels is shown in green. There is a possible peak at the bin that spans phase 0.15–0.20. This peak, however, is not significant (see Section 3.1.5).
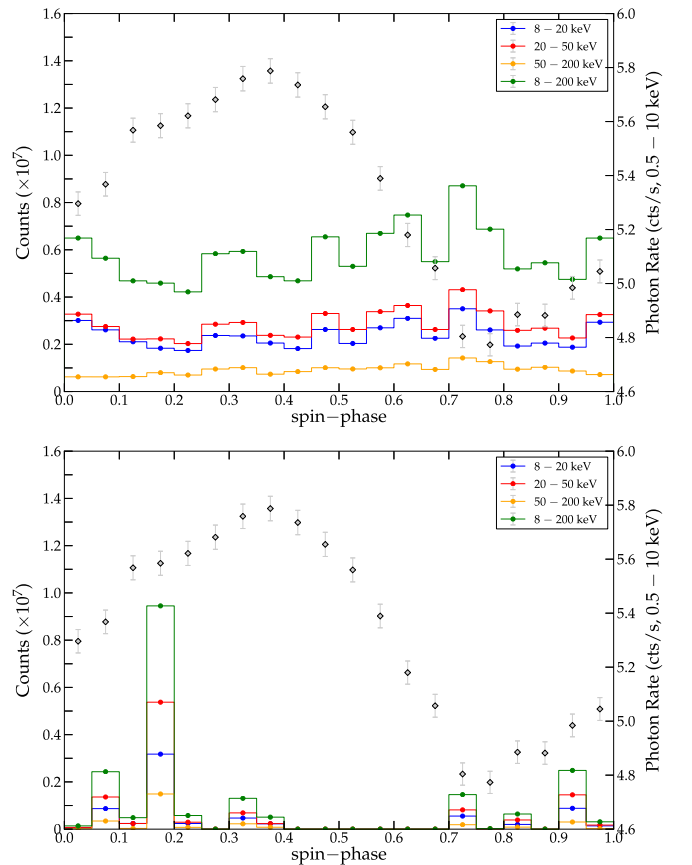
Figure 19. Folded light curve of all bursts from SGR J1550–5418 without the 10 brightest ones (top panel), and folded light curve of only the 10 brightest ones; color coding is the same as in Figure 18. The peak at phase bin 0.15–0.20 in Figure 18 is not apparent in the top panel, but is clearly present in the bottom panel.

fluence (van der Horst et al. 2012); here, we find a weaker T_{90} – fluence correlation (chance probability of 2.5×10^{-4}), and no correlation between T_{90} and the peak flux (Figure 12). However, we do find a marginal anti-correlation (chance probability of 7.1×10^{-6}) between T_{50} and the peak flux (see also Figure 13). This can be explained by the fact that for bursts in which the light curve is dominated by one very bright peak, the T_{50} is likely to encompass only that bright peak and not to include any lower level activity that is part of that burst (while the latter is included in the T_{90}). This is further illustrated in Figure 14 where we show a histogram of the T_{90} / T_{50} ratio. This histogram peaks between 2 and 3, but has a broad tail extending above 10, which shows that there is indeed a large amount of bursts that consist of a bright peak and a relatively long time span of lower level emission.

We estimated the peak fluxes on a 4 ms timescale, and investigated the E_{peak}–peak flux relation at this timescale for the first time in this study (Figure 15). We find that this correlation is considerably stronger than the one using the average fluxes reported previously by van der Horst et al. (2012). We fit the data to both a PL and a broken PL. The PL

Table 6
Durations, Peak Fluxes, and Fluences of SGR J0501+4516 Bursts

Trigger (yymmddfff)	T_{90} Start (UT)	T_{90} (ms)	T_{50} Start (UT)	T_{50} (ms)	8 ms Peak Flux[c,d] (erg s^{-1} cm^{-2})	Fluence[c,d] (erg cm^{-2})
080822529a	12:41:56.902	80 ± 16	12:41:56.902	38 ± 7	1.59E-06 ± 3.20E-07	7.05E-08 ± 6.20E-09
080822647a	15:41:17.712	226 ± 24	15:41:17.712	24 ± 24	7.04E-06 ± 6.70E-07	1.93E-07 ± 1.42E-08
080822981a	23:32:57.728	30 ± 15	23:32:57.728	12 ± 4	2.37E-06 ± 5.20E-07	4.41E-08 ± 6.70E-09
080823020a	00:28:09.908	48 ± 7	00:28:09.908	20 ± 7	6.61E-06 ± 5.90E-07	2.50E-07 ± 1.12E-08
080823091a	02:11:36.694	554 ± 40	02:11:36.694	386 ± 7	6.49E-06 ± 7.40E-07	8.28E-07 ± 3.04E-08
080823174a	04:10:19.222	330 ± 51	04:10:19.222	142 ± 7	1.63E-06 ± 3.70E-07	1.41E-07 ± 1.29E-08
080823248a	05:56:31.487	276 ± 34	05:56:31.487	34 ± 7	3.42E-06 ± 6.40E-07	2.22E-07 ± 1.80E-08
080823293a	07:01:09.971	164 ± 7	07:01:09.971	82 ± 3	2.89E-06 ± 3.40E-07	2.01E-07 ± 9.00E-09
080823293b	07:07:35.074	30 ± 11	07:07:35.074	10 ± 4	5.59E-06 ± 3.60E-07	9.54E-08 ± 5.60E-09
080823319a	07:39:32.253	122 ± 25	07:39:32.253	44 ± 4	4.03E-06 ± 4.90E-07	1.94E-07 ± 1.16E-08
080823330a	07:55:45.706	162 ± 13	07:55:45.706	32 ± 4	1.52E-05 ± 7.10E-07	6.71E-07 ± 1.55E-08
080823354a	08:30:01.587	94 ± 114	08:30:01.587	36 ± 9	2.97E-06 ± 3.70E-07	8.62E-08 ± 8.30E-09
080823429a	10:18:13.889	82 ± 13	10:18:13.889	20 ± 4	5.02E-06 ± 4.00E-07	1.42E-07 ± 7.60E-09
080823478a	11:27:32.348	246 ± 6	11:27:32.348	168 ± 4	6.96E-05 ± 2.80E-06	5.13E-06 ± 6.48E-08
080823623a	14:56:23.551	204 ± 21	14:56:23.551	94 ± 17	3.02E-06 ± 5.40E-07	2.11E-07 ± 1.50E-08
080823714a	17:08:49.132	398 ± 11	17:08:49.132	90 ± 12	3.11E-06 ± 4.70E-07	3.30E-07 ± 1.59E-08
080823847a	20:19:30.655	124 ± 11	20:19:30.655	34 ± 3	2.00E-05 ± 1.04E-06	7.86E-07 ± 2.26E-08
080823847b	20:27:55.038	110 ± 108	20:27:55.038	24 ± 4	1.03E-05 ± 7.10E-07	3.31E-07 ± 1.31E-08
080823986a	23:39:24.434	30 ± 10	23:39:24.434	18 ± 7	1.43E-06 ± 2.80E-07	4.37E-08 ± 4.90E-09
080824054a[b]	01:17:55.458	250 ± 3	01:17:55.458	102 ± 3	…	…
080824346a	08:18:24.400	28 ± 11	08:18:24.400	12 ± 4	3.29E-06 ± 5.00E-07	5.70E-08 ± 6.10E-09
080824828a	19:52:51.214	62 ± 16	19:52:51.214	32 ± 9	1.64E-06 ± 3.60E-07	6.39E-08 ± 7.20E-09
080825200a[b]	04:48:27.407	102 ± 8	04:48:27.407	22 ± 3	…	…
080825401a	09:37:42.156	114 ± 4	09:37:42.156	26 ± 4	3.70E-05 ± 1.28E-06	1.05E-06 ± 2.01E-08
080826136a	03:16:14.883	146 ± 7	03:16:14.883	26 ± 3	1.61E-04 ± 5.85E-06	5.07E-06 ± 7.78E-08
080826236a	05:40:19.407	100 ± 16	05:40:19.407	22 ± 4	4.74E-06 ± 5.70E-07	1.71E-07 ± 1.06E-08
080828875a	20:59:39.942	44 ± 22	20:59:39.942	22 ± 8	1.48E-06 ± 2.40E-07	5.28E-08 ± 5.10E-09
080903421a	10:06:35.303	60 ± 83	10:06:35.303	18 ± 9	4.06E-06 ± 6.70E-07	1.10E-07 ± 1.09E-08
080903787a	18:53:48.767	80 ± 6	18:53:48.767	22 ± 6	6.68E-06 ± 6.50E-07	1.39E-07 ± 1.01E-08

Notes.
[a] Untriggered Burst.
[b] Saturated Burst.
[c] By COMP model.
[d] 8–200 keV energy range.

**Table 7**
Time-integrated Spectral Modeling Results for SGR J0501+4516 Bursts

Trigger ID	COMP E_{peak} (keV)	COMP α	OTTB kT (keV)	BB kT (keV)	BB+BB kT1 (keV)	BB+BB kT2 (keV)
080822529a	40.83 ± 2.76	1.06 ± 0.70	44.65 ± 7.08	10.33 ± 0.60	…	…
080822647a	39.83 ± 5.98	−1.32 ± 0.34	40.95 ± 4.32	9.85 ± 0.42	4.24 ± 0.52	17.24 ± 2
080822981a	44.86 ± 5.02	1.48 ± 1.42	50.89 ± 16.3	11.62 ± 1.17	…	…
080823020a	36.37 ± 3.28	−1.27 ± 0.20	37.85 ± 2.35	9.53 ± 0.23	4.66 ± 0.34	16.99 ± 1.21
080823091a	42.09 ± 2.63	−1.17 ± 0.17	42.53 ± 2.27	10.27 ± 0.22	5.06 ± 0.39	17.40 ± 1.08
080823174a	57.53 ± 7.06	−0.52 ± 0.44	61.65 ± 9.66	12.86 ± 0.76	…	…
080823248a	51.94 ± 3.41	1.03 ± 0.55	68.30 ± 11.1	13.00 ± 0.68	…	…
080823293a	48.13 ± 1.85	0.52 ± 0.29	53.43 ± 4.12	11.82 ± 0.34	…	…
080823293b[a]	26.68 ± 8.25	−1.63 ± 0.26	35.26 ± 2.82	9.61 ± 0.32	3.3 ± 0.33	14.52 ± 1.12
080823319a	36.96 ± 3.22	−0.98 ± 0.30	36.92 ± 3.16	8.78 ± 0.31	5.13 ± 0.54	17.00 ± 1.88
080823330a	30.10 ± 1.10	−0.79 ± 0.14	28.96 ± 0.944	8.28 ± 0.12	4.87 ± 0.23	13.64 ± 0.68
080823354a	28.10 ± 2.89	0.09 ± 0.80	24.91 ± 3.71	7.43 ± 0.50	…	…
080823429a	55.32 ± 4.73	−0.86 ± 0.24	56.11 ± 4.88	12.71 ± 0.40	3.47 ± 0.38	16.93 ± 1.07
080823478a	34.50 ± 0.48	−0.12 ± 0.10	30.29 ± 0.553	9.36 ± 0.07	5.5 ± 0.26	12.50 ± 0.35
080823623a	48.70 ± 2.89	0.88 ± 0.51	53.22 ± 6.82	12.29 ± 0.57	…	…
080823714a	46.68 ± 1.69	1.50 ± 0.41	56.15 ± 5.25	12.04 ± 0.39	…	…
080823847a	36.57 ± 1.77	−1.12 ± 0.14	37.02 ± 1.53	9.41 ± 0.16	4.25 ± 0.23	14.92 ± 0.7
080823847b[a]	29.95 ± 2.22	−1.01 ± 0.23	30.01 ± 1.66	8.38 ± 0.20	4.78 ± 0.34	14.70 ± 1.23
080823986a	46.62 ± 5.84	−0.38 ± 0.61	48.65 ± 8.66	11.24 ± 0.73	…	…
080824346a	57.33 ± 7.00	−0.22 ± 0.48	67.20 ± 13.2	12.67 ± 0.81	…	…
080824828a	43.22 ± 3.98	0.50 ± 0.84	49.38 ± 9.24	10.60 ± 0.74	…	…
080825401a	37.76 ± 0.66	−0.03 ± 0.13	35.48 ± 1.04	9.74 ± 0.11	3.98 ± 0.32	11.53 ± 0.32
080826136a	36.51 ± 0.56	−0.09 ± 0.10	33.27 ± 0.754	9.59 ± 0.09	6.40 ± 0.32	14.14 ± 0.59
080826236a	51.88 ± 3.41	0.03 ± 0.36	56.03 ± 6.24	12.66 ± 0.46	3.77 ± 0.86	15.02 ± 1.11
080828875a	43.41 ± 5.69	−0.85 ± 0.47	43.15 ± 6.25	11.03 ± 0.62	3.31 ± 0.69	14.60 ± 1.74
080903421a	47.35 ± 7.63	−1.07 ± 0.48	47.26 ± 7.16	10.77 ± 0.62	5.72 ± 1.1	20.37 ± 3.78
080903787a	33.68 ± 3.75	−0.95 ± 0.39	33.42 ± 3.49	9.07 ± 0.40	4.78 ± 0.81	13.64 ± 1.93

Notes.
[a] Untriggered Burst.

Table 8
Durations, Peak Fluxes, and Fluences of 1E 1841–045 Bursts

Trigger (yymmddffff)	T_{90} Start (UT)	T_{90} [a] (ms)	T_{50} Start (UT)	T_{50} [a] (ms)	8 ms Peak Flux[b,c] (erg s cm^{-2})	Fluence[b,c] (erg cm^{-2})
110209218a	05:14:25.930	72 ± 23	05:14:25.934	16 ± 11	3.12E-06 $\pm$ 5.34E-07	5.1E-08 $\pm$ 4E-09
110217330a	07:55:55.241	72 ± 30	07:55:55.265	42 ± 3	2.91E-06 $\pm$ 4.62E-07	8.4E-08 $\pm$ 5E-09
110221029a	00:41:16.224	28 ± 11	00:41:16.242	8 ± 6	7.93E-06 $\pm$ 6.46E-07	1E-07 $\pm$ 1E-08
110616881a	21:09:08.420	40 ± 6	21:09:08.428	20 ± 6	1.29E-05 $\pm$ 1.15E-06	2.9E-07 $\pm$ 1E-08
110623612a	14:41:42.752	32 ± 14	14:41:42.756	12 ± 6	1.11E-05 $\pm$ 1.06E-06	1.9E-07 $\pm$ 1E-08
110625969a	23:26:03.165	56 ± 11	23:26:03.167	8 ± 11	9.50E-06 $\pm$ 1.00E-06	1.1E-07 $\pm$ 1E-08

Notes.
[a] 8–100 keV energy range.
[b] By COMP model.
[c] 8–200 keV energy range.
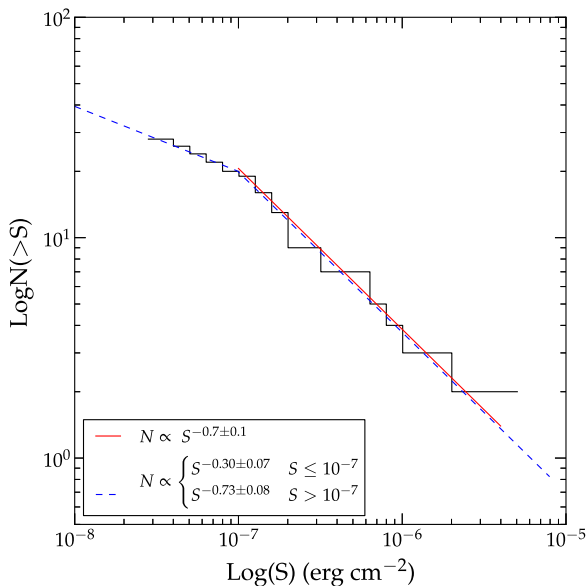
Figure 20. Log $N(>S)$ − Log (S) diagram of SGR J0501+4516. The data are fit to a single PL (red solid line) and a broken PL (blue dashed line). For the single PL, we only fit the data with $S > 1 \times 10^{-7}$ erg cm^{-2}.

Table 9
Time-integrated Spectral Modeling Results for 1E 1841–045 bursts

Trigger ID	COMP E_{peak} (keV)	α	OTTB kT (keV)	BB+BB kT1 (keV)	kT2 (keV)
110209218a	51^{+5}_{-4}	$-0.19^{+0.45}_{-0.41}$	60.93 ± 9.80	⋯	⋯
110217330a	45^{+3}_{-2}	$0.44^{+0.44}_{-0.4}$	41.48 ± 4.35	⋯	⋯
110221029a	41^{+2}_{-2}	$0.11^{+0.29}_{-0.27}$	43.24 ± 3.36	5.6 ± 1.1	13.1 ± 1.2
110616881a	28^{+2}_{-2}	$-0.9^{+0.2}_{-0.2}$	27.94 ± 1.37	⋯	⋯
110623612a	40^{+2}_{-2}	$-0.11^{+0.27}_{-0.26}$	38.42 ± 2.92	⋯	⋯
110625969a	37^{+2}_{-2}	$-0.04^{+0.37}_{-0.35}$	34.88 ± 3.66	⋯	⋯

index is -0.06 ± 0.01, and the broken PL indices are -0.23 ± 0.03 and 0.16 ± 0.03 with the break at 2.7×10^{-5} erg s cm^{-2}. The break value is almost an order of magnitude higher than that estimated using the average flux values (van der Horst et al. 2012), but closer to the break flux determined with time-resolved spectroscopy of the brightest SGR J1550–5418 bursts (Younes et al. 2014). The latter is also comparable to the break flux estimated for the time-resolved spectroscopy of bright bursts from SGR J0501+4516 (Lin et al. 2011a). We note that we find a considerably stronger correlation among the bursts below the break (Spearman rank = -0.422, chance probability of 5.9×10^{-14}) than among those reported in van der Horst et al. (2012). For the bursts above the break, we again see an improved but still insignificant correlation (chance probability of 0.17) compared to that found using the average flux (chance probability of 0.64).

3.1.4. Burst Peak Arrival Times—Pulse Phase Correlation Analysis

We have studied the burst peak arrival times with respect to the spin phase of the source. To determine a burst peak, for

each burst we fit the time-resolved spectra accumulated over 4 ms bins to a COMP model using *RMFIT*. The binning process was repeated for different bin edges to account for windowing effects. We assigned the time of the center of the brightest 4 ms as the peak in each burst. All times were barycenter corrected using the JPL ephemeris file as provided by HEASOFT-6.11.1; the phase of each burst peak was estimated using the spin ephemeris of Dib et al. (2012).

Figure 16 shows a histogram of all of the burst peak phases with the SGR J1550–5418 pulse profile measured with *XMM-Newton* (Lin et al. 2012) overplotted. We find that the peak arrival times are distributed uniformly across the spin phase (average bin height: $N = 17$ events, $\sigma = 5$ events). We tested for a correlation between the peak flux, fluence, and burst duration against the spin phase. Figure 17 shows the individual points, their weighted averages by 0.05 phase bins, and the SGR J1550–5418 pulse profile. We find no correlation between these three burst properties with spin phase.

3.1.5. Burst Profile Epoch Folding

Using *Swift*/XRT data (0.2–10 keV), Scholz & Kaspi (2011) found that the epoch folded light curves had one (fairly smooth) peak at 0.45–0.65 of the pulse phase. However, this was not found in an analysis of *Swift*/XRT bursts by Lin et al. (2012). We have performed a similar analysis using the GBM data to check this at higher energies. We epoch folded the background-subtracted light curves of each burst using the ephemeris of Dib et al. (2012). We then added all folded light

Table 10
Locations, Durations, Peak Fluxes, and Fluences for Bursts of Known Sources

Trigger (yymmddfff)	Source	Location[a]		T_{90} Start (UT)	T_{90} (ms)	T_{50} Start (UT)	T_{50} (ms)	4 ms Peak Flux[b,c] (erg cm^{-2})	Fluence[b,c] (erg cm^{-2})
		R.A.	Decl.						
090605862a	SGR J0418+5729	04 h 18 m 33.867s	+57° 32' 22.91"	20:30:48.875	40 ± 7	20:30:48.881	10 ± 4	1.00E-05 ± 5.80E-07	9.80E-08 ± 3.92E-09
090605876a	SGR J0418+5729	04 h 18 m 33.867s	+57° 32' 22.91"	21:01:35.011	80 ± 6	21:01:35.019	34 ± 4	1.71E-06 ± 1.50E-07	2.94E-08 ± 1.72E-09
100326867a	SGR 1806−20	18 h 08 m 39.337s	−20° 24' 39.85"	20:48:59.836	64 ± 9	20:48:59.848	32 ± 6	1.99E-06 ± 3.59E-07	8.44E-08 ± 5.46E-09
110714533a	SGR J1822.3−1606	18 h 22 m 18.00s	−16° 04' 26.8"	12:47:54.368	40 ± 18	12:47:54.368	8 ± 11	8.66E-06 ± 6.42E-07	5.81E-08 ± 4.52E-09
110729737a	AXP 4U 0142+61	01 h 46 m 22.407s	+61° 45' 03.19"	17:40:37.110	20 ± 6	17:40:37.114	12 ± 6	6.50E-06 ± 1.08E-06	1.33E-07 ± 9.72E-09
120421346a	AXP 1E 2259+586	23 h 01 m 08.295s	+58 ° 52' 44.45"	08:17:43.694	40 ± 33	08:17:43.694	8 ± 11	6.71E-06 ± 7.91E-07	5.73E-08 ± 5.40E-09
130617411a	SGR J1550−5418	15 h 50 m 54.12386s	−54° 18' 24.1141"	09:52:30.276	156 ± 16	09:52:30.300	88 ± 11	1.72E-06 ± 3.76E-07	1.27E-07 ± 6.66E-09

Notes.
[a] Source: Olausen & Kaspi (2013).
[b] By COMP model.
[c] 8–200 keV energy range.

Table 11
Time-integrated Spectral Modeling Results for Bursts of Known Sources

Trigger ID	Source	OTTB kT	COMP E_{peak}	α	BB kT
(yymmddfff)		(keV)	(keV)		(keV)
090605862a	SGR J0418+5729	33.46 ± 2.23	34.72 ± 1.85	-0.510 ± 0.260	8.70 ± 0.25
090605876a	SGR J0418+5729	19.71 ± 1.96	21.39 ± 2.55	-0.660 ± 0.520	6.06 ± 0.27
100326867a	SGR 1806–20	32.79 ± 3.19	34.23 ± 2.84	-0.600 ± 0.368	8.64 ± 0.39
110714533a	SGR J1822.3–1606	50.26 ± 6.14	50.06 ± 5.80	-0.929 ± 0.357	50.26 ± 6.14
110729737a	AXP 4U 0142+61	36.96 ± 4.17	38.46 ± 2.98	-0.324 ± 0.410	9.92 ± 0.44
120421346a	AXP 1E 2259+586	85.55 ± 16.70	74.30 ± 10.70	-0.469 ± 0.412	16.48 ± 0.96
130617411a	SGR J1550–5418	63.05 ± 6.78	50.78 ± 1.98	1.547 ± 0.416	13.12 ± 0.47

curves together to create the pulse profiles shown in Figure 18. We display the folded profiles in four energy bands, 8–20 keV, 20–50 keV, 50–200 keV, and 8–200 keV, together with the pulse profile in 0.5–10 keV. We note a peak at phase 0.15–0.20, which appears in all of the energy bands and is not associated with the pulse maximum or minimum.

We have studied the significance of this peak by calculating its deviation from the mean as $\sigma_i = (x_{max} - \bar{x})/\sigma_{19}$, where x_{max} is the value of the peak and $\bar{x}$ is the average of the histogram without that maximum bin. For the 8–200 keV energy range, we find $\sigma_i \sim 5.9$. To test the significance of this deviation, we performed a Monte Carlo simulation, randomly shifting all SGR J1550–5418 light curves in phase space by a random number chosen from a uniform distribution. After each shift, we created a new count-phase histogram and recalculated σ_i. This process was repeated 10,000 times, and we find that 1.24% of the time, σ_i would be at least as high as it is in the real data. This corresponds to a $\sim 2.5\sigma$ result, rendering this feature insignificant. Interestingly, we find that if we remove the top 10 brightest bursts from the histogram, the peak disappears (Figure 19) suggesting that the brightest bursts prefer a certain spin phase, a fact that may have been buried in the arrival time analysis. We tested this peak in the same way as described above and find that in this case, $\sigma_i \sim 11.4$. However, a Monte Carlo simulation of the 10 brightest bursts shows that this peak is only a $\sim 2.95\sigma$ result. Therefore, our findings confirm the results of Lin et al. (2012) that there is no strong evidence for a correlation between the burst counts and spin phase.

3.2. SGR J0501+4516

SGR J0501+4516 was discovered with *Swift*/BAT (Barthelmy et al. 2008; Holland & Sato 2008) when it emitted a magnetar-like burst on 2008 August 22, which also triggered GBM (Lin et al. 2011a). The entire source outburst lasted for about two weeks, with multiple bursts observed with *Swift*, GBM, *RXTE*, *Konus-Wind*, and *Suzaku* (Aptekar et al. 2009; Enoto et al. 2009; Kumar et al. 2010; Lin et al. 2011a). Göğüş et al. (2008) found the spin period with *RXTE*: ∼5.76 s; the combined *RXTE* and *Swift*/XRT data revealed a spin-down rate of $\dot{P} = 1.5 \times 10^{-11}$ s/s, which corresponds to a magnetic field of 2.0×10^{14} G (Woods et al. 2008; Rea et al. 2009; Göğüş et al. 2010). The most accurate location of SGR J0501+4516 was found with *Chandra* to be R.A. $= 05^h01^m06^s.76$, decl. $= +45°16'13''.92$ with an uncertainty of $0''.11$ (1σ; Göğüş et al. 2010). The source distance has been estimated to be ∼2 kpc (Xu et al. 2006; Lin et al. 2011a).

GBM triggered on 26 bursts during the entire outburst interval; an untriggered search as described in Kaneko et al. (2010) yielded 3 more bursts with TTE data, resulting in a total of 29 bursts. Two of these bursts saturated the High Speed Science Data Bus of GBM and were excluded from the detailed temporal and spectral analyses which are described in Lin et al. (2011a). In Tables 6–7, we provide the T_{90} and T_{50} durations in photon space and the spectral fitting parameters for these bursts. In Figure 20, we display the Log $N(>S)$ − Log (S) diagram for SGR J0501+4516 bursts computed in this study. We fit the histogram with both a PL and a broken PL. For the former we only fit the bins $\geqslant 1 \times 10^{-7}$ erg cm^{-2}, yielding an index of -0.7 ± 0.1. The broken PL indices are -0.30 ± 0.07 and -0.73 ± 0.08 below and above a break at 10^{-7} erg cm^{-2}, respectively. We note that in contrast to SGR J1550–5418, the single PL index and the high-fluence index for the broken PL are consistent with indices found for other magnetars (Section 3.1.2; Göğüş et al. 1999; Woods et al. 1999; Göğüş et al. 2001; Gavriil et al. 2004).

Finally, we note that a detailed variability analysis of the GBM bursts of SGR J0501+4516 did not result in a significant detection of QPOs (Huppenkothen et al. 2013).

3.3. 1E 1841–045

1E 1841–045 is a magnetar located at R.A. $= 18^h41^m19^s.343$, decl. $= -04°56'11''.16$ (from *Chandra* observations Wachter et al. 2004), and at a distance of $\sim 8.5^{+1.3}_{-1.0}$ kpc (Tian & Leahy 2008). ASCA observations have revealed a period of ∼11.8 s (Vasisht & Gotthelf 1997); the spin-down rate of $\dot{P} = 4.16 \times 10^{-11}$ s s^{-1} has been determined through ASCA, *RXTE*, and *BeppoSaX* observations (Gotthelf et al. 1999, 2002). *Swift*/BAT was first triggered by one burst on 2010 May 6 (Kumar & Safi-Harb 2010). This was followed by a period of activity between 2011 February 8 and July 2. During this time, *Swift* observed four bursts (e.g., Barthelmy et al. 2011; Melandri et al. 2011; Rowlinson et al. 2011). *Fermi*/GBM triggered on magnetar-like events six times during this time interval, with one of these triggers being one of the four *Swift* detections. The other five detections have no concurrent observations with other instruments. In addition, an untriggered burst search was performed over all of 2011 February and June 10–July 6 using the algorithm described in Kaneko et al. (2010). This search yielded only one burst, but one for which there is no TTE data, so it is excluded from our analyses. We argue that despite the lack of concurrent observations, given the coincidence in time and

Table 12
Locations, Durations, Peak Fluxes, and Fluences for Bursts of Unknown Sources

Trigger ID (yymmddfff)	Location–Galactic R.A. (°)	Decl. (°)	Err (°)	Location–Galactic l (°)	b (°)	T_{90} Start (UT)	T_{90} (ms)	T_{50} –Start (UT)	T_{50} (ms)	4 ms Peak Flux[a,b] (erg s^{-1} cm^{-2})	Fluence[a,b] (erg cm^{-2})
081106241a	268.0	−15.3	5.2	12.5	5.8	05:47:04.036	56 ± 11	05:47:04.052	24 ± 18	1.83E-06 ± 3.47E-07	7.08E-08 ± 4.90E-09
081129027a	272.3	−23.0	4.9	7.8	−1.6	00:38:12.655	116 ± 16	00:38:12.675	40 ± 6	3.06E-06 ± 6.51E-07	1.66E-07 ± 8.00E-08
090804852a	273.4	−19.2	3.7	11.6	−0.7	20:26:41.019	96 ± 33	20:26:41.027	28 ± 9	4.40E-06 ± 4.81E-07	1.42E-07 ± 6.43E-09
101114746a	264.7	−21.8	4.2	5.3	5.1	17:54:26.717	64 ± 25	17:54:26.725	8 ± 11	3.68E-06 ± 4.82E-07	6.38E-08 ± 4.99E-09
110107970a	271.6	−25.6	7.6	5.2	−2.3	23:16:28.380	80 ± 36	23:16:28.380	32 ± 23	1.86E-06 ± 3.42E-07	5.02E-08 ± 5.46E-09
110531601a	279.6	1.0	6.4	32.3	3.3	14:25:54.672	44 ± 23	14:25:54.680	16 ± 11	4.18E-06 ± 4.96E-07	8.35E-08 ± 5.32E-09
110807970a	276.9	−6.3	7.0	24.6	2.4	23:16:24.848	96 ± 23	23:16:24.864	48 ± 23	2.72E-06 ± 5.77E-07	1.03E-07 ± 7.38E-09
110810685a	285.8	−7.4	7.4	27.6	−6.0	16:26:28.188	40 ± 18	16:26:28.196	16 ± 11	2.04E-06 ± 3.86E-07	4.27E-08 ± 3.90E-09
111112325a	277.1	5.9	4.1	35.6	7.8	07:47:17.912	20 ± 6	07:47:17.916	8 ± 6	6.33E-06 ± 5.75E-07	8.70E-08 ± 4.48E-09
111220138a	236.7	−48.1	10.4	330.6	5.2	03:19:11.865	12 ± 6	03:19:11.869	4 ± 6	7.82E-06 ± 7.56E-07	6.04E-08 ± 4.76E-09
111225444a	280.7	0.2	5.2	32.1	2.0	10:38:46.236	224 ± 51	10:38:46.252	80 ± 36	2.27E-06 ± 3.80E-07	8.47E-08 ± 5.00E-09
120207380a	272.4	−30.3	6.3	1.4	−5.2	09:07:49.658	116 ± 13	09:07:49.670	49 ± 9	5.69E-06 ± 6.00E-07	2.10E-07 ± 8.43E-09
120728516a	282.2	−0.8	1.7	31.9	0.2	12:22:21.246	44 ± 6	12:22:21.258	16 ± 9	1.19E-05 ± 7.42E-07	3.92E-07 ± 8.71E-09
130113156a	277.6	4.2	5.6	34.2	6.6	03:45:10.258	20 ± 9	03:45:10.258	4 ± 6	5.61E-06 ± 6.73E-07	6.70E-08 ± 4.76E-09
130118345a	283.8	−2.6	1.2	31.1	−2.0	08:17:18.863	76 ± 6	08:17:18.879	36 ± 9	1.24E-05 ± 8.85E-07	8.04E-07 ± 1.44E-08
130507091a	280.3	−0.3	8.3	31.5	2.1	02:11:29.414	20 ± 9	02:11:29.418	8 ± 6	3.36E-06 ± 5.53E-07	4.37E-08 ± 4.68E-09
130702409a	279.9	−1.1	4.6	30.6	2.2	09:48:18.012	28 ± 16	09:48:18.016	8 ± 6	6.53E-06 ± 8.89E-07	7.63E-08 ± 6.60E-09
130913625a	278.9	−8.5	1.0	23.6	−0.4	15:10:28.436	112 ± 6	15:10:28.460	56 ± 6	2.00E-05 ± 1.30E-06	1.69E-06 ± 2.37E-08
130913757a	281.8	−7.5	7.1	25.7	−2.5	18:10:05.674	68 ± 13	18:10:05.714	20 ± 14	3.07E-06 ± 6.42E-07	6.70E-08 ± 8.06E-09

Notes.
[a] By COMP model.
[b] 8–200 keV energy range.
[c] This burst may be associated with the magnetar J1834.9–0846. However, due to large error for the GBM location and the crowdedness of the region, we cannot definitively associate it with this source.

position of these bursts, it is highly likely that they originate from 1E 1841−045 (see Lin et al. 2011b).

Detailed spectral and and temporal analyses of these GBM and *Swift* bursts are described in Lin et al. (2011b). Here, in Tables 8–9, we provide the T_{90} and T_{50} durations in photon space, and the spectral parameters for these bursts. New in this catalog compared to previous studies, we provide OTTB time-integrated spectral fits and 4 ms peak fluxes for these bursts (see Table 9).
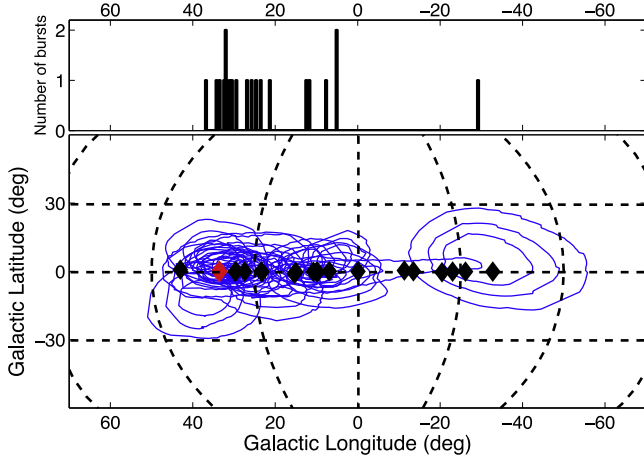
Figure 21. Locations in galactic coordinates of magnetar-like bursts with unconfirmed origin, displayed as 1, 2, and 3σ statistical error contours (blue lines). The known magnetars and magnetar candidates are shown as black diamonds, and the magnetar 3XMM J185246.6+0033.7 (Zhou et al. 2013) is highlighted in red. The histogram in the top panel is for the centroids of the GBM location contours.

3.4. Bursts from Other Known Magnetar Sources

In this section, we cover seven bursts, each originating from a known source as confirmed with *Swift* observations but with too few bursts to perform a statistical analysis as with the magnetars in the previous sections. These include two bursts from a new magnetar source, SGR J0418+5729, discovered with GBM and also observed with *Swift*/BAT and Konus-RF (van der Horst et al. 2009); the GBM data were published in van der Horst et al. (2010) and are also included in Tables 10–11. The other events originated from SGR 1806−20 (contemporaneous *Swift*/BAT detection; Bhat et al. 2010); SGR J1822.3−1606, which is a new source discovered and localized by *Swift* (Cummings et al. 2011; Pagani et al. 2011; von Kienlin & Kouveliotou 2011); AXP 4U 0142+61, for which GBM observed a burst simultaneous with a *Swift*/BAT burst (Bhat 2011; D. Palmer 2013, private correspondence); AXP 1E 2259+586, for which a single burst was observed with a location consistent with the source during an increased activity of the source's persistent emission (Foley et al. 2012; Archibald et al. 2013); SGR J1550−5418, which emitted a single burst in 2013 June, which was also detected with *Swift*/BAT (Holland et al. 2013) and was comparable in brightness to the bursts in the 2008 October period. For all bursts, we performed spectral and temporal analyses following the methods described in Section 2. The results of these analyses are presented in Tables 10–11.

## 4. MAGNETAR BURSTS OF UNCONFIRMED ORIGIN

GBM triggered on 19 bursts with magnetar-like temporal and spectral properties. Several of these bursts, however, were located in the vicinity of the Galactic Center, which is a very crowded region including many confirmed magnetars; see Table 12 for the burst locations. Due to the large error boxes of these bursts, we were not able to identify their origin

Table 13
Time-integrated Spectral Modeling Results for Bursts of Unknown Sources

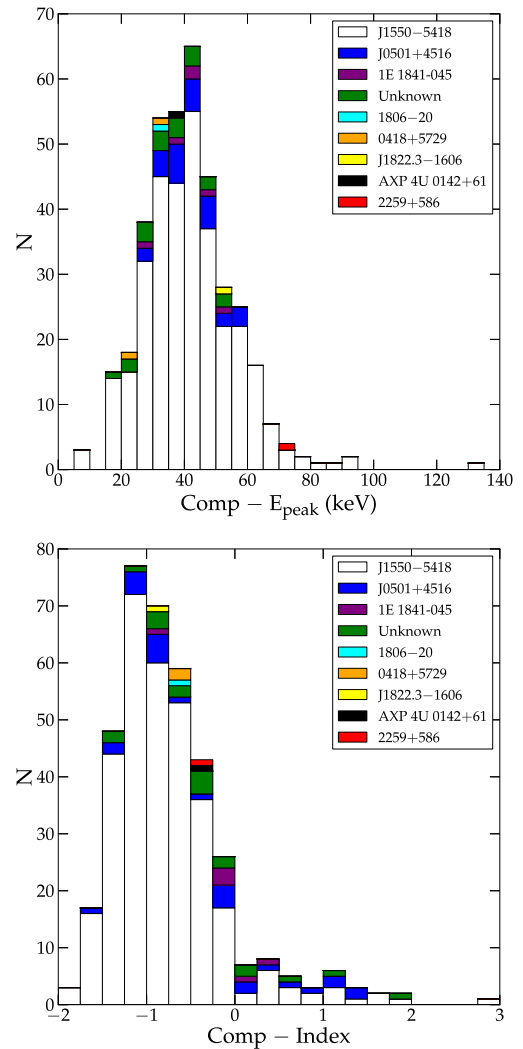| TRIGGER	PL α	OTTB kT (keV)	COMP Ep (keV)	α	BB kT (keV)	BB+BB Low kT (keV)	High kT (keV)
081106241a	−2.380 ± 0.094	25.73 ± 2.52	23.64 ± 4.63	−1.281 ± 0.354	7.34 ± 0.33	⋯	⋯
081129027a	−2.335 ± 0.097	26.67 ± 2.65	25.20 ± 4.17	−1.188 ± 0.367	7.34 ± 0.33	⋯	⋯
090804852a	−2.461 ± 0.071	22.58 ± 1.49	24.66 ± 1.68	−0.533 ± 0.321	6.81 ± 0.21	⋯	⋯
101114746a	−2.280 ± 0.105	31.49 ± 3.60	32.55 ± 3.56	−0.773 ± 0.443	8.70 ± 0.45	⋯	⋯
110107970a	−2.491 ± 0.153	21.67 ± 3.15	17.33 ± 8.80	−1.446 ± 0.599	6.80 ± 0.45	⋯	⋯
110531601a	−2.056 ± 0.087	42.00 ± 4.41	43.15 ± 2.55	0.179 ± 0.388	10.98 ± 0.45	⋯	⋯
110807970a[a]	−1.770 ± 0.085	63.81 ± 8.36	53.54 ± 3.41	0.532 ± 0.436	13.15 ± 0.62	⋯	⋯
110810685a	−1.936 ± 0.120	47.71 ± 7.69	44.42 ± 2.84	1.778 ± 0.284	47.71 ± 7.69	⋯	⋯
111220138a	−2.041 ± 0.105	44.24 ± 5.30	45.05 ± 4.16	−0.615 ± 0.354	11.37 ± 0.52	⋯	⋯
111112325a	−2.229 ± 0.078	31.72 ± 2.44	35.35 ± 1.86	−0.121 ± 0.321	31.72 ± 2.44	⋯	⋯
111225444a	−2.056 ± 0.081	39.85 ± 3.84	38.86 ± 1.76	1.028 ± 0.473	9.90 ± 0.40	⋯	⋯
120207380a	−2.470 ± 0.066	22.26 ± 1.33	25.17 ± 1.25	−0.229 ± 0.229	22.26 ± 1.33	⋯	⋯
120728516a	−2.278 ± 0.035	30.73 ± 1.04	33.27 ± 0.86	−0.398 ± 0.135	8.92 ± 0.12	3.83 ± 0.29	11.19 ± 0.36
130113156a	−2.026 ± 0.096	47.78 ± 5.94	48.00 ± 5.05	−0.751 ± 0.360	12.12 ± 0.59	⋯	⋯
130118345a	−2.406 ± 0.032	26.56 ± 0.74	27.65 ± 0.93	−0.828 ± 0.114	7.96 ± 0.10	3.95 ± 0.21	11.15 ± 0.35
130507091a	−1.991 ± 0.130	44.38 ± 7.19	42.62 ± 4.69	−0.303 ± 0.564	10.01 ± 0.68	⋯	⋯
130702409a	−2.069 ± 0.118	36.33 ± 5.06	36.72 ± 2.94	0.130 ± 0.529	9.25 ± 0.52	⋯	⋯
130913625a	−2.293 ± 0.024	29.81 ± 0.63	32.40 ± 0.56	−0.401 ± 0.086	8.68 ± 0.07	5.32 ± 0.19	13.04 ± 0.415
130913757a	−1.853 ± 0.138	57.71 ± 11.80	54.54 ± 8.05	−0.411 ± 0.589	12.82 ± 0.98	⋯	⋯

Notes.
[a] This burst may be associated with the magnetar J1834.9−0846. However, due to large error for the GBM location and the crowdedness of the region, we cannot definitively associate it with this source.
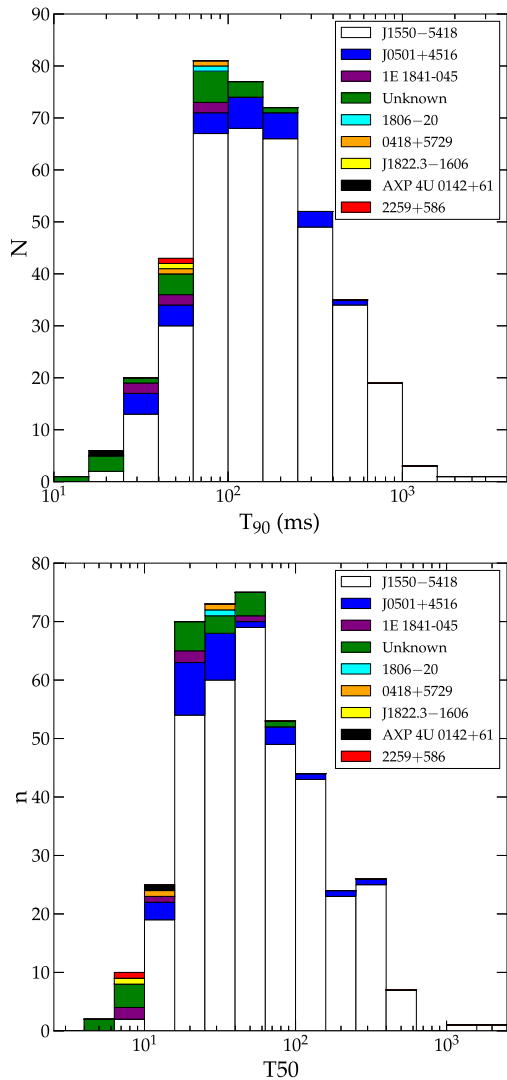
Figure 22. Distributions of the T_{90} and T_{50} durations for all magnetar bursts in this catalog.

Figure 23. Distributions of E_{peak} and the spectral index of the COMP model for all magnetar bursts in this catalog.

unambiguously, also because no other instruments with better localization capabilities recorded any of them. Figure 21 shows the locations of all 19 bursts with their 1, 2, and 3σ statistical error contours together with the locations of the known magnetars and magnetar candidates (Olausen & Kaspi 2013). All but one of the unknown bursts are in the same general location on the sky. The upper panel of Figure 21 displays the distribution of the contour centroids of the burst locations in Galactic longitude. We note a concentration of 8 events between 30° and 35°. Recently, Zhou et al. (2013) reported the discovery with *XMM-Newton* of a new magnetar, 3XMM J185246.6+0033.7 (red diamond on Figure 21). The source location ($l = 33°34'45''.1$, $b = -00°02'39''.9$) coincides with the highest density of unknown magnetar bursts, strongly suggesting that at least several bursts originate from this source (in particular those detected in 2013).

For this sample of bursts, we have also performed temporal and spectral analyses, the results of which are shown in Tables 12 and 13. Their analysis procedure is the same one we used for the bursts in Section 3.4, albeit using the locations determined with the GBM data.

5. DISCUSSION AND CONCLUSIONS

Here, we have compiled the 5 year GBM magnetar burst catalog comprising 446 events, 19 of which are from unknown sources and 427 are distributed across 7 known sources as shown in Table 1. We display the results of previously published temporal and spectral analyses for 357 events and include new results for the remaining 89. All of these data are compiled here to provide a single reference catalog to facilitate large-scale analyses of magnetar bursts for the community. The capabilities of *Fermi*/GBM allow for detailed spectral and temporal characterizations of magnetar bursts, which can be used to further our understanding of these bursts.

Figures 22–24 combine durations and spectral parameters for all 446 events. Each event is color coded per source, and the 19 unknown magnetar bursts are given the same color. Although SGR J1550–5418 bursts dominate the sample, we note several similarities in the spectral and temporal parameters across the bursts, regardless of their source. With respect to durations, all known source events tend to center around $T_{90} \sim 100$ ms (Figure 22). The unknown event durations tend to be shorter than most magnetar bursts with an average of $T_{90} \sim 61$ ms. However, the uncertainties on the individual durations are also
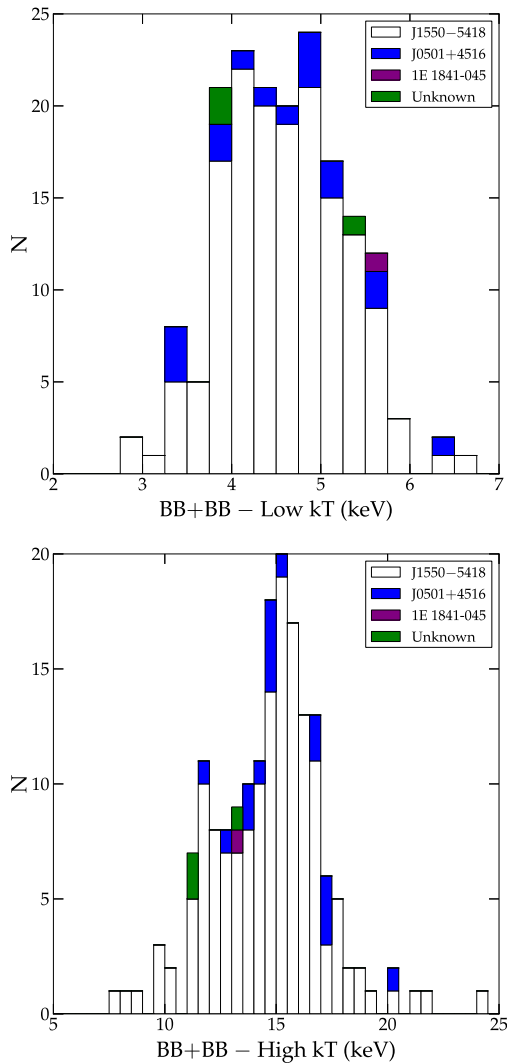
Figure 24. Distributions of the low- and high-temperature BB for all magnetar bursts in this catalog.

considerably high, largely due to the low intensities of some of these bursts, hampering any definitive conclusions on the possible differences in burst durations.

Regarding the spectral properties, the COMP parameters of all known events are very similar with $E_{\rm peak}$ centered at ~40 keV (Figure 23). The 19 unknown events have an arithmetic mean of $E_{\rm peak} \sim 37$ keV. The temperatures of the BB+BB center around ~4.5 and ~15 keV (Figure 24). The BB temperatures of the 19 unknown events have arithmetic means of ~4.3 and ~12.4 keV, which are very similar to those obtained from the SGR J1550–5418 bursts. For the former, we find an average 4 ms peak flux (8–200 keV) of 6.5×10^{-6} erg cm^{-2} s^{-1} and an average fluence of 2.3×10^{-7} erg cm^{-2}, which places them right in the middle of the flux-fluence diagram of SGR J1550–5418 (see also Figure 11).

Finally, the location distribution of eight events of unknown origin strongly indicates an association with the recently discovered magnetar 3XMM J185246.6+0033.7. A definite association of these bursts is not possible, however, due to the presence of multiple magnetar sources in that region.

REFERENCES

Archibald, R. F., Kaspi, V. M., Ng, C.-Y., et al. 2013, Natur, 497, 591
Aptekar, R. L., Cline, T. L., Frederiks, D. D., et al. 2009, ApJL, 698, L82
Aptekar, R. L., Frederiks, D. D., Golenetskii, S. V., et al. 2001, ApJS, 137, 227
Atteia, J.-L., Boer, M., Hurley, K., et al. 1987, ApJL, 320, L105
Barthelmy, S. D., Baumgartner, W. H., D'Elia, V., et al. 2011, GCN Circ., 11673
Barthelmy, S. D., Beardmore, A. P., Burrows, D. N., et al. 2008, GCN Circ., 8113
Bhat, P. N., Palmer, D., Kouveliotou, C., & Barthelmy, S. 2010, GCN Circ., 10549
Bhat, P. N. 2011, GCN Circ., 12231
Camilo, F., Ransom, S. M., Halpern, J. P., & Reynolds, J. 2007, ApJL, 666, L93
Cummings, J. R., Burrows, D., Campana, S., et al. 2011, GCN Circ., 12159
Dib, R., Kaspi, V. M., Scholz, P., & Gavriil, F. P. 2012, ApJ, 748, 3
Duncan, R. C., & Thompson, C. 1992, ApJL, 392, L9
Enoto, T., Nakagawa, Y. E., Rea, N., et al. 2009, ApJL, 693, L122
Esposito, P., Israel, G. L., Zane, S., et al. 2008, MNRAS, 390, L34
Foley, S., Kouveliotou, C., Kaneko, Y., & Collazzi, A. C. 2012, GCN Circ., 13280
Gavriil, F. P., Kaspi, V. M., & Woods, P. M. 2004, ApJ, 607, 959
Gelfand, J. D., & Gaensler, B. M. 2007, ApJ, 67, 1111
Göğüş, E. 2014, AN, 335, 296
Göğüş, E., Kouveliotou, C., Woods, P. M., et al. 2001, ApJ, 558, 228
Göğüş, E., Woods, P. M., Kouveliotou, C., et al. 1999, ApJL, 526, L93
Göğüş, E., Woods, P., & Kouveliotou, C. 2008, GCN Circ., 8118
Göğüş, E., Woods, P. M., Kouveliotou, C., et al. 2010, ApJ, 722, 899
Golenetskii, S. V., Ilinskii, V. N., & Mazets, E. P. 1984, Natur, 307, 41
Gotthelf, E. V., Gavriil, F. P., Kaspi, V. M., Vasisht, G., & Chakrabarty, D. 2002, ApJL, 564, L31
Gotthelf, E. V., Vasisht, G., & Dotani, T. 1999, ApJL, 522, L52
Götz, D., Mereghetti, S., Molkov, S., et al. 2006, A&A, 445, 313
Holland, S. T., & Sato, G. 2008, GCNR, 160, 1
Holland, S. T., Lien, A. Y., Marshall, F. E., et al. 2013, GCN, 14911
Huppenkothen, D., D'Angelo, C., Watts, A. L., et al. 2014, ApJ, 787, 128
Huppenkothen, D., Watts, A. L., Uttley, P., et al. 2013, ApJ, 768, 87
Kaneko, Y., Göğüş, E., & Kouveliotou, C. 2010, ApJ, 710, 1335
Kouveliotou, C., Norris, J. P., Cline, T. L., et al. 1987, ApJL, 322, L21
Kouveliotou, C., Meegan, C. A., Fishman, G. J., et al. 1993, ApJL, 413, L101
Kouveliotou, C., Dieters, S., Strohmayer, T., et al. 1998, Natur, 393, 235
Kouveliotou, C., Strohmayer, T., Hurley, K., et al. 1999, ApJL, 510, L115
Kouveliotou, C., von Kienlin, A., Fishman, G., et al. 2009, GCN Circ., 8915
Kumar, H. S., Ibrahim, A. I., & Safi-Harb, S. 2010, ApJ, 716, 97
Kumar, H. S., & Safi-Harb, S. 2010, ApJL, 725, L191
Lamb, R. C., & Markert, T. H. 1981, ApJ, 244, 94
Laros, J. G., Fenimore, E. E., Klebesadel, R. W., et al. 1987, ApJL, 320, L111
Lin, L., Göğüş, E., Baring, M. G., et al. 2012, ApJ, 756, 54
Lin, L., Göğüş, E., Kaneko, Y., & Kouveliotou, C. 2013, ApJ, 778, 105
Lin, L., Kouveliotou, C., Baring, M. G., et al. 2011a, ApJ, 739, 87
Lin, L., Kouveliotou, C., Göğüş, E., et al. 2011b, ApJL, 740, L16
Mazets, E. P., Golenetskij, S. V., & Guryan, Y. A. 1979b, SvAL, 5, 343
Mazets, E. P., Golentskii, S. V., Ilinskii, V. N., Aptekar, R. L., & Guryan, I. A. 1979a, Natur, 282, 587
Meegan, C., Lichti, G., Bhat, P. N., et al. 2009, ApJ, 702, 791
Melandri, A., Barthelmy, S. D., Chester, M. M., et al. 2011, GCN Circ., 12103
Mereghetti, S. 2008, A&ARv, 15, 225

Olausen, S. A., & Kaspi, V. M. 2013, arXiv:1309.4167v2
Pagani, C., Beardmore, A. P., & Kennea, J. A. 2011, ATel, 3493
Palmer, D. 2009, GCN Circ., 8901
Rea, N., Israel, G. L., Turolla, R., et al. 2009, MNRAS, 396, 2419
Rowlinson, A., Barthelmy, S. D., Beardmore, A. P., et al. 2011, GCN Circ., 12079
Scholz, P., & Kaspi, V. M. 2011, ApJ, 739, 94
Tian, W. W., & Leahy, D. A. 2008, ApJ, 677, 292
Tiengo, A., Vianello, G., Esposito, P., et al. 2010, ApJ, 710, 227
van der Horst, A. J., Connaughton, V., Kouveliotou, C., et al. 2009, GCN Circ., 9499
van der Horst, A. J., Connaughton, V., Kouveliotou, C., et al. 2010, ApJL, 711, L1
van der Horst, A. J., Kouveliotou, C., Gorgone, N. M., et al. 2012, ApJ, 749, 122

Vasisht, G., & Gotthelf, E. V. 1997, ApJL, 489, L129
von Kienlin, A., & Kouveliotou, C. 2011, GCN Circ., 12179
von Kienlin, A., Gruber, D., Kouveliotou, C., et al. 2012, ApJ, 755, 150
Wachter, S., Patel, S. K., Kouveliotou, C., et al. 2004, ApJ, 615, 887
Watts, A. L., Kouveliotou, C., van der Horst, A. J., et al. 2010, ApJ, 719, 190
Woods, P. M., Gogus, E., & Kouveliotou, C. 2008, ATel, 1691
Woods, P. M., Kouveliotou, C., van Paradijs, J., et al. 1999, ApJL, 519, L139
Woods, P. M., & Thompson, C. 2006, in Compact Stellar X-ray Sources, ed. W. H. G. Lewin, & M. van der Klis (Cambridge: Cambridge Univ. Press), 547
Younes, G., Kouveliotou, C., van der Horst, A. J., et al. 2014, ApJ, 785, 52
Xu, Y., Reid, M. J., Zheng, X. W., & Menten, K. M. 2006, Sci, 311, 54
Zhou, P., Chen, Y., Li, X.-D., et al. 2013, arXiv:1310.7705v